Non-peer reviewed EarthArXiv preprint

This manuscript is the revised version of the preprint uploaded to EarthArXiv in May 2019.

It has been submitted for publication to Basin Research on the 26 Apr. 2019, was rejected on the 7 Oct. 2019, and was resubmitted to the same journal on the 6 Jan. 2020.

This preprint version of the manuscript has not undergone peer-review. Newer versions may be moderately different with slight variations in content.

Authors encourage downloading the latest manuscript version from EarthArXiv before usage.

Authors welcome comments, feedback and discussions anytime. Please, feel free to contact the first author at r.j.g.charton@tudelft.nl

Permian to Neogene Source-and-Sink maps: A semi-quantitative analysis of vertical movements in Morocco and surroundings

Authors

Rémi Charton, Department of Geoscience and Engineering, Delft University of Technology, P.O. Box 5048, 2600 GA Delft, The Netherlands
r.j.g.charton@tudelft.nl

Giovanni Bertotti, Department of Geoscience and Engineering, Delft University of Technology, P.O. Box 5048, 2600 GA Delft, The Netherlands
g.bertotti@tudelft.nl

Aude Duval Arnould, School of Earth and Environmental Sciences, The University of Manchester, M13 9PL Manchester, United Kingdom
aude.duval-arnould@manchester.ac.uk

Joep E. A. Storms, Department of Geoscience and Engineering, Delft University of Technology, P.O. Box 5048, 2600 GA Delft, The Netherlands
j.e.a.storms@tudelft.nl

Jonathan Redfern, School of Earth and Environmental Sciences, The University of Manchester, M13 9PL Manchester, United Kingdom
jonathan.redfern@manchester.ac.uk

Acknowledgments

This study was part of the first author's doctoral thesis project, with financial support from the Netherlands research centre for Integrated Solid Earth Sciences (ISES) and the North Africa Research Group (NARG). We acknowledge the ONHYM for providing data to the NARG. All NARG members are thanked for scientific discussions and support. Angel Arantegui and Tim Luber are thanked for discussions about Early Cretaceous source-to-sink systems in the Tarfaya and Essaouira-Agadir basins, respectively. Emmanuel Roquette, Delphine Rouby, Antonio Teixell, and Mohamed Gouiza are acknowledged for proofreading an earlier version of the manuscript. Emilie Chaillan is thanked for digitizing the Cretaceous outcrops from the NW African geological maps. Finally, we deeply thank two anonymous reviewers for their constructive comments that greatly help improving the original manuscript.

Abstract

Available time-Temperature (t-T) modelling published results from Morocco and its surroundings have been digitized and a temperature-to-depth conversion was applied. The results predict high exhumation rates, comparable to values typical of rift flank, domal or structural uplifts, in the Anti-Atlas (0.1 km/Myr) during the Early to Middle Jurassic and in the High Atlas (0.1 km/Myr) and Rif (up to 0.5 km/Myr) during the Neogene. During other periods, erosional exhumation rates in the Meseta, High-Atlas, Anti-Atlas, and Reguibat shield are around 0.04±0.02 km/Myr.

The exhumation and burial rates were then used as input for interpolation at the country scale, in order to quantify the volume of rocks that were eroded during the several erosional exhumation episodes. Estimates of cumulative eroded volumes from Permian onwards are between ca. $15x10^5$ and $2x10^5$ km^3 (in the Reguibat Shield and Meseta, respectively). Periods of high rates of denudation in the investigated source areas include the Permian, the Jurassic, the Early Cretaceous (Berriasian to Barremian), and the Neogene.

Ten erosional (quantitative) and depositional (qualitative) “source-and-sink” maps have been constructed, covering the period between the Variscan Orogeny and the Present-Day (Permian to Neogene). Emphasis is placed on the Jurassic and Cretaceous periods. The maps are based on the extent of exhumed domains (first part of this study) and on the integration of data from new geological fieldwork, outcrop spatial distribution, lithofacies from onshore and offshore basin, biostratigraphic data, well data, palaeogeography, and depositional environment maps. The results illustrate changes in the Permian to Neogene source-to-sink systems and allow for the analysis of the dynamic nature of their components.

Keywords

Time-temperature modelling, Morocco, vertical movements, paleo-reconstruction, exhumation rates

1. Introduction

Continental passive margins and their hinterlands, especially in the Atlantic realm (fig. 1), are the locus of a significant amount of studies that evidence pre-, syn-, and post-rift episodic km-scale upward (i.e. exhumation) and downward (i.e. burial) movements (e.g. Green et al., 2018). Pre-rift exhumation episodes are recorded in the vicinity of the future Atlantic Ocean (e.g. Juez-Larre and Andriessen, 2006; Ruiz et al., 2011; Jelinek et al., 2014; Japsen et al., 2016a). Syn-rift exhumation episodes have been described in the Atlantic rift flanks (e.g. Oukassou et al., 2013; Jelinek et al., 2014; Wildman et al., 2015; Japsen et al., 2016a, Charton et al., 2018) and in the plate interior (e.g. Leprêtre et al., 2013), while syn-rift burial episodes in the unstretched continental crust have been documented in fewer places (e.g. Juez-Larre and Andriessen, 2006; Ghorbal et al., 2008). Post-rift km-scale vertical movements have been documented along the North (e.g. Japsen et al., 2006; Japsen et al., 2016a; 2016b), Central (e.g. Frizon de Lamotte et al., 2009; Bertotti and Gouiza, 2012; Amidon et al., 2016) Equatorial (e.g. Hayford et al., 2008; Ye, 2016; Wildman et al., 2018) and South (e.g. Jelinek et al., 2014; Wildman et al., 2015) Atlantic margins.

Vast regions along Atlantic rifted continental margins are characterised by the exposure of pre-rift rocks (e.g. in Norway, Canada, Greenland, Morocco, Mauritania, Brazil…). There, LTT and time-Temperature (t-T) modelling techniques provided understanding of the thermal history, as this is especially valuable for geologically ill-constrained areas characterised by no or little sedimentary cover (e.g. Gallagher et al., 1998; Ghorbal et al., 2008; Japsen et al., 2009; Teixell et al., 2009; Japsen et al., 2012b; Jelinek et al., 2014). These techniques are commonly selected as proxies to reconstruct vertical movements (e.g. Teixell et al., 2009), as they are key to reconstructing past source-to-sink systems (e.g. Helland-Hansen et al., 2016). Because the LTT ages record the cooling of rock samples,

they are linked either to thermal relaxation and/or exhumation (also called denudation when erosional in nature; e.g. Pagel et al., 2014; Malusà and Fitzgerald, 2019).

Bertotti and Gouiza (2012) proposed, in the eastern margin of the Central Atlantic, that anomalous vertical movements in the exhuming domain are concurrent to excessive downward movements in the subsiding domain. Exhumation and burial episodes occur in regions characterised by both stretched and non-stretched lithosphere, demonstrating that processes other than rifting are at work, or that the effects of the rifting and drifting extend beyond the rifted margin and their direct flanks. Several authors have qualitatively tested aspects of these vertical movements with numerical models (e.g. Leroy et al., 2008; Gouiza, 2011; Cloetingh and Burov, 2011; Yamato et al., 2013). However, to better constrain the models, a quantification of these movements over geological time and, more importantly, at the scale of the margin, is required (e.g. Ye et al., 2017; Wildman et al., 2019).

Over thirty LTT and time-Temperature (t-T) modelling published studies have been conducted in Morocco and its surroundings. There, the large majority of the derived LTT ages span the period between the Variscan and Atlas orogenies (ca. 300-40 Ma). These cooling ages were interpreted as resulting from vertical movements (e.g. Ghorbal et al., 2008; Sebti et al., 2009; Leprêtre et al., 2013; Gouiza et al., 2017a; Charton et al., 2018), and have sometimes been labelled as km-scale "unexpected" exhumation and "unpredicted" burial episodes, with the mechanism to generate this movement remaining enigmatic to-date (e.g. Ghorbal et al., 2008). As a prerequisite to constrain the responsible mechanism(s) in future works (potential candidates reviewed in Charton, 2018), vertical movements rates are to be investigate, enabled with temperature-to-depth conversion of the t-T models (e.g. Gouiza et al., 2017).

The objectives of this paper are 1) to use a simple workflow that quantifies eroded material fluxes from basement areas investigated by LTT/t-T studies, using Morocco as a test area and 2) to provide insights into the post-Variscan paleogeographic evolution of Morocco and its surroundings via the construction of source-and-sink maps.

This study should be considered as a framework for future studies investigating source-to-sink systems, creating an opportunity for definition and quantification of sediments pathways and fluxes along the entire Moroccan rifted margin and into the interior of its adjacent continental crust. The aim of these maps is not to precisely define the paleo-drainage systems, as the resolution of our datasets is in all cases too coarse, but to illustrate the dynamic nature of the source-to-sink systems and of their components during the Phanerozoic post-orogenic, syn-rift and post-rift phases.

2. Geological history of Morocco

The Central Atlantic continental margins extend from Morocco to Guinea in the east and Canada to the USA to the west (fig. 1; Davison, 2005; Withjack and Schlische, 2005). Morocco is located in Northwest Africa between the Central Atlantic oceanic crust, the West African Craton, and the Atlas orogenic system. The relief (fig. 2A) varies from high mountainous regions (Rif and Atlas belts), elevated plains (Hauts Plateaux and Ouarzazate Basin), high massifs (Central Massif, Rehamna, Jebilets, Massif Ancient, Anti-Atlas, Reguibat Shield, and Ougarta), non-elevated coastal plains (Meseta, Souss Basin, Tarfaya Basin, and Dakhla Basin), and the Saharan domain marked by ergs and sabkhas (salt flats).

The geological history of Morocco (fig. 2B) is punctuated by a number of major events from the Precambrian to the present-day (fig. 2C). Prior to the Central Atlantic rifting period, Morocco was subjected to the Eburnean and Panafrican orogenies during the Paleoproterozoic and Neoproterozoic (Piqué et al., 2006), respectively. These orogenies deformed the oldest sediments and crystalline basement of the Western African Craton, and are exposed in the Reguibat shield, Mauritanides, and in the core of the Anti-Atlas. Marine clastic-dominated sedimentation occurred during the Early Palaeozoic and deposits are preserved and exposed in the Meseta massifs, Anti-Atlas, and Tindouf basin (Michard et al., 2008).

The Late Palaeozoic Variscan orogeny (fig. 2C; basin inversion, crustal folding, intense thrusting, nappe structures, granitic intrusion…) affected the Palaeozoic cover and Precambrian basement of the Meseta, High Atlas, and Anti-Atlas (e.g. Michard et al., 2010). It was followed between Late Permian to Triassic by a post-orogenic collapse, of which termination is marked in Morocco by the so-called Variscan (or often 'Hercynian') unconformity (e.g. Frizon de Lamotte et al., 2004).

Morocco experienced two partly-coeval episodes of rifting during Triassic and Jurassic times: The Central Atlantic (ca. 230-190 Ma; Labails et al., 2010; Frizon de Lamotte et al., 2015) and Atlasic (also called Tethysian; ca. 240-185 Ma, aborted; Piqué et al., 2006; fig. 2C) rifts. The orientation of the Central Atlantic rift was partly inherited from Variscan structures, as rift structures occurred around and parallel to the trend of the Palaeozoic belt. The Atlasic rift belongs to the Tethysian realm and is oriented at ca. 45° to the Central Atlantic rift (fig. 2). In the rift zones, grabens and half graben were filled with continental syn-rift deposits in the Doukkala, Argana/Essaouira-Agadir, Tarfaya coastal basins and High/Middle Atlas basins. At ca. 201 Ma, the Central Atlantic Magmatic Province (CAMP; figs. 2B and C) is characterised by the emplacement of mafic dykes and sills (e.g. Davies et al., 2017), followed by flood basalts dated until ca. 190 Ma (Verati et al., 2007).

The onset of Pangaea break-up marking continental drift and initiation of the proto-Atlantic occurred at the beginning of the Jurassic. The precise age is debated between 190 and 170 Ma (e.g. Labails et al., 2010; Davison, 2005). The development of the Moroccan passive margin during the Jurassic and Early Cretaceous witnessed the accumulation of neritic and deeper marine sediments in the present-day offshore, the coastal basins, the High/Middle Atlas, and in the Meseta basins. The Peri-Atlantic Alkaline Pulse (PAAP) is recorded by plutons and flood basalt in the conjugate margins of the Central and South Atlantic oceans, between 125 and 80 Ma (Matton and Jebrak, 2009; Montero et al., 2016).

The opening of the South Atlantic at ca. 85 Ma led to the African and European plate convergence from the Late Cretaceous to the present-day, and may support far-field intraplate stresses responsible for folding and basin inversion in the High and Middle Atlas and in the Rif chains (Guiraud, 1998). The ongoing Atlas orogenesis that peaked in the Eocene is characterised by the deformation and upheaval of the Rif, the Middle Atlas, and the High Atlas (Michard et al., 2008). Finally, Cenozoic volcanism (Missenard and Cadoux, 2011) and surface uplift, observed along two axes, from the

Canary Islands to the Siroua massif (Anti-Atlas) and from the latter to the Rif belt, have been interpreted as associated to a mantle anomaly (Zeyen et al., 2005; Teixell et al., 2005; Missenard, 2006).

3. Converting time-temperature modelling into source-and-sink maps: material, methods, intermediary results, and uncertainties

3.1. From t-T models to eroded material fluxes

3.1.1. t-T modelling database and geological constraint review

In Morocco and its surroundings, over thirty LTT published studies have been conducted in the last 25 years (e.g. Mansour, 1991; Malusà et al., 2007; Ghorbal et al., 2008; Ruiz et al., 2011; Sehrt et al., 2018; see exhaustive list as of March 2018 in Charton, 2018). This provides an extensive database of over 1000 LTT ages in the study area (including (U-Th)/He ages from apatite crystals (AHe), Apatite Fission Track (AFT) ages, (U-Th)/He ages from zircon crystals (ZHe), and Zircon Fission Track (ZFT) ages). The spatial distribution of the samples highly depends on the superficial lithology (fig. 2B), as samples must contain either apatite or zircon crystals/grains. For this reason, exposed Precambrian crystalline basement rocks, meta-psammites within the otherwise (marine) metapelite dominated Palaeozoic column, Meso-Cenozoic clastic sediments, and dykes/sills of all ages could be analysed for LTT in the studied area.

LTT studies often use the produced ages, fission track density and length as inputs for t-T inverse modelling (e.g. Pagel, 2014; Malusà and Fitzgerald, 2019). Such modelling allows testing of several t-T paths by guiding the model realisations with user-defined constraints. The method provides a comprehensive illustration of the t-T path of the analysed sample, highlighting cooling and heating event(s). Amongst the above-mentioned LTT studies, twenty performed and published t-T modelling, resulting in 117 t-T models (figs. 3 and 4; see complete list of references in table 1). The programs that were used in these studies for the inverse modelling of LTT data are HeFTy (Ketcham, 2005), AFT Solve (Ketcham et al., 2000), and QTQt (Gallagher, 2012; also, see Vermeesch and Tian (2014) for a comparison of HeFTy and QTQt codes) providing comparable thermal histories. The programs outputs are labelled as ‘acceptable’, ‘good’, ‘best-fit’, or ‘weighted average’ (referring to a goodness

of fit) paths for HeFTy/AFTSolve and 'probability' range, 'maximum likelihood' or 'expected' paths for QTQt.

The age/depth or age/temperature geological constraints added to t-T modelling between 300 and 0 Ma are discussed in this part. In the study area, two types of geological constraints are used: 1) sediments that are overlying the sampled basement, with or without an erosion gap, provide a constraint to surface temperatures (ca. 10-40°C) for the estimated time of deposition. In the case of detrital thermochronology, the stratigraphic age of the sampled sediments is used as a constraint, also at surface temperatures. 2) When the age and temperatures of emplacement or metamorphism of the sampled basement are known, a corresponding radiometric constraint is implemented.

In the Rif belt, Pliocene sediments and Miocene $^{40}Ar/^{39}Ar$ and K-Ar radiometric dating were used as constraints (Romagny et al., 2014; Azdimousa et al., 2013). In the Meseta, constraints based on the Variscan granite emplacement and Permian, Triassic, and Cenomanian sedimentary record in the basins surroundings the Variscan massifs were added to the t-T modelling (Saddiqi et al., 2009, Ghorbal et al., 2008; Barbero et al., 2011). In the Variscan High Atlas (Massif Ancien), Triassic and poorly dated Early Cretaceous sediments overlying Precambrian basement rocks permitted authors to add surface-temperature constraints to the models (Ghorbal, 2009; Balestrieri *et al* 2008; Barbero et al., 2007; Domenech et al., 2016). In the central Anti-Atlas, emplacement data from the Jurassic intrusive rocks served as a constraint (Barbero et al., 2007). In the Tarfaya basin, Sehrt et al. (2017b) used the Aptian and Albian stratigraphic age of sampled sediments for the t-T modelling. In the Reguibat Shield, a geological constraint at surface temperatures was defined for the Early/Middle Cretaceous, as sediments (poorly dated) are exposed in the Tarfaya and Tindouf basins (Leprêtre et al., 2013; 2015; 2017). In the eastern Reguibat Shield, the poorly dated Upper Cretaceous sediments

of the Reggane basin were used to guide t-T models (Leprêtre et al., 2017). Overall, these studies used t-T model constraints fairly consistently.

The Variscan metamorphism (Ruiz et al., 2011, Charton et al., 2018, Malusà et al., 2007) and the emplacement of the CAMP dykes (see Gouiza et al., 2017) were used as geological constraints at placing the sampled rocks at great temperature/depths. The Triassic sediments in the north of the belt (Ghorbal, 2009), Middle Jurassic sediments (Charton et al., 2018), poorly dated terrestrial Infra-Cenomanian sediments in the western, central, and eastern Anti-Atlas (e.g. Ruiz et al., 2011; Oukassou et al., 2013) and Cenomanian fluvial sediments overlying the Variscan basement on the eastern Anti-Atlas (Gouiza et al., 2017) were used as evidence of the presently outcropping Anti-Atlas basement rocks being close to surface temperatures.

However, comparison between t-T models of the Anti-Atlas suggests major discrepancies (Gouiza et al., 2017; fig. 4D). One of the aspects of the modelling, to which these discrepancies can be attributed, is the use of different t-T modelling constraints. Despite the established use of an Early Cretaceous modelling constraint in the Anti-Atlas (Ruiz et al., 2011; Oukassou et al., 2013; Sehrt et al., 2017a), recent re-dating is leading to less and less of the terrestrial beds around the belt are still considered as Lower Cretaceous (reviewed in Gouiza et al., 2017; Charton et al, 2018; Arantegui et al., 2019). In the eastern part of the belt, extensive paleontological work conducted by Benyoucef and co-authors showed that the red beds are Cenomanian (e.g. Benyoucef et al., 2015). In the central Anti-Atlas, no recent study on the local undifferentiated clastics has been conducted, but a time constraint is the Cenomanian limestones positioned higher in the stratigraphic column (e.g. Fetah et al., 1990). The clastics could hence be Cenomanian in age, similarly to the sediments in eastern Anti-Atlas. Finally, in the western Anti-Atlas, recent work by Arantegui (2018) presents new biostratigraphic data that conclusively dates the local redbeds, also mapped as Lower Cretaceous, as Bathonian (Middle

Jurassic) or older (most-likely Triassic or Liassic). Overall, this invalidates the use of an Early Cretaceous constraint that was previously used to guide basement rock surface temperatures in the Anti-Atlas close. In this work, we consider as valid all of the abovementioned new modelling constraints used for the Anti-Atlas, and disregard the previous Early Cretaceous surface temperatures geological constraint.

3.1.2. From time-temperature models to vertical movement rates

In order to quantify volumes of eroded material on the top of the presently exposed rocks in the study area, we apply a temperature-to-depth conversion on selected t-T results (e.g. Gouiza et al., 2017; fig 5). One of the prerequisites to apply such a conversion to t-T results is that cooling must mean exhumation, as opposed to thermal relaxation (see Malusà and Fitzgerald, 2019b for a complete review). Exhumation, as defined in England and Molnar (1990), can be explain as the decrease of the distance between a buried rock and Earth's surface. It does not mean 'uplift', as exhumation may in principle occur by the erosion of a rock overburden, without involving motion of the rock in regards to its absolute elevation. In the present contribution, we only consider studies that have interpreted cooling events as exhumation ones.

The conclusion reached in nearly all t-T studies, conducted in Morocco and surroundings, including our previous work (Bertotti and Gouiza, 2012; Gouiza et al., 2017; Charton et al., 2018), is that samples with cooling ages younger than their stratigraphic ages record vertical movements. This allows cooling and heating events to be translated into exhumation and burial, respectively. The exceptions to this general, and regional, conclusion are the results for some of the samples collected in the High Atlas (post-rift thermal relaxation; Barbero et al., 2007), in the Canary Islands (Cenozoic post-volcanism thermal relaxation; Wipf et al., 2010) and in the Siroua massif (Cenozoic post-magmatism/volcanism thermal relaxation; Ghorbal, 2009).

Weighted average/expected curves were digitized when available (else the best-fit/maximum likelihood curves) using WebPlotDigitizer (Ankit Rohatgi; https://automeris.io/WebPlotDigitizer/). We applied five conditions to select representative and valid t-T curves, resulting in a total of 56 selected t-T curves (detailed in table 1). We consider that modelling results have to i) start before 20 Ma (about the extent of youngest considered period), ii) be based on HeFTy, AFT solve or QTQt results, iii) if

different models using the same LTT data exist, be from the most recent realizations (e.g. in Leprêtre et al., 2013 and Leprêtre, 2015), iv) should be based on one sample as opposed to vertical profiles (justified by the fact that we are using punctual measurements allowing for spatial interpolation), and v) be compatible with the geological history of each region as discussed in the previous part.

To achieve the temperature-to-depth conversion (fig. 6), different paleo-geothermal gradients were used based on the location of the selected t-T curves (i.e. independently known, c.f. Malusà and Fitzgerald, 2019; fig. 5) and keeping the surface temperature constant at 20°C. The considered geothermal gradients are based on several studies, which serve as analogues for the past geodynamic setting in Morocco. Luth and Willingshofer (2008; see references therein) obtained geothermal gradients of 23-35°C/km for the Alps. Based on these values, we considered an average geotherm of 29°C/km for the Variscan orogeny. The geotherm in the rift zone of the East African Rift system is ca. 40°C/km (van der Beek et al., 1998) and between 25 and 32°C/km in the Rio Gande Rift (Bridwell, 1976). We consider a geotherm of 34°C/km as representative for the High Atlas Rift zone. The flanks of the East African Rift systems display geothermal gradients between 25 and 30°C/km (van der Beek et al., 1998) and we use 27°C/km as an analogue for the Central Atlantic/High Atlas rift flanks. As an analogue for the post-rift Moroccan passive margin at 80 Ma (mature passive margin) and for intra-continental domain of the Reguibat Shield, we considered a geotherm of 24°C/km. Lastly, Zarhloule (2004) obtained present-day values from Moroccan Passive margin of 20 to 35°C/km. The selected geotherms take into account the thermal relaxation that follows after the rift-related heating phase.

The role of applying a changing paleo-geothermal gradient per area is to 1) match the changing thermal frame of the upper 10 km of the crust based on known geodynamic events (e.g. High Atlas rifting; e.g. Gouiza et al., 2017) and 2) provide a favourite model to obtain values of rates and fluxes with ranges, as opposed to only ranges using constant geotherms.

To estimate the overall range of depth-converted results, we used two constant geotherms of 20 and 40°C/km. Both values are realistic, given the present-day values of geothermal gradients in Morocco (Zarhloule, 2004), and are considered in this case as end-member values. The low and high constant geotherms, applied to the digitized temperature envelopes, expectedly yield the maximum and minimum depths throughout the considered period of time, respectively (cf. dashed lines in figure 6). The resulting rates are shown in figure 7.

3.1.3. Vertical movement rates

Exhumation and burial rates (km/Myr; fig. 7) were calculated from the depth-converted t-T curves (fig. 5). We define seven periods of time for these calculations (periods ***a*** to ***g***), resulting in up to seven vertical movement rates for each curves: Permian (***a***; 299-252Ma), Triassic (***b***; 252-201Ma), Early to Middle Jurassic (***c***; 201-163Ma), Late Jurassic to Early Cretaceous (***d***; 163-125Ma), Cretaceous (***e***; 125-66Ma), Palaeogene (***f***; 66-23Ma), and Neogene (***g***; 23-0Ma). The selection of time periods is based on the observed resolution of the t-T results, on recognition of key events in the regional sedimentary record, and on the timing of exhumation and burial events as recorded by t-T modelling. The calculated rates range from -0.09 (burial) to 0.49 (exhumation) km/Myr.

The first order interpretation gained from this figure is that there were four periods of active and widespread denudation in the studied area: the Permian, Early to Middle Jurassic, Late Jurassic to Early Cretaceous, and Neogene (periods ***a***, ***c***, ***d***, and ***g***, respectively). During the Permian (period ***a***), sampled basement in the Meseta (e.g. Ghorbal et al., 2008) and the Anti-Atlas (e.g. Oukassou et al., 2013) were strongly exhumed (0 to 0.12 km/Myr), while those of the Reguibat Shield (e.g. Leprêtre et al., 2015) were stable (ca. -0.01 km/Myr). During the Triassic (period ***b***), the exhumation in the Meseta and the Anti-Atlas slows down (0.01 to 0.05 km/Myr). The High Atlas and most of the Meseta and Reguibat samples are subsiding (0 to -0.08 km/Myr). In the Early to Middle Jurassic (period ***c***), the Variscan rocks of the Anti-Atlas (Gouiza et al., 2017a) are greatly exhumed (0 to 0.16 km/Myr). For this region, we observe an acceleration of the exhumation from the Triassic to the Jurassic, characterised by the highest rates recorded in this study, with the exception of Neogene exhumation rates. Concomitantly, the regions surrounding the Anti-Atlas were mostly subsiding in the north (0 to -0.09 km/Myr) and mildly exhuming in the south (0 to 0.06 km/Myr). The Late Jurassic to Early Cretaceous period (***d***) is marked by the stability or subsidence of the Anti-Atlas (0 to -0.05 km/Myr), whereas the sampled basement of the Meseta (e.g. Saddiqi et al., 2009), the Reguibat shield (e.g.

Leprêtre, 2015), and the High Atlas to some extent (e.g. Ghorbal, 2009), were exhuming (0 to 0.09 km/Myr). During the Cretaceous (period ***e***), the exhumation in the Meseta, the High Atlas and the Reguibat Shield regions slows down, and all areas are rather stable (weak exhumation and subsidence) with motion rates between ca. 0.03 and -0.03 km/Myr. Exhumation is renewed throughout the Anti-Atlas during the Palaeogene (period ***f***; 0.01 to 0.03 km/Myr), while other areas remain characterised by rates similar to those of the Late Cretaceous. Finally, the Neogene (**g**) period was characterised by a significant acceleration in exhumation; which increases from a typical value below 0.10 km/Myr, to reach 0.20 km/Myr in the High Atlas (e.g. Ghorbal, 2009) and 0.49km/Myr in the Rif belt (Romagny et al., 2014).

3.1.4. Generating exhumation maps

In order to estimate the volume of material that has been removed through time in the examined area, we first build seven 'exhumation maps' (fig. 9), using the calculated exhumation rates as recorded by t-T modelling. This takes into account burial rates and simplified stratigraphy columns for the Permian to Neogene onshore and offshore basins in the study area (fig. 8) to define areas undergoing subsidence.

Data points for of the exhumation maps consist of the exhumation and subsidence rates calculated using the variable paleo-geothermal gradients (fig. 7). For the computation of volume ranges, we use rates obtained by using the previously defined constant geotherms of 20 and 40°C/km temperature range converted to depth.

The dataset, composed of vertical movement rates, is characterised by dense data (basement massifs in Meseta/Anti-Atlas) and sparse data areas (Reguibat Shield). Data clusters are separated by preserved basins for which no LTT/t-T results are available. To add geological meaning to the exhumation maps, by including documented subsiding areas, we added synthetic points on the basis of stratigraphic columns, which are compiled in figure 8. For each preserved sedimentary basin, up to four points were created depending on the extent of the area. If sediments were deposited during one of the selected periods and are still preserved in a basin, we attribute a negative rate to all the synthetic points of this basin. When sediments are not recorded in a basin, because they were not deposited or not preserved, we attribute to synthetic points a rate of 0 km/Myr.

More synthetic points are needed away from the present day coastline, in order to guide the interpolation while retaining geological meaning. To this end, the Continental-Ocean Boundary (COB; Miles et al., 2012) is used as a boundary to yield synthetic exhumation/subsidence rates. Prior to the Jurassic, there was no oceanic crust being generated, and therefore no COB was present.

Nevertheless, for the Permian and Triassic interpolations (periods ***a*** and ***b***), we consider a similar position for the boundary location in order to yield synthetic rates. For the Permian, the COB line is attributed an exhumation rate of 0.1 km/Myr. This is to account for the collapse (peneplain) of the Variscan chain, which is documented in Morocco as occurring somewhere between the Carboniferous and the Triassic (e.g. Michard et al., 2008). Exhumation rates during post-orogenic collapse have been used in other published models and documented between 0.15 and 0.7 km/Myr (e.g. Clift et al., 2004; Mazzoli et al., 2010; Casini et al., 2015). We consider in this study a lower exhumation rate of 0.1 km/Myr, comparable to the highest rate we calculated for the Permian (period ***a***). From the Triassic onwards (periods ***b*** to ***g***), we attributed a subsidence rate to the COB of -0.011 km/Myr. This is equivalent to adding a number of synthetic points with subsiding rates, as above-defined, in the slope or basinal domains. These values are not necessarily realistic, but acceptable as this area is not the focus of study.

For the interpolation of the vertical movement rates, we use the nearest neighbour algorithm (available in Surfer version 8; Golden Software, Inc.). This algorithm is simple to implement, with an interpolation grid that can be extended across the entire study area, and allows for the addition of faults. The interpolation grid extends from 0 to -18°W and 20 to 36°N (112x100 lines with fixed spacing) and ends at the COB in the west. For the Triassic, Palaeogene, and Neogene periods (***b***, ***f***, and ***g***, respectively), the Atlas system faults (whether they were normal or inverse faults) are added as boundaries for the interpolation (after geological map in Frizon de Lamotte et al., 2004).

The “Nearest Neighbor” is a fairly simple approach, but it has some limitations as it gives better results with regularly spaced data points. In addition, the algorithm does not extrapolate the rates above and below input values. The interpolated rates are calculated from the closest data/synthetic points. When located exactly in the middle, between two points, the lowest value will be attributed to the

interpolated rates, which is most-likely responsible for artefacts observed in the exhumation maps (fig. 9). These artefacts are illustrated by narrow zones with important changes of rates over short distances.

The descriptions of the exhumation maps and observed patterns are presented alongside the source-and-sink maps (section 4.).

3.1.5. Eroded material fluxes

Sediment fluxes may be quantified by calculating the volume of deposited sediments in the sink, the erosion rate in the source, or using other techniques that investigate the paleo-drainage system (e.g. Wold and Hay, 1990; Gallagher et al., 1998; Barnes and Heins, 2008; Matenco et al., 2013). Understanding hinterland vertical movements, sediment budgets, pathways, and entry points are crucial for hydrocarbon exploration, to predict reservoir presence and quality and to map potential play fairways (e.g. Schneider and Issler, 2019).

Volume calculations of eroded material per million years (see similar approaches in other areas: Guillocheau et al., 2012; Grimaud et al., 2017; expressed in km^3/Myr), thereafter called "eroded material flux", are performed with the Surfer software between the interpolated surface and a plane characterised by a null motion rate (0 km/Myr). The volumes are also separately calculated, by masking other areas, for three regions of high interest: the Meseta, High Atlas, Anti-Atlas, and the Reguibat Shield (table 2). The eroded material fluxes obtained in this work are an estimation of the volume of removed material, per million years, during documented exhumation events. Because LTT data nor t-T modelling do take into account the lithology and erodibility of the overburden (Flowers and Ehlers, 2018), the obtained fluxes cannot be considered as total terrigeneous sediment fluxes. Therefore, the calculated volume of material removed from the source areas (table 2) will be higher than the volume of terrestrial material deposited in the sink areas. This is especially valid when eroding marine-dominated series, where carbonates will dissolve.

The calculated volumes of eroded material for the seven exhumation maps range from $0.76x10^6$ to $0.07x10^6$ km^3 /Ma for the Jurassic and Triassic, respectively (fig. 9 and table 1). For the regions of specific interest, the eroded material fluxes are between ca. 600 and 11,000 km^3/Ma for the Reguibat

Shield, ca. 700 and 8,000 km^3/Ma for the Anti-Atlas, and ca. 100 and 2,300 km^3/Ma for the Meseta and High Atlas massifs (fig. 9).

3.1.6. Uncertainties and limitations of the used workflow

Together with the uncertainty inherent in the ranges for the rates and volumes, other uncertainties need to be recognised to fully understand the limitations of the presented workflow. Typically, LTT analyses in Morocco have ~10% error for both (U-Th)/He and FT systems (Charton, 2018). The t-T modelling shows a substantial temporal and thermal uncertainty associated to all realisations (e.g. good and acceptable envelopes for HeFTy) and this uncertainty increases with time (fig. **4**).

Furthermore, nearly all t-T modelling studies reviewed in this work (table **1**) consider post-Variscan cooling events as resulting from erosional exhumation events. As reviewed in Malusà and Fitzgerald (2019b), cooling does not systematically mean erosional exhumation, but may be linked to thermal relaxation or tectonic exhumation, depending on the geological context. The studies used for the interpolation of the exhumation rates (table 1) have all explained the observed cooling events as resulting from erosional exhumation. If the interpretation from previous workers is erroneous, then the related t-T path(s) should not have been used to obtained exhumation rates, which would in turn results in different exhumation maps.

Other factors such as the paleo-geothermal gradients and the constant surface temperature have impact on the error range. Indeed, assumptions regarding the thermal structure of the crust are that, for each region, the gradients and surface temperature are invariable. However, it is obvious that surface temperature will vary locally and regionally while, the geotherms may be influenced locally by independent parameters. Moreover, the paleo-geotherms are not adapted dynamically as a function of erosion and deposition, while they can impact the upper crust thermal structure (erosion may lead to an increase of the paleo-geotherm while sedimentation may lead to its decrease; Ehlers, 2005; Gouiza et al., 2017a).

Moreover, using different analogues for geothermal gradients may, or not, have an impact on the workflow. For instance, in the Mediterranean Sea, a paleo-geothermal gradient of >80°C/km was constrained on the base of t-T modelling for the rift zone of the Tethysian rifting (Malusà et al., 2016). In the view of this finding, a value of 34°C/km might be seen as low. However, using such a gradient would not affect greatly the obtained exhumation/burial rates, as considered t-T realisations for the rifting period in the High Atlas show a flat path fairly close to surface temperature (fig. 4C). On the other hand, using higher/lower gradients in the Rift flanks during the Triassic for example, may result in significantly lower/higher exhumation rates.

Another source of uncertainty lies in the use of non-restored base maps for the exhumation maps, as some areas may have changed in shape and/or surface (the High Atlas before the Cenozoic orogeny for instance). Further, the use of null vertical movement rates for synthetic points introduces an error, as non-recorded sediments might have been eroded (i.e. burial rates should have been used during the assumed time of deposition) or never deposited (i.e. null or exhumation rates). Other potential errors associated with the interpolation method and volume calculations are more difficult to quantify. Overall, we estimate the error for the rates and calculated eroded material fluxes to ~20% for the Permian (periods ***a***), ~15% for the Mesozoic (periods ***b*** to ***e***) and to ~10% for the Cenozoic (periods ***f*** and ***g***).

3.2. From exhumation maps to source-and-sink maps

3.2.1. Source-and-sink maps: principle and inputs

Source-to-sink studies encompass the investigation of the exhumation history of the hinterland ('source'), the spatial distribution of fluvial and coastal deposits ('to'), and the architecture of continental traps, shallow and deep marine depocenters ('sink'; e.g. Allen, 2008; Sømme et al., 2009; Helland-Hansen et al., 2016). The availability of robust sedimentary, stratigraphic, geochronology, provenance, palaeontology, LTT, and numerical analyses allows integration to improve source-to-sink models (e.g. Helland-Hansen et al., 2016). Source-to-sink studies have limitations, depending on, for instance, the spatial and temporal resolutions of each component, or simply on the existence and quality of the sedimentary record. Because the nature of data used in this contribution (LTT/t-T) do not constrain nor depend on the transport of sediments ('to'), the presented maps are not labelled as 'Source-to-Sink' but instead as Source-and-Sink (SandS) maps.

A recent effort at generating paleogeography maps by combining AFT data with more classical datasets has been carried out in NW Africa (Ye et al., 2017), at the sub-continental scale. The work resulted in several paleo-reconstructions around the equatorial Atlantic African margin, and that since the early Mesozoic. This work allowed the inclusion of exhuming areas, as based on LTT and t-T results, onto what can also be described as qualitative SandS maps. Overall, Ye et al. (2017) and our contribution are very similar in terms of deliverables, and therefore ours maps are, by design, greatly inspired from the former.

Initially, we digitized the geological map of Morocco at 1:1,000,000 (Hollard et al., 1985). For neighbouring regions not covered by the Moroccan map, we digitized the map of NW Africa compiled by the UNESCO in 1990 (fig **2B**). It provided widespread control points for our maps, with the exception of the Permian, for which there are few penetrations in the basins and even less exposed

at outcrop. The outcrop and fossil data in Morocco is extensive, as suggested by the title of the recent special edition on Morocco from the journal "Geologues" (Number 194, septembre 2017): "Le Maroc, paradis des geologues", providing a wealth of outcrop and fossil data (table B).

Several "modifications" of the stratigraphy were added to this composite map (fig. 2B), based on new fieldwork or new published data, especially around the Anti-Atlas (see details in Gouiza et al., 2017; Charton et al., 2018; Arantegui et al., 2019) and in the Central High-Atlas. In the latter, the so-called "Couches Rouges" terrestrial redbeds are found associated with Middle Jurassic and middle Cretaceous (Aptian) marine carbonates (Charrière and Haddoumi, 2016) have historically been attributed a Middle and Late Jurassic age (Hollard et al., 1985). Recent biostratigraphy work constrained the ages of the redbeds more precisely to the Middle and Late Jurassic, but also to the Barremian (Early Cretaceous; reviewed in Charrière and Haddoumi, 2016).

The well database (fig. 11) is composed of DSDP and IODP well reports, confidential oil exploration well reports and completion logs accessed from the "Office National des Hydrocarbures et des Mines" (ONHYM). Detailed well data from published works (notably Michard et al., 2008), and limited well data such as total depth, reached formation, or stratigraphy in published studies or company reports was also used.

Several types of paleo-reconstructions are used as the basis for depositional environments (sub-continental scale, e.g. Ye et al., 2017; to local scale, e.g. Luber, 2018) and tectonic regime (e.g. Brahim et al., 2002). Depositional environment reconstructions at the scale of North Africa of Guiraud et al. (2005) for the Phanerozoic were used to broadly constrain all SandS maps. A recent work, conducted at a similar scale, offers a view of Cretaceous paleo-environments based on regional Cretaceous stratigraphy columns (An et al., 2017). This work was, however, not used as most depositional environment outlines were incompatible with our compilation of paleo-reconstruction from

Morocco. Similarily, paleogeography maps of Scotese (Paleomap project, 2013) are shown in the inserts below each SandS maps, but were not used in their construction. In many instances, we modified the shown outlines according to new evidence (t-T, outcrop, fossil, and/or well data). Sedimentary provenance analysis conducted in Morocco and surroundings for the Permian to Neogene periods are scarce; four recent works investigated the provenance with detrital zircon U-Pb (Pratt et al., 2015; Marzoli et al., 2017; Domènech et al., 2018; Azdimousa et al., 2019), one study used traced elements and radiogenic Nd-Sr isotopes (Ali et al., 2014), one using neodymium isotopes and major/trace elements from DSDP wells (Mourlot et al., 2018), and one produced detrital LTT ages (Sehrt, 2014). Several studies have also documented paleo-current directions in fluvial systems (e.g. Brown, 1980; Baudon et al., 2009, Fabuel-Perez et al 2009, Mader et al., 2017). Finally, we use the previously presented exhumation maps to constrain the source domains, while modifying their extent based on the control points described above.

3.2.2. Building the source-and-sink maps

Large scale reconstructions of the Moroccan geological history have been carried out in several studies in the past decades (e.g. Ranke et al., 1982; Le Roy et al., 1997; Nemčok et al., 2005; Sibuet et al., 2012; Ye et al., 2017) and this data has been collated and integrated into our study. The majority of the maps used in this review focused on depositional environments, palaeogeography, tectonic plate reconstruction, and more local structural/stress maps, based on extensive data collections.

Using the knowledge gathered hitherto in the previous part of this study, we construct ten Source-and-Sink (SandS) maps, which illustrate the timing, extent, and rate of exhumation episodes documented with LTT and t-T modelling results. Using geological maps, several other databases (well, outcrop, fossil, and provenance data), and previous paleogeography work, we also reconstructed the gross depositional environments. The SandS maps presented illustrate the source, transitional, and sink domains from the Permian to Neogene, within a simplified structural framework.

The presented maps are defined according to the geological time chart division (with a strong focus on the Cretaceous and Jurassic periods). The time-windows covered by the maps are as follow: Permian (300 to 252 Ma; fig. 12), Triassic (252 to 201 Ma; fig. 13), Early Jurassic (201 to 174 Ma; fig. 14), Middle Jurassic (174 to 163 Ma; fig. 15), Late Jurassic (163 to 145 Ma; fig. 16), (early) Early Cretaceous (145 to 125 Ma; fig. 17), middle Cretaceous (125 to 90 Ma; fig. 18), (mid-late) Late Cretaceous (90 to 66 Ma; fig. 19), Palaeogene (66 to 23 Ma; fig. 20), and Neogene (23 to 0 Ma; fig. 21).

Four types of depositional environments are described in this study: terrestrial, transitional, shallow marine, and marine. For most of the map control points, the depositional environments were already interpreted in the associated study (table 3). In other instances, we interpreted the depositional environment based on lithology and/or fossil data. The transitional environments presently suggest

a coastal situation, but may account for areas characterised by fluctuation(s) between shallow marine and terrestrial environments. Source areas with low exhumation rates (between 0 and 0.01km/Myr) may momentarily act as sedimentary by-pass zones, and therefore not necessarily eroding zones, as exemplified with the Neogene map (fig. 21). Inversely, terrestrial domains may also have contain local sedimentary sources, which is highlighted in the SandS maps by with hatched (and dashed) lines.

Overall, the construction of the map was done graphically by superimposing all the above-mentioned input layers. Source areas and faults were placed first, then data pertaining to the sink domains. Each feature (outcrop, well, fossil…) was then manually associated with a small coloured halo corresponding to the dominant depositional environment. The extent of the source area were modified at this stage, and finally the maps are completed by connecting depositional environments together. The descriptions of the SandS maps and observed patterns are presented in Section 4.

3.2.3. Limitations of the source-and-sink maps

Data quality, data density and temporal resolution are highly variable across the area covered by the SandS maps. This leads to variable robustness of the presented maps, which complicates the comparisons from one to another. Dating is the primary uncertainty, as several Phanerozoic layers in Morocco and the surrounding area have undifferentiated ages (e.g. Hollard et al., 1985). This is for instance the case for Permo-Triassic, Middle to Late Jurassic, and Early to Middle Cretaceous redbeds ("Continentale Intercalaire"), all three of which are widely mapped across the study area, but their ages are weakly constrained. These intervals may be intercalated by biostratigraphically marine sequences or radiometrically dated magmatic intrusions, but these biostratigraphic or geochronological studies are generally local and extrapolation still has to be made to similar but non-constrained facies.

The proposed Permian map is characterised by the less certain dominant depositional environments, as it is constrained with limited data. While the Neogene is a data-rich time interval and the corresponding map is of higher resolution. Another limiting aspect is introduced by the definition of the time-windows that each map covers. The temporal resolution of the Permian and Triassic maps is coarse, as they encompass ca. 50 Myr, compared to the short Middle Jurassic interval (ca. 11 Myr). It is also important to note that the Triassic map is mostly composed of Late Triassic data, as Early and Middle Triassic sediments are rarely documented in the stratigraphy of Morocco. Although much of the Triassic sediments are mapped as undifferentiated, where dated they are mainly Late Triassic and the best dating occurs at the end of the sequence, where CAMP dykes and sills are radiometrically dated. However, exhumation rates were calculated for the entire Triassic, which will result in a reduction in overall rate and will have introduced a bias on the map.

Ye et al. (2017) used the slope of the contact between the sediment and its basement as a proxy to reconstruct the original extent of the basin (after Sloss and Scherer, 1975), which in turns provide the areal extent of the exhuming/emerged zones. We do not apply something similar in our contribution, as we lack the data on the slope values. These angles are often small and hard to measure in the field. Therefore, little published data exist on this subject. Moreover, it is sometimes unknown in remote places of Morocco if the sediments are truncated, onlapping, or simply completely missing. Therefore we make the hypothesis that the interpolation results (using data from both the source and the sink) are a fair approximation of the extent of the source areas.

Moreover, our SandS maps use the present-day unrestored geography and geology as base maps. In many areas this is acceptable, however this should be taken into account when using them and discussing implications for areas such as the Atlas and Rif belts, for which Cenozoic upheaval was mostly caused by N-S shortening (e.g. Michard et al., 2008).

4. Source-and-Sink (SandS) maps

4.1. Pre-rift: Permian and Triassic maps

During the Permian (fig. 12), erosion occurred in the remnants of the Variscan chain (e.g. Lorenz, 1988; Hmich et al., 2006), located mostly in the Meseta and Western Anti-Atlas. Known Permian basins are the Eastern Meseta, Doukkala and Argana Valley basins. From the interpolated area, we estimate the volume of produced sediments to be about $1.0x10^6$ km^3, of which little is preserved today. Our working hypothesis is that Permian sediments were re-worked during the Triassic and/or that the erosion of the Variscan chain yielded little coarse terrestrial material. Subsiding domains predicted by the t-T modelling results are the Central and Eastern Reguibat Shield (Leprêtre et al., 2015).

From the Permian to the Early Triassic (periods ***a*** to ***b***; figs. 12 and 13), the source area shifted from most of the domain affected by the Variscan orogeny to only part of it: The Meseta, the Anti-Atlas, and the eastern Reguibat Shield. The appearance of transitional depositional environments is another important change, resulting from marine incursions from the Tethysian realm as far as the Tarfaya basin (e.g. Ranke et al., 1982; Scotese, 2012; Leleu et al., 2016). The erosion that occurred in the Anti-Atlas during the Triassic is supported by sedimentary provenance analyses and paleo-currents conducted in the Massif Ancien (Brown, 1980; Baudon et al., 2009; Domènech et al., 2018), evidencing a drainage divide perpendicular to the Anti-Atlas trends.

4.2. Syn-rift: Triassic and Early Jurassic maps

During the Triassic (period ***b***; fig. **13**), the northern Meseta (estimated volume of eroded material: ca. 6,000 km^3), the Anti-Atlas (ca. 35,000 km^3), and the Reguibat Shield (ca. 30,000 km^3) were being eroded. A large portion of the Meseta shows considerable burial (e.g. Ghorbal et al., 2008), which is comparable to Triassic burial documented in the Central Atlantic and High Atlas rift zones (e.g. Gouiza et al., 2010; Moragas et al., 2016, respectively). The Central Atlantic and Atlas rift zones were subsiding, except perhaps for a part of the Massif Ancien which acted as a major drainage divide as suggested in Domenech et al., 2018 (fig. **13**). This massif is indeed described as forming positive structural relief sourcing Triassic sediments to the Argana and Oukaimeden valley (e.g. Baudon et al., 2012). The t-T modelling results do not cover the time before 200 Ma in the Central and Eastern Anti-Atlas (Gouiza et al., 2017), but red clastics overlying Precambrian basement in the northern Central Anti-Atlas are mapped as Triassic. No recent study on these sediments has been conducted, however, basaltic flows covering them have yielded ages of 205.9±7.9 and 207.8±6.5 Ma (Fiechtner et al., 1992), suggesting that these deposits are Triassic (or older). This implies that, while the core of the Anti-Atlas continued to exhume (c. 0.04 km/Myr), its northern margin was stable or subsiding (including the Souss and Ouarzazate basins).

From the Late Triassic to Early Jurassic epochs (periods ***b*** to ***c***; figs. **13** and **14**), marine domains progressively covered the Atlas and Central Atlantic rift. The only significant change in source areas is an exhumation event occurring in the western Reguibat Shield (up to 0.06 km/Myr) and starting in the Early Jurassic (Leprêtre et al., 2015; fig. **14**). A recent provenance study by Marzoli et al. (2017), using detrital zircon U-Pb ages, shows that sediments interfingering with the CAMP basalts in the western High Atlas have been sourced from the Meseta domain.

4.3. Early Post-rift: Early Jurassic to early Early Cretaceous maps

The Early and Middle Jurassic epochs (period *c*; figs. 14 and 15) are marked by enhanced erosion in the Anti-Atlas and Reguibat Shield, and to some extent in the Meseta (see volumes of eroded material in table 3). From all the periods defined in this study, period *c* is the most active in terms of eroded material flux for the Anti-Atlas. It is likely that the Anti-Atlas formed a topographic swell as obtained exhumation rates are higher in the central part of the belt (up to 0.16 km/Myr; e.g. Gouiza et al., 2017; fig. 14). Middle Jurassic redbeds are recorded in the onshore basins north and west of the Anti-Atlas (Tarfaya, Agadir-Essaouira, Central High Atlas, Ifni Margin, and Souss basins; see table 3 and references therein). In the basins south and east of the Anti-Atlas, no Jurassic sediments are recognised (e.g. Hollard et al., 1986; Michard et al., 2008). This supports the idea of an exhuming Anti-Atlas and Reguibat Shield, linked by an exhuming or stable Tindouf area.

The siliciclastic fraction within the overall carbonate sedimentation is abundant in the Central High Atlas during the Early Jurassic and in the Essaouira-Agadir Basin during most of the Early and Middle Jurassic (Duval-Arnould, 2019). Coarse grained clastic sediments are deposited in the Central and Western High Atlas during the Toarcian, and the rest of the Early Jurassic is dominated by carbonate sedimentation with up to 40 % of fine grained siliciclastics (10-20% average). Middle Jurassic rocks are composed of clay to coarse clastics (alluvial plain) and mixed carbonate-siliciclastics in the Western and Central High Atlas, respectively (Malaval, 2016; Joussiaume, 2016). These observations point towards the presence of an active source of clastic sediments in the vicinity of these basins for the Early to Middle Jurassic, matching the results of t-T studies conducted in the Anti-Atlas (e.g. Ruiz et al., 2011; Oukassou et al., 2013; Gouiza et al., 2017).

The Early and Middle Jurassic epochs (period *c*; figs. 14 and 15) are fairly similar in terms of depositional environments. Moreover, the exhumation patterns are identical on both maps as they

originate from the same exhumation map, presented as figure 9C. Provenance studies carried out on Middle Jurassic sediments show evidences of sedimentary transport from the Meseta to the Middle Atlas (based on detrital zircon geochronology; Pratt et al., 2015), and from the Anti-Atlas to the Essaouira-Agadir basin (based on paleocurrents; Stets, 1992). Triassic salt mobilisation occurred in the High Atlas and Essaouira-Agadir salt basins from the Early until the Middle Jurassic (e.g. Moragas et al., 2018), assumably where the sedimentary columns were the thicker (shallow marine environment; figs. 14 and 15). Salt mobilisation in the High Atlas basin stopped prior to the Late Jurassic, but continue in the coastal basin until the Late Cretaceous (Moragas et al., 2018). Depositional environments in the Essaouira-Agadir basin change from fluvial to lagoonal during the Early Jurassic, from continental/transitional to shallow marine (dolomites) in the Middle Jurassic, and then remain shallow marine / shelfal during the Late Jurassic (Duval-Arnould, 2019). In the Sidi Ifni area, Arantegui (2018) documented a Bathonian (Middle Jurassic) age for shallow marine and lacustrine deposits exposed along the coast (Charton et al., 2018; Arantegui et al., 2019).

Although most vertical movement rates are negative in the Anti-Atlas (i.e. burial rates), one of them is positive in the western part of the belt (fig. 7D). This could be due to a t-T modelling inconsistency or it could be a remnant, non-structural, relief from the previous period. A sedimentary provenance study conducted in the north Tarfaya Basin (Ali et al., 2014) for Lower Cretaceous sediments showed they were sourced from the Reguibat Shield only. It suggests that the one positive vertical movement rate calculated for the western Anti-Atlas for period ***d*** should be discarded, and that the t-T modelling results for that specific sample are inconsistent. We therefore considered no active source area in the western Anti-Atlas during the Late Jurassic in the corresponding SandS map (fig. 16).

From the Middle to Late Jurassic, our results show a shift in the areas of sediment production, from the Anti-Atlas to the Meseta. The Late Jurassic (period ***d***; fig. 16) shows a major shift in the sediment

source areas: the Anti-Atlas is no longer an active source while the Meseta becomes strongly exhumed (up to 0.07 km/Myr; e.g. Ghorbal et al., 2008). A high-resolution clay mineralogy study, carried out in folded Jurassic sediments of the Essaouira-Agadir Basin (Ouajhain et al., 2011), shows a clear shift in either the sediment source lithology or area, between the Middle and Late Jurassic, passing from a chlorite- to an illite-dominated assemblage. It is possible that Middle Jurassic erosion of the Anti-Atlas reached down to the Precambrian, hence cutting through the metamorphosed Palaeozoic series and eventually sourcing chlorite minerals to surrounding basins. The Meseta is also a documented source area during the Late Jurassic, as suggested by paleo-currents measured in the western High Atlas (Stets, 1992). The Upper Jurassic was not deposited in the Central High Atlas, but fluvial deposits of Callovian age are recorded, while in the Western High Atlas, the Malm is dominated by carbonate sedimentation interbedded with fine siliciclastics in the Kimmeridgian (Duval-Arnould, 2019).

The transition between the Jurassic and Cretaceous (period *d*; fig. 16 and 17) was, according to our current dataset at least, fairly quiescent. The coastline shifted towards the north in the Middle Atlas/Rif areas, and towards the west in the Tarfaya basin. The latter change was accompanied by the onset of large Early Cretaceous deltaic systems (Tan-Tan and Boujdour deltas; fig. 17). The entire Reguibat Shield was an active source of sediments since the Early Jurassic and remains one during the Early Cretaceous. This suggests that an acceleration of the exhumation or a change in source lithology in the Reguibat Shield must have occurred in the earliest Cretaceous, supplying the siliciclastics to the Tan-Tan and Boujdour deltas. It is likely that the erosion in the Reguibat Shield reached the granitic basement at the end of the Jurassic, with removal of the meta-pelites from the overlying Early Palaeozoic basin.

Exhumation of the Meseta massifs (rates of up to 0.1 km/Myr; ca. 750 km^3/Ma) from Late Jurassic to Early Cretaceous (period ***d***) was first described in Ghorbal et al. (2008). The preserved onshore basins of the Meseta do not record Upper Jurassic sediments, excepted in the coastal Doukkala basin (fig. 17). This suggests that a surface larger than that of the presently outcropping basement was being eroded.

In the Late Jurassic and Early Cretaceous, it is unknown if the Tindouf basin was sourcing sediments to the Tarfaya Basin deltas, a transitional sink, or simply stable, as no LTT cooling ages have been measured. Nevertheless, values of vitrinite reflectance from the Silurian (Kuuskraa *et al,* 2013), in the northern Tindouf basin, suggest that these sediments were previously buried deeper and significantly thick overburden is missing, which was deposited and subsequently eroded between the Carboniferous and the Late Cretaceous. As most of the Anti-Atlas and the central Reguibat Shield were subsiding during the Late Jurassic/Early Cretaceous (figs. 17 and 18), we assume that 1) the missing overburden was deposited during this period in the northern Tindouf Basin, and 2) in the absence of evidence, the basin was fairly stable elsewhere.

A sedimentary provenance study was conducted in the north Tarfaya Basin for Lower Cretaceous to Cenozoic sediments (Ali et al., 2014). Their results showed that the Lower Cretaceous sediments were sourced from the Reguibat Shield, while upper Cretaceous sediments were sourced from both the Reguibat Shield and the Anti-Atlas (fig. 18). During period ***d***, the Reguibat Shield witnessed substantial erosion (ca. 8,200 km^3/Myr). It appears that the source area of the sediments deposited in the Boujdour and Tan-Tan Lower Cretaceous deltas is the Reguibat Shield (and potentially part of the south Tindouf basin), with over 700,000 km^3 of eroded material.

4.4. Late Post-rift and syn-Atlas kinematics: middle Cretaceous to Neogene maps

The Cretaceous (periods ***d*** and ***e***; figs. 17, 18, and 19) is characterised by another shift in source areas. The Anti-Atlas presently outcropping basement, which was subsiding during the Early Cretaceous, is exhumed again from the middle Cretaceous onwards (up to 0.04 km/Myr; Gouiza et al., 2017; fig. 18). Meanwhile, the southern massifs of the Meseta underwent burial during the middle Cretaceous after a prolonged exhumation episode (e.g. Ghorbal et al., 2008).

In Morocco, widespread coarse sediments are described from the Early Cretaceous (e.g. Davison, 2005; Frizon de Lamotte et al., 2009, Luber, 2017). In the north Tarfaya basin, Arantegui (2018) has shown that the undifferentiated Lower Cretaceous clastic succession is characterised by fluvial and tidal flat environments, with alluvial fan conglomerates at the base in contact with Cambrian metamorphosed sediments. The study further provides an updated biostratigraphy of Aptian-Albian (middle Cretaceous) transitional to shallow marine deposits exposed along coastal outcrops. The mean paleo-current direction for the fluvial units indicates a local transport direction towards the northwest.

The transition from shallow marine to continental deposition environments occurred between the early and the middle Cretaceous in the Essaouira-Agadir basin. The continental environment records a general paleocurrent direction towards the west and a significant regression, probably tectonically controlled, during the Latest Barremian to Early Aptian (Luber, 2017). In the Late Aptian and Albian times, the area was drowned once again with the establishment of shallow marine conditions.

Sedimentary provenance analyses suggest that only the Reguibat Shield (including the Mauritanides) were sourcing clastic sediments to the north Tarfaya basin during the Early Cretaceous, while the Anti-Atlas was part of the siliciclastic supply to the coastal basin from Late Cretaceous onwards (Ali et al., 2014). Pratt et al. (2015) collected Albian sediments deposited in the Rif basin, and traced the

provenance to two sources: the Meseta and a presently unknown source area. Finally, Mourlot et al. (2018) undertook a large scale provenance study targeting Albian to Maastrichtian sediments from DSDP wells (from north to south offshore Morocco sites 370, 416, 415, and 369 were sampled) along the NW African coast. They used the major and trace element concentrations from these marine sediments, as well as neodymium isotopes, to constrain continental crust signatures. Their results show that the DSDP wells north of Agadir have preserved a signature from the Meseta, the Anti-Atlas, and the Reguibat Shield during the middle Cretaceous. DSDP Well 369, in the offshore Tarfaya basin, has a continuous record of sediments with a Reguibat Shield signature throughout the Albian and Late Cretaceous (Mourlot et al., 2018). Finally, Azdimousa et al. (2019) analysed detrital zircon for U-Pb ages and documented similar potential source areas for Aptian-Albian, Palaeogene (Eocene), and Neogene (early Miocene) sediments deposited in the north-western Rif. These potential source areas, namely the Meseta, the Triassic sediments from the High Atlas, or the northern West African Craton (Azdimousa et al., 2019), would require a local, regional, or sub-continental drainage systems, respectively. In our maps, we have displayed only the most local required system, i.e. between the exhuming Meseta massifs and the northern tip of the Rif (figs. 18, 20, and 21).

A Cenomanian-Turonian carbonate platform with low detrital influx prevailed in the Central High Atlas, while in the Atlantic domain, Turonian organic-matter rich black shales were deposited in fault bounded restricted basins where relatively deeper marine environment prevailed (Wang, 2018). Cenomanian-Turonian outcrops are characterised by a widespread occurrence around the Anti-Atlas (fig. 18) with similar facies (Eastern Anti-Atlas; Guimera et al., 2011) and onlapping on the Palaeozoic basement (western Anti-Atlas; Abioui et al., 2019). Sauropods and crocodilian ichnofacies from the Guir Hamada (Benyoucef et al., 2015) showed that an emerged land was neaby these sediments,

which, according to our compilation of t-T curves, was the Anti-Atlas (Gouiza et al., 2017; Charton, 2018; Abioui et al., 2019).

During the middle Cretaceous, the central Anti-Atlas became an active source area and the Meseta exhumation slowed down significantly (from up to 0.06 down to 0.02 km/Myr). By the end of the Cretaceous, the entire Anti-Atlas s.s. was sourcing sediments to surrounding basins, and most of the Meseta and High Atlas domains were subsiding and progressively drowned.

In the late Early to Late Cretaceous period (period ***e***; fig. 19), subsiding domains are dominant in the study area. This period is characterised by a rise in global sea level (Cenomanian-Turonian transgression; e.g. Piqué et al., 2006), which transgressed into the interior of Morocco and Algeria (e.g. Upper Cretaceous deposits in the Guir Hamada; e.g. Benyoucef et al., 2015). It appears to have partially submerged the Reguibat shield, the Tindouf basin (except its central part), and the borders of the Anti-Atlas. Anti-Atlas erosion (ca. 900 km^3/Ma) is dominated in the centre, and later extends to the eastern and western regions.

Finally, the Palaeogene and the Neogene periods (periods ***f*** and ***g***; fig. 20 and 21) are characterised by the Atlas orogeny, which is expressed by high exhumation rates in the High Atlas and Rif (up to 0.20 and 0.49 km/Myr, respectively) and to a lesser extent in the Anti-Atlas and Reguibat Shield Rif (up to 0.05 and 0.10 km/Myr, respectively). We estimate the volume of eroded material from the studied area during the Palaeogene and Neogene to ca. $0.5x10^6$ and $0.7x10^6$ km^3, respectively.

During the Palaeogene (fig. 20), a large portion of the study area was emerged. Epicontinental basins developed around the exhuming massifs of the Meseta and the High Atlas, and shallow marine setting persisted in the Tarfaya basin. Paleontological evidence comes from remains of fish, lizards and mammals (e.g. whales and turtles; see palaeontology references in table 3).

The Neogene period (fig. 21) shows only minor differences with the present-day situation, with nearly all of Morocco emergent. Important sediment source areas are the Meseta, the High Atlas, the Anti-Atlas, and the Reguibat Shield. Some shallow marine sinks were developed in the North Tarfaya, southern Settat and Gharb basins, and along the Mediterranean coast in the Rif domain.

5. Discussion

5.1. Implications for Moroccan source-to-sink systems

Our results show that sedimentary source areas in Morocco throughout since the Permian have varied in size and were not always active simultaneously (fig. 22). The present-day extent of the Precambrian and Variscan basement match fairly well the stacked of exhuming areas. Few exceptions exist however, and they can be explain either geologically or by a shortcoming in the way exhumation maps (fig. 9) are designed. If basement rocks are exposed and no exhuming area polygon covers it (fig. 22), then either 1) there are no known t-T models published from these rocks or 2) the exhumation occurred prior to the Permian (without subsequent burial). In the opposite case, if an polygon covers an area where no basement is exposed, then either 1) the denudation was not strong enough to reach down to the basement , 2) Cenozoic sediments are now covering basement subcrops, or 3) the algorithm interpolated too far away from t-T result locations.

However, regardless of timing and eventual shortcomings, we conclude that the Anti-Atlas, High Atlas, and massifs of the Meseta have all been important contributors to the surroundings sedimentary basins through the investigated periods. Furthermore, the Reguibat Shield is a vast and long-lived source areas (fig. 9), and may therefore be the most important supplier of clastics material to Meso-Cenozoic basins in Morocco and its surroundings; either directly as exemplified for the Tarfaya Basin (Ali et al., 2014) or further away through several sediment recycling cycles. As suggested by figure 8, increasing occurrences of terrigeneous intervals are recognised southwards, which is in good agreement with the presence of the Reguibat Shield as major source area. Moreover, the study of Ye et al. (2017) depicts via its paleo-reconstructions the importance of the Reguibat Shield as a sedimentary source. Important fluvial systems must have existed between the massif and the Taoudeni Basin (southernmost basin on figure 2) and the Mauritania-Senegal Basin (so called ‘MSGBC

Basin'). These connections have likely existed during the Triassic, the Berriasian (Early Cretaceous), Cenozoic, and to a lesser extent during the Aptian-Albian and Late Cretaceous (Ye et al., 2017).

In the recent provenance study from Azdimousa et al. (2019), an Aptian-Albian tentative paleo-reconstruction depicts a drainage system carrying material from the central West African Craton (i.e. Reguibat Shield and surroundings) towards the Rif. They further conclude that this is one of three potential source areas for the analysed sediments in the Rif. Assuming that the most regional drainage system proposed in this work is a correct model, it would require fluvial system of 1500-2000 km long. In the view of our findings, this system would have to span over or around a stable Tindouf Basin, exhuming central Anti-Atlas and northern Meseta massifs, and a marine sedimentary basin. Therefore, we submit that sediment recycling allows for the following scenario: during the early Early Cretaceous (fig. 17), material from the Reguibat Shield is transported and deposited over the at-the-time buried Anti-Atlas, to be later reworked in the middle Cretaceous (fig. 18) and transported northwards.

Important basins that have accumulated a near complete succession of deposits since the Permo-Triassic are the coastal Essaouira-Agadir and Tarfaya basins as well as the passive margin in the offshore domain (Tari and Jabour, 2013; fig. 8). Evidence such as these point towards fairly stable subsiding regions, meaning that the upheaval leading to the erosional exhumation was indeed bounded to the documented source areas. The drainage systems linking the investigated massifs and these two basins may have therefore been somewhat perennial.

Past drainage systems are not bound by the extent of this study, and much larger sedimentary pathways (i.e. Source and sink domains of a larger system) may have existed in Morocco, with a distant source. Depending on the overall slope from the plate interior towards Morocco, sedimentary material may have been transported from the Leo Shield in the South to the Reguibat Shield, and

then towards the Tarfaya Basin. Similarly, material may have been carried from the Hoggar region to the Atlantic coastal basins, by-passing the Anti-Atlas, Tindouf Basin, and/or Reguibat Shield. Potential source(s) of sediments adjacent or distant to the study area should therefore also be considered when investigating source-to-sink systems.

5.2. Comparing eroded material flux to terrestrial sedimentation rates

The total estimated eroded volume rates (table 2) can be compared to published sedimentation rates Helm (2009; fig. 23). The study by Helm calculated sedimentation rates for several segments along the offshore West African margin, including the Moroccan segment. The sedimentation rates in the offshore domain and the coastal basins were obtained from nine interpreted seismic profiles perpendicular to the coast, and extended by extrapolation and/or well control to the basin (using DSDP wells). Terrestrial sedimentation rates from the Triassic to the Neogene were then estimated and adjusted to the portion of terrigeneous sediments recorded in the used control wells. It is important to note that the age resolution is not identical across Helm (2009) and this study; in other words, the start and end dates of calculated intervals are not systematically concordant.

An assumption is that, in an ideal situation, results from the eroded material flux modelling should approximate the terrestrial sedimentation (i.e. disregarding routing of sediment in onshore basins, climate, lithology of the source area or suspension load, and the terrestrial component exiting the system to further offshore). This comparison shows that the siliciclastic volumes deposited in the offshore/coastal basins and the eroded volume of material from the interpolation grid are, for the most part, of the same order of magnitude (fig. 23). Furthermore, rates are very similar during the Triassic, early Early Cretaceous, Late Cretaceous, Palaeogene, and Neogene. Overall the correlation is good, except for the rates obtained during the Jurassic period. According to our results, between 10,000 to 30,000 km^3/Myr of material were eroded, while the offshore seems to record much lower volumes, about 1000 to 2000 km^3/Myr of siliciclastic sediments. This discrepancy could be explained by considering the eroded lithologies at this time. A hypothesis is that erosion in the Reguibat Shield, Anti-Atlas, Tindouf, and Meseta may have removed fine-grained and/or carbonated meta-sediments from the upper part of the Palaeozoic section. Hence, little coarse terrestrial material would be

recorded in the Atlantic basins, were platform limestones are dominant. Additionally, fluvial system pathways could have re-routed sediments to the east.

5.3. Prerequisites, advantages, and possible improvements to the proposed workflow

The workflow presented here broadly constrains source-to-sink systems and domains through time, using t-T modelling as the basis for SandS maps construction. The prerequisites to apply this workflow elsewhere are limited to the availability of dense t-T datasets and prior geological knowledge. Any candidate study area should be characterised by the presence of exposed crystalline basement that has been subjected to LTT/t-T investigation. This workflow requires independent and prior, but not extensive, knowledge about sedimentary basins, palaeo-thermal regimes (see Malusà and Fitzgerald, 2019) and paleogeography. In order to construct detailed SandS maps, published geological data must be obtained, corroborated and interpreted in terms of depositional environments (including borehole data when available). Additionally, in areas where horizontal movements were substantial, exhumation maps should be generated from restored basemaps.

The workflow may be used to test several exhumation scenarios (i.e. exhumation rates, timing, and location) against the stratigraphic record, and may be further validated with sedimentary provenance analyses. Volumes can be calculated without prior information on actual sediment fluxes or budgets, but may be compared with existing results (as exemplified in section 5.2 of this work; Helm, 2009). Provenance studies are also not a requirement to build exhumation maps, but they may facilitate the construction of the SandS maps. As with all studies, the quality and quantity of available data will improve the results, but this methodology allows exhumation rates and eroded material fluxes to be estimated without the need for new fieldwork campaigns, using confidential well data, or analyses of samples, making it a powerful first-order tool for evaluating underexplored and fairly remote areas.

These results can be updated and improved as more t-T data points are made available, away from clusters in well-studied basement areas and by gathering subsidence curves from preserved basins or extracting burial rates for their interpolation with exhumation rates. It may subsequently be

extended to include landscape evolution modelling, using the vertical movement rates as input, which will help in defining the most-likely sediment entry points into the sinks, as well as providing a first-order estimate of the paleo-altimetry (e.g. Salles et al., 2017).

Finally, this workflow could be greatly improved if associated with a systematic investigation of the contact between t-T modelled basement areas and their sedimentary cover (e.g. Ye et al., 2017). Indeed, identifying the truncation surfaces where sediments extend onto basement areas, and interpolating these surfaces for the time of deposition, can offer valuable insights, while mapping onlapping features can be used to identify if basement areas were palaeo-highs (topographic or bathymetric).

6. Conclusions

t-T modelling results have been used as a proxy to define and quantify exhumation events from the Permian to the present-day in eastern Morocco and its surroundings. A series of exhumation maps is presented from which erosion patterns and eroded material fluxes have been extracted. This allows analysis of the possible mechanism(s) responsible for these vertical movements. The presented findings have implications for the evolution of the Central Atlantic passive margins and for our understanding of the Permian to Neogene Moroccan source-to-sink systems.

The reconstructed evolution of vertical movements and erosion at the scale of the passive margin can be divided into 3 areas: The Reguibat Shield, the Anti-Atlas, and the High Atlas/Meseta. The Reguibat Shield is marked by burial from the Permian to the Triassic, followed by exhumation from the Jurassic onwards (0.01-0.06 km/Myr; ca. 1,400,000 km^3). We infer that the Reguibat shield was the only source of sediments for the Boujdour and the Tan-Tan Cretaceous deltas, offshore Tarfaya basin.

The sampled Anti-Atlas basement rocks were deeply buried in the Permian and were exhumed between the Triassic and the Middle Jurassic (0.01-0.16 km/Myr; ca. 300,000 km^3). Burial during the Late Jurassic/Early Cretaceous was followed by a final exhumation from the Late Cretaceous onwards (0.01-0.05 km/Myr; ca. 180,000 km^3).

Presently outcropping Variscan rocks in the High Atlas and Meseta were close to the surface during the Permian/Late Triassic, followed by burial until the Middle Jurassic, exhumation in the Late Jurassic/Early Cretaceous (exhumation rates: 0.01-0.09km/Myr; eroded material: ca. 28,000 km^3), renewed burial during the Late Cretaceous and a finally exhumation during the Cenozoic (0.01-0.20 km/Myr; ca. 37,000 km^3). The burial event was synchronous to Atlantic rifting, and sample analysis

indicates rapid burial from close to the surface down to 4 km, suggesting that subsidence associated with the Central Atlantic and/or the High Atlas rift zone(s) extended over nearly the entire Meseta.

This study presents 10 source-and-sink maps, integrating data from palaeo- structural, erosional, and depositional maps for the Permian to the present-day.

During the Permian, terrestrial basins located across the Meseta were sourced with eroded material of the Variscan chain. In the Middle to Late Triassic, widespread rifting allowed more extensive deposition across Morocco. Active sedimentary source areas were the northern Meseta, the western Anti-Atlas, and the central Reguibat Shield. Initially most of Morocco was dominated by continental deposits, with a gradual transgression inland from Tethys to the east and the proto-Atlantic to the west extending terrestrial/transitional marine environments, across the High Atlas, the Meseta, and the Tarfaya basins as well as part of the Reguibat Shield.

Throughout the Jurassic, shallow marine and marine environments dominate, with periods of discrete siliciclastic input. Active sedimentary source areas were the Anti-Atlas, the Reguibat Shield, and the Meseta massifs. A substantial shift of source area was evidenced from the Anti-Atlas to the Meseta/High Atlas at the transition between the Middle and the Late Jurassic (ca. 163 Ma).

In the Early Cretaceous, terrestrial environments cover a substantial portion of the study area, especially between 145 and 125 Ma. Another considerable shift of source area was evidenced from the Meseta/High Atlas to the Anti-Atlas at the transition between the early Early and the middle Cretaceous (ca. 125 Ma). Finally, during the Cenozoic, almost all the presently outcropping basement areas provided source material to the coastal and foreland basins.

The presented workflow enables past large-scale source-to-sink domains to be constrained, which is lacking by design in local LTT studies (e.g. Charton et al., 2018). The prerequisites, if applied

elsewhere, are limited to the availability of t-T datasets and prior geological knowledge. These results may be further improved as more t-T data points are made available and/or if associated with a systematic investigation of the contact between t-T modelled basement areas and their sedimentary cover.

References

Abioui, M., Ferry, S., Grosheny, D., Içame, N., Robert, E., Benssaou, M.. (2019). The Cretaceous marine onlap on Palaeozoic deposits (Smara–Lâayoune Basin, South Morocco). Comparison with neighbouring regions: Comptes Rendus Geoscience, in press, 10p.. doi:10.1016/j.crte.2019.09.003.

Adaci, M., Tabuce, R., Mebrouk, F., Bensalah, M., Fabre, P.-H., Hautier, L., Jaeger, J.-J., Lazzari, V., Mahboubi, M., Marivaux, L. and Otero, O.. (2007). Nouveaux sites à vertébrés paléogènes dans la région des Gour Lazib (Sahara Nord-occidental, Algérie): Comptes Rendus Palevol, 6, p. 535–544. doi:10.1016/j.crpv.2007.09.001

Aït Boughrous, A., Boulanouar, M., Yacoubi, M. and Coineau, N.. (2007). The first Microcharon (Crustacea Isopoda, Microparasellidae) from the Moroccan North Saharan Platform. Origin and palaeobiogeography: Contribution to Zoology, 76, p. 19–32. doi:10.1163/18759866-07601003

Ali, S., Stattegger, K., Garbe-Schönberg, D., Frank, M., Kraft, S. and Kuhnt, W.. (2014). The provenance of Cretaceous to Quaternary sediments in the Tarfaya basin, SW Morocco: Evidence from trace element geochemistry and radiogenic Nd–Sr isotopes: Journal of African Earth Sciences, 90, p. 64–76. doi:10.1016/j.jafrearsci.2013.11.010

Allen, P.A.. (2008). From landscapes into geological history: Nature, 451, p. 274.

Ambroggi, R. and Lapparent, A.. (1954). Découverte d'empreintes de pas de Reptiles dans le Maestrichtien d'Agadir (Maroc): Compte Rendu sommaire des séances de la Société géologique de France, p. 51–52.

Amidon, W.H., Roden-Tice, M., Anderson, A.J., McKeon, R.E. and Shuster, D.L.. (2016). Late Cretaceous unroofing of the White Mountains, New Hampshire, USA: An episode of passive margin rejuvenation?: Geology, 44, p. 415–418. doi:10.1130/G37429.1

An, K., Hanlin C., Xiubin L., Fang W., Shufeng Y., Zhixin W., Zhaoming W., Guangya Z., and Xiaoguang T.. (2017). Major transgression during Late Cretaceous constrained by basin sediments in northern Africa: implication for global rise in sea level: Frontiers of earth science, 11, no. 4 (2017): 740-750. doi.org/10.1007/s11707-017-0661-0

Andreu, B. and Tronchetti, G.. (1994). Ostracodes et foraminifères du Crétacé supérieur du synclinal d'El Koubbat, Moyen Atlas, Maroc: Biostratigraphie, Paléoenvironements, Paléobiogéopgraphie, systématique des ostracodes: Congrès français de stratigraphie, 1, Toulouse.

Aquit, M., Kuhnt, W., Holbourn, A., Hassane Chellai, El, Stattegger, K., Kluth, O. and Jabour, H.. (2013). Late Cretaceous paleoenvironmental evolution of the Tarfaya Atlantic coastal Basin, SW Morocco: Cretaceous Research, 45, p. 288–305. doi:10.1016/j.cretres.2013.05.004

Arab, M., Bracène, R., Roure, F., Zazoun, R.S., Mahdjoub, Y. and Badji, R.. (2015). Source rocks and related petroleum systems of the Chelif Basin, (western Tellian domain, north Algeria): Marine and Petroleum Geology, 64, p. 363–385. doi:10.1016/j.marpetgeo.2015.03.017

Arabi, El, E.H., Ferrandini, J. and Essamoud, R.. (2003). Triassic stratigraphy and structural evolution of a rift basin: The Eç Çour basin, High atlas of Marrakech, Morocco: Journal of African Earth Sciences, 36, p. 29–39. doi:10.1016/S0899-5362(03)00020-4

Arantegui, A.. (2018). Characterisation of Mesozoic Depositional Systems along the Atlantic Passive Margin of Morocco. North Aaiun-Tarfaya Basin: University of Manchester, Ph.D. Thesis, 169 p.

Arantegui, A., Jerrett, R., Schröder, S., Bulot, L.G., Gatto, R., Monari, S. and Redfern, J.. (2019). Constraining Mesozoic early post-rift depositional systems evolution along the eastern Central Atlantic margin: Sedimentary Geology, 386, p. 31-51. doi:10.1016/j.sedgeo.2019.03.005

Azdimousa, A., Bourgois, J., Poupeau, G., Vázquez, M., Asebriy, L. and Labrin, E.. (2013). Fission track thermochronology of the Beni Bousera peridotite massif (Internal Rif, Morocco) and the exhumation of ultramafic rocks in the Gibraltar Arc: Arabian Journal of Geosciences, 7, p. 1993–2005. doi:10.1007/s12517-013-0924-3

Azdimousa, A., Jabaloy-Sánchez, A., Talavera, C., Asebriy, L., González-Lodeiro, F. and Evans, N.J.. (2019). Detrital zircon U-Pb ages in the Rif Belt (northern Morocco): Paleogeographic implications: Gondwana Research, 70, p.133-150: doi:10.1016/j.gr.2018.12.008

Balestrieri, M.L., Moratti, G., Bigazzi, G. and Algouti, A.. (2009). Neogene exhumation of the Marrakech High Atlas (Morocco) recorded by apatite fission-track analysis: Terra Nova, 21, p. 75–82. doi:10.1111/j.1365-3121.2008.00857.x

Barbero, L., Jabaloy, A., Gómez-Ortiz, D., Pérez-Peña, J.V., Rodríguez-Peces, M.J., Tejero, R., Estupiñán, J., Azdimousa, A., Vázquez, M. and Asebriy, L.. (2011). Evidence for surface uplift of the Atlas Mountains and the surrounding peripheral plateaux: Combining apatite fission-track results and geomorphic indicators in the Western Moroccan Meseta (coastal Variscan Paleozoic basement): Tectonophysics, 502, p. 90–104. doi:10.1016/j.tecto.2010.01.005

Barbero, L., Teixell, A., Arboleya, M.-L., Río, P.D., Reiners, P.W. and Bougadir, B.. (2007). Jurassic-to-present thermal history of the central High Atlas (Morocco) assessed by low-temperature thermochronology: Terra Nova, 19, p. 58–64. doi:10.1111/j.1365-3121.2006.00715.x

Barnes, J.B. and Heins, W.A.. (2009). Plio-Quaternary sediment budget between thrust belt erosion and foreland deposition in the central Andes, southern Bolivia: Basin Research, 21, p. 91–109. doi:10.1111/j.1365-2117.2008.00372.x

Baudon, C., Fabuel-Perez, I. and Redfern, J.. (2009). Structural style and evolution of a Late Triassic rift basin in the Central High Atlas, Morocco: Controls on sediment deposition: Geological Journal, 44, p. 677–691. doi:10.1002/gj.1195

Baudon, C., Redfern, J. and Van Den Driessche, J.. (2012). Permo-Triassic structural evolution of the Argana Valley, impact of the Atlantic rifting in the High Atlas, Morocco: Journal of African Earth Sciences, 65, p. 91–104. doi:10.1016/j.jafrearsci.2012.02.002

Beauvais, L.. (1986). Monographie des madréporaires du Jurassique inférieur du Maroc: Palaeontographica, 194, p. 1–68.

Benest, M.. (1985). Evolution de la plate-forme de l'Ouest algérien et du Nord-Ouest marocain au cours du Jurassique supérieur et au début du Crétacé : Stratigraphic, milieux de depot et dynamique sedimentaire: Documents du Laboratoire de Geologie de Lyon, 95, 581p.

Benvenuti, M., Moratti, G. and Algouti, A.. (2017). Stratigraphic and structural revision of the Upper Mesozoic succession of the Dadès valley, eastern Ouarzazate Basin (Morocco): Journal of African Earth Sciences, 135, p. 1–45. doi:10.1016/j.jafrearsci.2017.01.018

Benyoucef, M., Malti, F.-Z., Adaci, M., Fellah, A.H., Abbache, A., Cherif, A., Sidhoum, R. and Bensalah, M.. (2015). Évolution lithostratigraphique, paléoenvironnementale et paléogéographique du flysch de Ben-Zireg (Viséen inférieur, Algérie): Geodiversitas, 37, p. 5–29. doi:10.5252/g2015n1a1

Benzaggagh, M.. (2016). Tholeitic basalts and ophiolitic complexes of the Mesorif Zone (External Rif, Morocco) at the Jurassic-Cretaceous boundary and the importance of the Ouerrha Accident in the palaeogeographic and geodynamic evolution of the Rif Mountains: Boletín geológico y minero, 127, p. 389–406.

Benzaggagh, M., Latil, J.-L., Oumhamed, M. and Ferré, B.. (2017). Stratigraphic succession (Albian to lower? Cenomanian) and upper Albian ammonites and biozones from the Talerhza Basin (South Riffian Ridges, northern Morocco): Cretaceous Research, 73, p. 71–90. doi:10.1016/j.cretres.2017.01.005

Bertotti, G. and Gouiza, M.. (2012). Post-rift vertical movements and horizontal deformations in the eastern margin of the Central Atlantic: Middle Jurassic to Early Cretaceous evolution of Morocco: International Journal of Earth Sciences, 101, p. 2151–2165. doi:10.1007/s00531-012-0773-4

Best, M.W. and Boekschoten, G.J.. (1981). On the coral fauna in the Miocene reef at Baixo, Porto Santo (Eastern Atlantic): Netherlands Journal of Zoology, 32, p. 412–418.

Blain, H.-A., Sesé, C., Rubio-Jara, S., Panera, J., Uribelarrea, D. and Pérez-González, A.. (2013). Reconstitution paléoenvironnementale et paléoclimatique du Pléistocène supérieur ancien (MIS 5a) dans le Centre de l'Espagne: Les petits vertébrés (Amphibia, Reptilia & Mammalia) des gisements de HAT et PRERESA (Sud-est de Madrid). Revue de l'Association française pour l'étude du Quaternaire, 24, p. 191–205. Doi : 10.4000/quaternaire.6604

Boleli, E.. (1952). Plateau des phosphates ''hydrogéologie du Maroc'': Notes et Mémoires du Service Géologique du Maroc, 77, p. 197–204.

Bourillot, R., Neige, P., Pierre, A. and Durlet, C.. (2008). Early-Middle Jurassic Lytoceratid Ammonites with constrictions from Morocco: Palaeobiogeographical and evolutionary implications: Palaeontology, 51, p. 597–609. doi:10.1111/j.1475-4983.2008.00766.x

Brahim, L.A., Chotin, P., Hinaj, S., Abdelouafi, A., Adraoui, El, A., Nakcha, C., Dhont, D., Charroud, M., Alaoui, F.S., Amrhar, M., Bouaza, A., Tabyaoui, H. and Chaouni, A.. (2002). Paleostress evolution in

the Moroccan African margin from Triassic to Present: Tectonophysics, 357, p. 187–205. doi:10.1016/S0040-1951(02)00368-2

Bridwell, R.J.. (1976). Lithospheric thinning and the late Cenozoic thermal and tectonic regime of the northern Rio Grande rift: New Mexico Geological Society Field Conference, 27, Vermq'o Park.

Broutin, J., Aassoumi, H., Wartiti, El, M., Freytet, P., Kerp, H., Quesada, C. and Toutin-Morin, N.. (1998). The Permian basins of Tiddas, Bou Achouch and Khenifra (Central Morocco). Biostratigraphic and palaeophytogeographic implications. Mémoires du Muséum national d'histoire naturelle, 179, p. 257–278.

Broutin, J., Ferrandini, J. and Saber, H.. (1989). Implications stratigraphiques et paléogéographiques de la découverte d'une flore permienne euraméricaine dans le Haut-Atlas occidental (Maroc): Comptes rendus de l'Académie des sciences, 308, p. 1509–1514.

Brown, R.H.. (1980). Triassic rocks of Argana Valley, southern Morocco, and their regional structural implications: AAPG Bulletin, 64, p. 988–1003.

Burkhard, M., Caritg, S., Helg, U., Robert-Charrue, C. and Soulaimani, A.. (2006). Tectonics of the Anti-Atlas of Morocco: Comptes Rendus Geoscience, 338, p. 11–24. doi:10.1016/j.crte.2005.11.012

Casini, L., Cuccuru, S., Puccini, A., Oggiano, G. and Rossi, P.. (2015). Evolution of the Corsica-Sardinia Batholith and late-orogenic shearing of the Variscides: Tectonophysics, 646, p. 65–78. doi:10.1016/j.tecto.2015.01.017

Cavin, L., Tong, H., Boudad, L., Meister, C., Piuz, A., Tabouelle, J., Aarab, M., Amiot, R., Buffetaut, E., Dyke, G., Hua, S. and Le Loeuff, J.. (2010). Vertebrate assemblages from the early Late Cretaceous of southeastern Morocco: An overview: Journal of African Earth Sciences, 57, p. 391–412. Doi:10.1016/j.jafrearsci.2009.12.007

Chalouan, A., Michard, A., Kadiri, El, K., Negro, F., de Lamotte, D.F., Soto, J.I. and Saddiqi, O.. (2008). The Rif Belt. In: Continental Evolution: The Geology of Morocco, Springer, p. 203–302.

Charrière, A. and Haddoumi, H.. (2016). Les «Couches rouges» continentales jurassico-crétacées des Atlas marocains (Moyen Atlas, Haut Atlas central et oriental): Bilan stratigraphique, paléogéographies successives et cadre géodynamique: Boletín geológico y minero, 127, p. 407–430.

Charton, R., Bertotti, G., Arantegui, A. and Bulot, L.. (2018). The Sidi Ifni transect across the rifted margin of Morocco (Central Atlantic): Vertical movements constrained by low-temperature thermochronology: Journal of African Earth Sciences, 141, p. 22-32. doi:10.1016/j.jafrearsci.2018.01.006

Charton, R.. (2018). Phanerozoic Vertical Movements in Morocco: PhD Thesis, TUDelft, 165p. doi: 10.4233/uuid:fda35870-18d9-4ca3-9443-199a1dcb0250

Chevalier, J.P. and Choubert, G.. (1962). Les madréporaires miocènes du Maroc: Éditions du Service géologique du Maroc, 173, p. 1–74.

Chopin, F., Corsini, M., Schulmann, K., Houicha, El, M., Ghienne, J.-F. and Edel, J.-B.. (2014). Tectonic evolution of the Rehamna metamorphic dome (Morocco) in the context of the Alleghanian-Variscan orogeny: Tectonics, 33, p. 1154–1177. doi:10.1002/2014TC003539

Choubert, G., Faure-Muret, A. and Hottinger, L.. (1966). Aperçu géologique du bassin côtier de Tarfaya: Editions du Service géologique du Maroc, 285 p.

Clift, P.D., Dewey, J.F., Draut, A.E., Chew, D.M., Mange, M. and Ryan, P.D.. (2004). Rapid tectonic exhumation, detachment faulting and orogenic collapse in the Caledonides of western Ireland: Tectonophysics, 384, p. 91–113. doi:10.1016/j.tecto.2004.03.009

Cloetingh, S. and Burov, E.. (2011). Lithospheric folding and sedimentary basin evolution: a review and analysis of formation mechanisms: Basin Research, 23, p. 257–290. doi:10.1111/j.1365-2117.2010.00490.x

Dartevelle, E. and Schwetz, J.. (1937). Mollusques récoltés dans le Bas-Congo: Annales de la Société Royale Zoologique de Belgique, 68, p. 49–65.

Davies, J.H.F.L., Marzoli, A., Bertrand, H., Youbi, N., Ernesto, M. and Schaltegger, U.. (2017). End-Triassic mass extinction started by intrusive CAMP activity: Nature Communications, 8, 15596. doi:10.1038/ncomms15596

Davison, I.. (2005). Central Atlantic margin basins of North West Africa: Geology and hydrocarbon potential (Morocco to Guinea): Journal of African Earth Sciences, 43, p. 254–274. doi:10.1016/j.jafrearsci.2005.07.018

Dhondt, A.V., Malchus, N., Boumaza, L. and Jaillard, E.. (1999). Cretaceous oysters from North Africa: Origin and distribution: Bulletin de la Société Géologique de France, 170, p. 67–76.

Domenech, M.. (2015). Rift opening and inversion in the Marrakech High Atlas: integrated structural and thermochronologic study: Universitat Autònoma de Barcelona, Ph.D. Thesis, 157 p.

Domènech, M., Stockli, D. and Teixell, A.. (2018). Detrital zircon U-Pb provenance and paleogeography of Triassic rift basins in the Marrakech High Atlas: Terra Nova, 30, p. 310-318. doi:10.1111/ter.12340

Domènech, M., Teixell, A. and Stöckli, D.F.. (2016). Magnitude of rift-related burial and orogenic contraction in the Marrakech High Atlas revealed by zircon (U-Th)/He thermochronology and thermal modeling: Tectonics, 35, p. 2609–2635. doi:10.1002/2016TC004283

Doubinger, J., 1956. Contribution à l'étude des flores autuno-stéphaniennes: Société géologique de France, 35, p. 1–180.

Duval-Arnould A.. (2019). Controls on stratigraphic development of shelf margin carbonates: Jurassic Atlantic margin – Essaouira-Agadir Basin, Western Morocco : PhD Thesis, University of Manchester, 287p.

Echarfaoui, H., Hafid, M. and Salem, A.A.. (2002). Analyse sismo-stratigraphique du bassin d'Abda (Maroc occidental), exemple de structures inverses pendant le rifting atlantique: Comptes Rendus Geoscience, 334, p. 371-377. doi:10.1016/S1631-0713(02)01768-6

Ehlers, T.A.. (2005). Crustal Thermal Processes and the Interpretation of Thermochronometer Data: Reviews in Mineralogy and Geochemistry, 58 , p. 315–350. doi:10.2138/rmg.2005.58.12

El Haimer, F.Z.. (2014). Mouvements verticaux post-Varisques des domaines Mesetien et Atlasique: Thermochronology basse température sur apatite et zircon: Université Hassan II, Ph.D. Thesis, 124 p.

El Harfi, A., Lang, J., Salomon, J. and Chellai, E.. (2001). Cenozoic sedimentary dynamics of the Ouarzazate foreland basin (Central High Atlas Mountains, Morocco): International Journal of Earth Sciences, 90, p. 393–411. doi:10.1007/s005310000115

Ellouz, N., Patriat, M., Gaulier, J.-M., Bouatmani, R. and Sabounji, S.. (2003). From rifting to Alpine inversion: Mesozoic and Cenozoic subsidence history of some Moroccan basins: Sedimentary Geology, 156, p. 185–212. doi:10.1016/S0037-0738(02)00288-9

Ennouchi, E., 1954. La faune néolithique de Toulkine (Haut Atlas): Comptes rendus des séances mensuelles de la société des sciences naturelles et physiques du Maroc, 20, p. 140–141.

Ettachfini, M., Rey, J., Taj-Eddine, K., Tavera, J.M.. (1998). The Valanginian of the Safi Basin (Atlantic Morocco) and its ammonite fauna. Palaeobiogeographical implications: Comptes Rendus de l'Académie des Sciences, 5, p. 319–325.

Fabuel-Perez, I., Redfern, J. and Hodgetts, D.. (2009). Sedimentology of an intra-montane rift-controlled fluvial dominated succession: The Upper Triassic Oukaimeden Sandstone Formation, Central High Atlas, Morocco: Sedimentary Geology, 218, p. 103–140. doi:10.1016/j.sedgeo.2009.04.006

Fabre, J., Arnaud-Vanneau, A., Belhadj, Z., and Monod, T.. (1996). Evolution des terrains méso-cénozoïques d'une marge à l'autre du craton ouest africain, entre le Tanezrouft (Algérie) et l'Adrar de Mauritanie: Mémoires du Service Géologique de l'Algérie , 8, p. 187–229.

Fetah, M., Bensaid, M. and Dahmani, M.. (1990). Carte Géologique du Maroc: Zawyat Ahancal (1:100,000): Ministere de l'Energie et des Mines.

Fiechtner, L., Friedrichsen, H. and Hammerschmidt, K.. (1992). Geochemistry and Geochronology of Early Mesozoic Tholeiites From Central Morocco: Geologische Rundschau, 81, p. 45–62. doi:10.1007/BF01764538

Flowers, R.M. and Ehlers, T.A.. (2018). Rock erodibility and the interpretation of low-temperature thermochronologic data: Earth and Planetary Science Letters, 482, p. 312–323. doi:10.1016/j.epsl.2017.11.018

Frizon de Lamotte, D., Crespo-Blanc, A., Saint-Bézar, B., Comas, M., Fernandez, M., Zeyen, H., Ayarza, P., Robert-Charrue, C., Chalouan, A. and Zizi, M.. (2004). TRANSMED Transect I: Iberian Meseta–Guadalquivir Basin–Betic Cordillera–Alboran Sea–Rif–Moroccan Meseta–High Atlas–Sahara Platform. In: The TRANSMED Atlas: The Mediterranean Region from Crust to Mantle, Springer, p. 141.

Frizon de Lamotte, D., Fourdan, B., Leleu, S., Leparmentier, F. and de Clarens, P.. (2015). Style of rifting and the stages of Pangea breakup: Tectonics, 34, p. 1009–1029. doi:10.1002/2014TC003760

Frizon de Lamotte, D., Leturmy, P., Missenard, Y., Khomsi, S., Ruiz, G., Saddiqi, O., Guillocheau, F. and Michard, A.. (2009). Mesozoic and Cenozoic vertical movements in the Atlas system (Algeria, Morocco, Tunisia): An overview: Tectonophysics, 475, p. 9–28. doi:10.1016/j.tecto.2008.10.024

Frizon de Lamotte, D., Raulin, C., Mouchot, N., Wrobel-Daveau, J.-C., Blanpied, C., and Ringenbach, J.-C.. (2011). The southernmost margin of the Tethys realm during the Mesozoic and Cenozoic: Initial geometry and timing of the inversion processes: Tectonics, 30, TC3002. doi:10.1029/2010TC002691.

Gaffney, E.S., Tong, H. and Meylan, P.A.. (2006). Evolution of the side-necked turtles: The families Bothremydidae, Euraxemydidae, and Araripemydidae: Bulletin of the American Museum of Natural History, 300, 698 p. doi: 10.1206/0003-0090(2006)300[1:EOTSTT]2.0.CO;2

Gallagher, K.. (2012). Transdimensional inverse thermal history modeling for quantitative thermochronology: Solid Earth, 117, p. 2156–2202. doi:10.1029/2011JB008825

Gallagher, K., Brown, R. and Johnson, C.. (1998). Fission track analysis and its applications to geological problems: Annual Review of Earth and Planetary Sciences, 26, p. 519–572. doi:10.1146/annurev.earth.26.1.519

Ghorbal, B.. (2009). Mesozoic to Quaternary thermo-tectonic evolution of Morocco (NW Africa): Vrije Universiteit Amsterdam, Ph.D. Thesis, 226 p.

Ghorbal, B., Bertotti, G., Foeken, J. and Andriessen, P.. (2008). Unexpected Jurassic to Neogene vertical movements in ‘stable’ parts of NW Africa revealed by low temperature geochronology: Terra Nova, 20, p. 355–363. doi:10.1111/j.1365-3121.2008.00828.x

Gimeno-Vives, O., Mohn, G., Bosse, V., Haissen, F., Zaghloul, M. N., Atouabat, A., & Frizon de Lamotte, D.. (2019). The Mesozoic margin of the Maghrebian Tethys in the Rif belt (Morocco): Evidence for polyphase rifting and related magmatic activity: Tectonics, 38, 2894–2918. doi.org/10.1029/2019TC005508

Gingerich, P.D. and Zouhri, S.. (2015). New fauna of archaeocete whales (Mammalia, Cetacea) from the Bartonian middle Eocene of southern Morocco: Journal of African Earth Sciences, 111, p. 273–286. doi:10.1016/j.jafrearsci.2015.08.006

Gomez, F., Beauchamp, W. and Barazangi, M.. (2000). Role of the Atlas Mountains (northwest Africa) within the African-Eurasian plate-boundary zone: Geology, 28, p. 775–778. doi:10.1130/0091-7613(2000)28<775:ROTAMN>2.0.CO;2

Gouiza, M.. (2011). Mesozoic source-to-sink systems in NW Africa: Geology of vertical movements during the birth and growth of the Moroccan rifted margin: Vrije Universiteit Amsterdam, Ph.D. Thesis, 170 p.

Gouiza, M., Charton, R., Bertotti, G., Andriessen, P. and Storms, J.E.A.. (2017). Post-Variscan evolution of the Anti-Atlas belt of Morocco constrained from low-temperature geochronology: International Journal of Earth Sciences, 106, p. 593–616. doi:10.1007/s00531-016-1325-0

Groune, K., Halim, M., Benmakhlouf, M., Arsalane, S., Lemee, L. and Ambles, A.. (2013). Organic geochemical and mineralogical characterization of the Moroccan Rif bituminous rocks: Journal of Materials and Environmental Science, 4, 472-481.

Green, P.F., Japsen, P., Chalmers, J.A., Bonow, J.M. and Duddy, I.R.. (2018). Post-breakup burial and exhumation of passive continental margins: Seven propositions to inform geodynamic models: Gondwana Research, 53, p. 58–81. doi:10.1016/j.gr.2017.03.007

Grimaud, J. , Rouby, D. , Chardon, D. and Beauvais, A.. (2018). Cenozoic sediment budget of West Africa and the Niger delta: Basin Research, 30, p. 169-186. doi:10.1111/bre.12248

Guillocheau, F., Rouby, D., Robin, C., Helm, C. and Rolland, N.. (2012). Quantification and causes of the terrigeneous sediment budget at the scale of a continental margin: a new method applied to the Namibia-South Africa margin: Basin Research, 24, pp.3-30. doi: 10.1111/j.1365-2117.2011.00511.x

Guimerà, J., Arboleya, M.L. and Teixell, A.. (2011). Structural control on present-day topography of a basement massif: the Central and Eastern Anti-Atlas (Morocco): Geologica Acta: an international earth science journal, 9, p. 55-65. doi:10.1344/105.000001643

Guiraud, R.. (1998). Mesozoic rifting and basin inversion along the northern African Tethyan margin: An overview: Geological Society, London, Special Publications, 132, p. 217–229. doi:10.1144/GSL.SP.1998.132.01.13

Guiraud, R., Bellion, Y., Benkhelil, J. and Moreau, C.. (1987). Post-Hercynian Tectonics in Northern and Western Africa: Geological Journal, 22, p. 433–466. doi:10.1002/gj.3350220628

Guiraud R., Bosworth, W., Thierry, J., Delplanque, A.. (2005). Phanerozoic geological evolution of Northern and Central Africa: An overview: Journal of African Earth Sciences, 43, p. 83-143. doi:10.1016/j.jafrearsci.2005.07.017.

Haddoumi, H., Charriere, A. and Mojon, P.-O.. (2010). Stratigraphie et sedimentologie des «Couches rouges» continentales du Jurassique-Cretace du Haut Atlas central (Maroc): implications paleoogeographiques et geodynamiques: Geobios, 43, p. 433–451. Doi : 10.1016/j.geobios.2010.01.001

Hafid, M., Zizi, M., Bally, A.W. and Ait Salem, A.. (2006). Structural styles of the western onshore and offshore termination of the High Atlas, Morocco: Comptes Rendus Geoscience, 338, p. 50–64. doi:10.1016/j.crte.2005.10.007

Helland-Hansen, W., Sømme, T.O., Martinsen, O.J., Lunt, I. and Thurmond, J.. (2016). Deciphering Earth's Natural Hourglasses: Perspectives On Source-To-Sink Analysis: Journal of Sedimentary Research, 86, p. 1008–1033. doi:10.2110/jsr.2016.56

Helm, C.. (2009). Quantification des flux sédimentaires anciens à l'échelle d'un continent: Le cas de l'Afrique au Méso-Cénozoïque: Université Rennes, Ph.D. Thesis, 364 p.

Herbig, H. G., and Trappe, J.. (1994). Stratigraphy of the Subatlas Group (Maastrichtian-Middle Eocene, Morocco): Newsletters on Stratigraphy, 125-165. doi:10.1127/nos/30/1994/125

Hill, R.V., Mccartney, J.A., Roberts, E., Bouaré, M., Sissoko, F. and O'leary, M.A.. (2008). Dyrosaurid (Crocodyliformes: Mesoeucrocodylia) Fossils from the Upper Cretaceous and Paleogene of Mali: Implications for Phylogeny and Survivorship across the K/T Boundary: American Museum Novitates, 3631, p. 1–21. doi:10.1206/598.1

Hmich, D., Schneider, J.W., Saber, H., Voigt, S. and Wartiti, El, M.. (2006). New continental Carboniferous and Permian faunas of Morocco: implications for biostratigraphy, palaeobiogeography and palaeoclimate: Geological Society, London, Special Publications, 265, p. 297–324. doi:10.1144/GSL.SP.2006.265.01.14

Hollard, H., Choubert, G., Bronner, G., Marchand, J. and SOUGY, J.. (1985). Carte Géologique du Maroc, (1:1,000,000 ; 2 sheets): Notes et Mémoires du Service Géologique du Maroc.

Ibrahim, N., Varricchio, D.J., Sereno, P.C., Wilson, J.A., Dutheil, D.B., Martill, D.M., Baidder, L. and Zouhri, S.. (2014). Dinosaur Footprints and Other Ichnofauna from the Cretaceous Kem Kem Beds of Morocco: PLoS ONE, 9, p. e90751–15. doi:10.1371/journal.pone.0090751

Japsen, P., Bonow, J.M., Green, P.F., Chalmers, J.A. and Lidmar-Bergström, K.. (2006). Elevated, passive continental margins: Long-term highs or Neogene uplifts? New evidence from West Greenland: Earth and Planetary Science Letters, 248, p. 330–339. doi:10.1016/j.epsl.2006.05.036

Japsen, P., Bonow, J.M., Green, P.F., Chalmers, J.A. and Lidmar-Bergström, K.. (2009). Formation, uplift and dissection of planation surfaces at passive continental margins - a new approach: Earth Surface Processes and Landforms, 34, p. 683–699. doi:10.1002/esp.1766

Japsen, P., Bonow, J.M., Green, P.F., Cobbold, P.R., Chiossi, D., Lilletveit, R., Magnavita, L.P. and Pedreira, A.. (2012b). Episodic burial and exhumation in NE Brazil after opening of the South Atlantic: Geological Society of America Bulletin, 124, p. 800–816. doi:10.1130/B30515.1

Japsen, P., Chalmers, J.A., Green, P.F. and Bonow, J.M.. (2012a). Elevated, passive continental margins: Not rift shoulders, but expressions of episodic, post-rift burial and exhumation: Global and Planetary Change, 90-91, p. 73–86. doi:10.1016/j.gloplacha.2011.05.004

Japsen, P., Green, P.F. and Bonow, J.M.. (2016b). Burial and exhumation history of the Labrador-Newfoundland margin: First observations: Geological Survey of Denmark and Greenland, 35, p. 91–94.

Japsen, P., Green, P.F., Bonow, J.M., Chalmers, J.A. and Rasmussen, E.S.. (2016a). Burial and exhumation history of southernmost Norway estimated from apatite fission-track analysis data constrained by geological observations and stratigraphic landscape analysis: NGF Abstract and Proceedings, 1, p. 26–28.

Jelinek, A.R., Chemale, F., Jr, van der Beek, P.A., Guadagnin, F., Cupertino, J.A. and Viana, A.. (2014). Denudation history and landscape evolution of the northern East-Brazilian continental margin from apatite fission-track thermochronology: Journal of South American Earth Sciences, 54, p. 158–181. doi:10.1016/j.jsames.2014.06.001

Jenny, J. and Jossen, J.A.. (1982). Découverte d'empreintes de pas de Dinosauriens dans le Jurassique inférieur (Pliensbachien) du Haut-Atlas central (Maroc): Comptes Rendues hébdomanaires Séances Academie de Sciences, 294, p. 223–226.

Joussiaume, R.. (2016). Les relations entre diapirisme et sédimentation: Exemple du Jurassique moyen de la région d'Imilchil, Haut-Atlas central, Maroc: PhD Thesis, Universite de Bordeaux.

Jouve, S., Larochene, M.O., Bouya, B. and Amaghzaz, M.. (2005). A new dyrosaurid crocodyliform from the Palaeocene of Morocco and a phylogenetic analysis of Dyrosauridae: Acta Palaeontologica Polonica, 50, p. 1–14.

Juez-Larre, J. and Andriessen, P.. (2006). Tectonothermal evolution of the northeastern margin of Iberia since the break-up of Pangea to present, revealed by low-temperature fission-track and (U–Th)/He thermochronologyA case history of the Catalan Coastal Ranges: Earth and Planetary Science Letters, 243, p. 159–180. doi:10.1016/j.epsl.2005.12.026

Kammerer, C.F., Nesbitt, S.J. and Shubin, N.H.. (2011). The first silesaurid dinosauriform from the Late Triassic of Morocco: Acta Palaeontologica Polonica, 57, p. 277–284. doi:10.4202/app.2011.0015

Karroum, M., Mandour, El, A., Khattach, D., Cassas, A., Himi, M., Rochdane, S., Laftouhi, N.-E. and Khalil, N.. (2014). Fonctionnement hydrogéologique du bassin de la Bahira (Maroc central): apport de l'analyse des données géologiques et gravimétriques: Canadian Journal of Earth Sciences, 51, p. 517-526. Doi : 10.1139/cjes-2013-0130

Ketcham, R.A.. (2005). Forward and Inverse Modeling of Low-Temperature Thermochronometry Data: Reviews in Mineralogy and Geochemistry, 58, p. 275–314. doi:10.2138/rmg.2005.58.11

Ketcham, R.A., Donelick, R.A. and Donelick, M.B.. (2000). AFTSolve: A program for multi-kinetic modeling of apatite fission-track data: Geological Materials Research, 2, p. 1–32.

Koeniguer, J.-C.. (1967). Etude paléoxylologique du Rio de Oro: Notas y Comunicaciones Insituto Geologico y Minero de España, 96, p. 39–66.

Kuuskraa, V., Stevens, S.H. and Moodhe, K.D.. (2013). Technically recoverable shale oil and shale gas resources: An assessment of 137 shale formations in 41 countries outside the United States: US Energy Information Administration, 27 p.

Labails, C., Olivet, J.-L., Aslanian, D. and Roest, W.R.. (2010). An alternative early opening scenario for the Central Atlantic Ocean: Earth and Planetary Science Letters, 297, p. 355–368. doi:10.1016/j.epsl.2010.06.024

Lagnaoui, A., Klein, H., Saber, H., Fekkak, A., Belahmira, A. and Schneider, J.W.. (2016). New discoveries of archosaur and other tetrapod footprints from the Timezgadiouine Formation (Irohalene Member, Upper Triassic) of the Argana Basin, western High Atlas, Morocco - Ichnotaxonomic implications: Palaeogeography, Palaeoclimatology, Palaeoecology, 453, p. 1–9. doi:10.1016/j.palaeo.2016.03.022

Le Roy, P., Piqué, A., Le Gall, B., Ait Brahim, L., Morabet, A.M. and Demnati, A.. (1997). Les bassins cotiers triasico-liasiques du Maroc occidental et la diachronie du rifting intra-continental de l'Atlantique central: Bulletin de la Société Géologique de France, 168, p. 637–648.

Lee, C.W.. (1983). Bivalve mounds and reefs of the Central High Atlas, Morocco: Palaeogeography, Palaeoclimatology, Palaeoecology, 43, p. 153–168. doi:10.1016/0031-0182(83)90052-4

Leeder, M.R.. (2006). Sedimentology and sedimentary basins: From turbulence to tectonics: John Wiley & Sons, 608 p.

Leleu, S., Hartley, A.J., van Oosterhout, C., Kennan, L., Ruckwied, K. and Gerdes, K.. (2016). Structural, stratigraphic and sedimentological characterisation of a wide rift system: The Triassic rift system of the Central Atlantic Domain: Earth Science Reviews, 158, p. 89–124. Doi:10.1016/j.earscirev.2016.03.008

Leprêtre, R.. (2015). Evolution Phanerozoïque du Craton Ouest Africain et de ses bordures Nord et Ouest: Université Paris 11, Ph.D. Thesis, 423 p.

Leprêtre, R., Barbarand, J., Missenard, Y., Gautheron, C., Pinna-Jamme, R. and Saddiqi, O.. (2017). Mesozoic evolution of NW Africa: implications for the Central Atlantic Ocean dynamics: Journal of the Geological Society, 174, p. 817–835. doi:10.1144/jgs2016-100

Leprêtre, R., Barbarand, J., Missenard, Y., Leparmentier, F. and Frizon de Lamotte, D.. (2013). Vertical movements along the northern border of the West African Craton: The Reguibat Shield and adjacent basins: Geological Magazine, 151, p. 1–14.

Leprêtre, R., Frizon de Lamotte, D., Combier, V., Gimeno-Vives, O., Mohn, G., & Eschard, R.. (2018). The Tell-Riforogenic system (Morocco, Algeria, Tunisia) and the structural heritage of the southern Tethys margin: BSGF. BSGF-Earth Sciences Bulletin, 189, 10. doi.org/10.1051/bsgf/2018009

Leprêtre, R., Missenard, Y., Barbarand, J., Gautheron, C., Saddiqi, O. and Pinna-Jamme, R.. (2015). Post-rift history of the eastern Central Atlantic passive margin: insights from the Saharan region of South Morocco: Solid Earth, 120, p. 4645–4666. doi:10.1002/2014JB011549

Leroy, M., Gueydan, F. and Dauteuil, O.. (2008). Uplift and strength evolution of passive margins inferred from 2-D conductive modelling: Geophysical Journal International, 172, p. 464–476. doi:10.1111/j.1365-246X.2007.03566.x

Lorenz, J.C.. (1988). Synthesis of Late Paleozoic and Triassic redbed sedimentation in Morocco. In: The Atlas System of Morocco Springer, p. 139–168.

Luber, T.. (2017). Integrated Analysis of Lower Cretaceous Stratigraphy and depositional systems: The Essaouira-Agadir basin of Morocco: University of Manchester, Ph.D. Thesis, 257 p.

Lundin, E.R. and Doré, A.G.. (2017). The Gulf of Mexico and Canada Basin: Genetic Siblings on Either Side of North America: GSA Today, 27, p. 4–11. doi:10.1130/GSATG274A.1

Luth, S.W. and Willingshofer, E.. (2008). Mapping of the post-collisional cooling history of the Eastern Alps: Swiss Journal of Geosciences, 101, p. 207–223. doi:10.1007/s00015-008-1294-9

Mader, N.K., Redfern, J. and El Ouataoui, M.. (2017). Sedimentology of the Essaouira Basin (Meskala Field) in context of regional sediment distribution patterns during upper Triassic pluvial events: Journal of African Earth Sciences, 130, p. 293–318. doi:10.1016/j.jafrearsci.2017.02.012

Mahammed, F., Läng, E., Mami, L., Mekahli, L., Benhamou, M., Bouterfa, B., Kacemi, A., Chérief, S.-A., Chaouati, H. and Taquet, P.. (2005). The ‘giant of Ksour’, a Middle Jurassic sauropod dinosaur from Algeria: Comptes Rendus Palevol, 4, p. 707–714. doi:10.1016/j.crpv.2005.07.001

Malaval, M.. (2016). Enregistrement sédimentaire de l'activité diapirique associée à la ride du Jbel Azourki, Haut Atlas central, Maroc: impact sur la géométrie des dépôts et la distribution des faciès des systèmes carbonatés et mixtes du Jurassique inférieur: PhD Thesis, Universite Bordeaux 3.

Manspeizer, W., Puffer, J.H. and Cousminer, H.L.. (1978). Separation of Morocco and eastern North America: A Triassic-Liassic stratigraphic record: Geological Society of America Bulletin, 89, p. 901–920. doi:10.1130/0016-7606(1978)89<901:SOMAEN>2.0.CO;2

Malusà, M.G., Polino, R., Feroni, A.C., Ellero, A., Ottria, G., Baidder, L. and Musumeci, G.. (2007). Post-Variscan tectonics in eastern Anti-Atlas (Morocco): Terra Nova, 19, p. 481–489. 10.1111/j.1365-3121.2007.00775.x

Malusà, M.G., Danisik, M., Kuhlemann, J.. (2016). Tracking the Adriatic-slab travel beneath the Tethyan margin of Corsica-Sardinia by low-temperature thermochronology: Gondwana Research, 31, p. 135-149. 10.1016/j.gr.2014.12.011

Malusà, M.G., Fitzgerald, P.G.. (2019a). Fission-Track Thermochronology and its Application to Geology: Springer Textbooks in Earth Sciences, Geography and Environment. Springer, Cham, 393 p.. 10.1007/978-3-319-89421-8

Malusà, M.G., Fitzgerald, P.G.. (2019b). From Cooling to Exhumation: Setting the Reference Frame for the Interpretation of Thermochronologic Data. In: Malusà M., Fitzgerald P. (eds). Fission-Track Thermochronology and its Application to Geology: Springer Textbooks in Earth Sciences, Geography and Environment. Springer, Cham , p. 147-164.

Mansour, E.M.. (1991). Thermochronologie par la méthode des traces de fission dans l'apatite. Application aux massifs de l'Argentera-Mercantour (Alpes occidentales) et des Jebilet (Meseta marocaine): Université Joseph-Fourier - Grenoble I, PhD Thesis, 197 p.

Marivaux, L., Adnet, S., Benammi, M., Tabuce, R. and Benammi, M.. (2017). Anomaluroid rodents from the earliest Oligocene of Dakhla, Morocco, reveal the long-lived and morphologically

conservative pattern of the Anomaluridae and Nonanomaluridae during the Tertiary in Africa: Journal of Systematic Palaeontology, 15, p. 539–569. doi:10.1080/14772019.2016.1206977

Marzoli, A., Davies, J.H.F.L., Youbi, N., Merle, R., Corso, J.D., Dunkley, D.J., Fioretti, A.M., Bellieni, G., Medina, F., Wotzlaw, J.-F., McHone, G., Font, E. and Bensalah, M.K.. (2017). Proterozoic to Mesozoic evolution of North-West Africa and Peri-Gondwana microplates: Detrital zircon ages from Morocco and Canada: Lithos, 278, p. 1–44. 10.1016/j.lithos.2017.01.016

Matenco, L., Andriessen, P. and Network, T.S.. (2013). Quantifying the mass transfer from mountain ranges to deposition in sedimentary basins: Source to sink studies in the Danube Basin–Black Sea system: Global and Planetary Change, 103, p. 1–18. doi:10.1016/j.gloplacha.2013.01.003

Matte, P.. (2001). The Variscan collage and orogeny (480–290 Ma) and the tectonic definition of the Armorica microplate: A review: Terra Nova, 13, p. 122–128. doi:10.1046/j.1365-3121.2001.00327.x

Matton, G. and Jébrak, M.. (2009). The Cretaceous Peri-Atlantic Alkaline Pulse (PAAP): Deep mantle plume origin or shallow lithospheric break-up?: Tectonophysics, 469, p. 1–12. doi:10.1016/j.tecto.2009.01.001

Mazzoli, S., Ascione, A., Buscher, J.T., Pignalosa, A., Valente, E. and Zattin, M.. (2014). Low-angle normal faulting and focused exhumation associated with late Pliocene change in tectonic style in the southern Apennines (Italy): Tectonics, 33, p. 1802–1818. Doi:

10.1002/2014TC003608

Mazzoli, S., Jankowski, L., Szaniawski, R. and Zattin, M.. (2010). Low-T thermochronometric evidence for post-thrusting (<11 Ma) exhumation in the Western Outer Carpathians, Poland: Comptes Rendus Geoscience, 342, p. 162–169. doi:10.1016/j.crte.2009.11.001

Mekahli, L., Elmi, S. and Benhamou, M.. (2004). Biostratigraphy, sedimentology and tectono-eustatic events of the Lower and Middle Jurassic of the Ksour Mountains (Western Saharian Atlas, Southern Algeria): International Geological Congress, 32, Florence.

Merino-Tomé, Ó., Della Porta, G., Pierre, A. and Kenter, J.A.. (2017). Intact seismic-scale platforms and ramps in the Lower to Middle Jurassic of Morocco: Implications for stratal anatomy and lithofacies partitioning: AAPG Bulletin, 101, p. 205–513. doi:10.1306/011817DIG17029

Michard, A., Saddiqi, O., Chalouan, A. and de Lamotte, D.F.. (2008). Continental Evolution: The Geology of Morocco: Springe, 424 p.

Michard, A., Soulaimani, A., Hoepffner, C., Ouanaimi, H., Baidder, L., Rjimati, E.C. and Saddiqi, O.. (2010). The South-Western Branch of the Variscan Belt: Evidence from Morocco: Tectonophysics, 492, p. 1–24. Doi: 0.1016/j.tecto.2010.05.021

Michard, A., Ibouh, H. and Charrière, A.. (2011). Syncline-topped anticlinal ridges from the High Atlas: a Moroccan conundrum, and inspiring structures from the Syrian Arc, Israel: Terra Nova, 23, p. 314–323. doi:10.1111/j.1365-3121.2011.01016.x

Middlemiss, F.A., 1980. Lower Cretaceous Terebratulidae from south-western Morocco and their biogeography: Palaeontology, 23, p. 515–556.

Miles, P., Bouysse, P., and De Souza, K.. (2012). Structural Map of the Atlantic Ocean, CCGM-CGMW.

Missenard, Y.. (2006). Le relief des Atlas Marocains: Contribution des processus asthénosphériques et du raccourcissement crustal, aspects chronologiques: Université de Cergy Pontoise, Ph.D. Thesis, 236 p.

Missenard, Y. and Cadoux, A.. (2011). Can Moroccan Atlas lithospheric thinning and volcanism be induced by Edge-Driven Convection?: Terra Nova, 24, p. 27–33. doi:10.1111/j.1365-3121.2011.01033.x

Monbaron, M.. (1978). New Occurrences Of Big Dinosaurian Bones In The Jurassic-Cretaceous Basin Of Taguelft (Atlas Of Beni-mellal, Morocco): Comptes Rendus Hebdomadaires Des Seances De L'Academie Des Sciences, 287, P. 1277–1279.

Monbaron, M. and Taquet, P.. (1981). Découverte du squelette complet d'un grand Cétiosaure (Dinosaure Sauropode) dans le bassin jurassique moyen de Tilougguit (Haut-Atlas central, Maroc): Compte Rendu de l'Academie des Sciences de Paris, 292, p. 243–246.

Montero, P., Haissen, F., Mouttaqi, A., Molina, J.F., Errami, A., Sadki, O., Cambeses, A. and Bea, F.. (2016). Contrasting SHRIMP U–Pb zircon ages of two carbonatite complexes from the peri-cratonic terranes of the reguibat shield: Implications for the lateral extension of the West African craton: Gondwana Research, 38, p. 238–250. doi:10.1016/j.gr.2015.12.005

Moragas, M. , Vergés, J. , Saura, E. , Martín-Martín, J. , Messager, G. , Merino-Tomé, Ó. , Suárez-Ruiz, I. , Razin, P. , Grélaud, C. , Malaval, M. , Joussiaume, R. and Hunt, D. W.. (2018). Jurassic rifting to post-rift subsidence analysis in the Central High Atlas and its relation to salt diapirism: Basin Research, 30, 336-362. doi:10.1111/bre.12223

Mourlot, Y., Roddaz, M., Dera, G., Calvès, G., Kim, J.-H., Chaboureau, A.-C., Mounic, S., Raisson, F.. (2018). Geochemical evidence for large-scale drainage reorganization in Northwest Africa during the Cretaceous. Geochemistry, Geophysics, Geosystems, 19, 1690– 1712. 10.1029/2018GC007448

Mulder, E.W., Bardet, N., Godefroit, P. and Jagt, J.W.. (2000). Elasmosaur remains from the Maastrichtian type area, and a review of latest Cretaceous elasmosaurs (Reptilia, Plesiosauroidea): Bulletin de l'Institut royal des Sciences naturelles de Belgique, 70, p. 161–178.

Najih, A., Montero, P., Verati, C., Charaf Chabou, M., Fekkak, A., Baidder, L., Ezzouhairi, H., Bea F., Michard A.. (2019). Initial Pangean rifting north of the West African Craton: Insights from late Permian U-Pb and 40Ar/39Ar dating of alkaline magmatism from the Eastern Anti-Atlas (Morocco): Journal of Geodynamics, 132, doi:10.1016/j.jog.2019.101670.

Nemčok, M., Stuart, C., Segall, M.P. and Allen, R.B.. (2005). Structural development of southern Morocco: Interaction of tectonics and deposition: Annual Bob F. Perkins Research Conference, 25, Houston p. 151–202.

Nouri, J., Díaz-Martínez, I. and Pérez-Lorente, F.. (2011). Tetradactyl Footprints of an Unknown Affinity Theropod Dinosaur from the Upper Jurassic of Morocco (C. Lalueza-Fox, Ed.): PLoS ONE, 6, p. e26882–7. doi:10.1371/journal.pone.0026882

Ouajhain, B., Daoudi, L., Laduron, D., Rocha, F. and Naud, J.. (2011). Jurassic Clay Mineral Sedimentation Control Factors in the Essaouira Basin (Western High Atlas, Morocco): Geologica Belgica, 14, p. 129–141.

Oujidi, M. and Elmi, S.. (2000). Evolution de l'architecture des monts d'Oujda (Maroc oriental) pendant le Trias et au debut du Jurassique : Bulletin de la Société géologique de France, 171, pp.169-179. doi:10.2113/171.2.169

Oukassou, M., Charrière, A., Lagnaoui, A., Gibb, S., Michard, A. and Saddiqi, O.. (2016). First occurrence of the Ichnogenus Selenichnites from the Middle Jurassic Strata of the Skoura Syncline

(Middle Atlas, Morocco). Palaeoecological and palaeoenvironmental context: Comptes Rendus Palevol, 15, p. 461–471. doi:10.1016/j.crpv.2015.09.013

Oukassou, M., Saddiqi, O., Barbarand, J., Sebti, S., Baidder, L. and Michard, A.. (2013). Post-Variscan exhumation of the Central Anti-Atlas (Morocco) constrained by zircon and apatite fission-track thermochronology: Terra Nova, 25, p. 151–159. doi:10.1111/ter.12019

Ourribane, M., Chellai, E.H. and Zaghbib-Turki, D.. (2000). Rôle des microbialites et des «micro-encroûtants» dans la lithification récifale: Exemples du Jurassique supérieur de l'Atlas maghrébin (Maroc et Tunisie): Comptes Rendus de l'Académie des Sciences, 330, p. 407–414. Doi : 10.1016/S1251-8050(00)00157-9

Pagel, M., Barbarand, J., Beaufort, D., Gautheron, C. and Pironon, J.. (2014). Bassins sédimentaires Les marqueurs de leur histoire thermique: Ed Sciences, Société Géologique de France, 226 p.

Piqué, A., Soulaimani, A., Laville, E., Amrhar, M., Bouabdelli, M., Hoepffner, C. and Chalouan, A.. (2006). Géologie du Maroc: Editions Geode, 287 p.

Pratt, J.R., Barbeau, D.L., Jr., Garver, J.I., Emran, A. and Izykowski, T.M.. (2015). Detrital Zircon Geochronology of Mesozoic Sediments in the Rif and Middle Atlas Belts of Morocco: Provenance Constraints and Refinement of the West African Signature: The Journal of Geology, 123, p. 177–200. doi:10.1086/681218

Rage, J.-C.. (1976). Les Squamates du Miocène de Beni Mellal, Maroc: Géologie méditerranéenne, 3, p. 57–69.

Rage, J.-C. and Wouters, G.. (1979). Découverte du plus ancien Palaeopheidé (Reptilia, Serpentes) dans le Maestrichtien du Maroc: Geobios, 12, p. 293–296.

Ranke, U., Rad, von, U. and Wissmann, G.. (1982). Stratigraphy, Facies and Tectonic Development of the On- and Offshore Aaiun-Tarfaya Basin — A Review. In: Geology of the Northwest African Continental Margin, Springer, p. 86–105.

Romagny, A., Münch, P., Cornée, J.J., Corsini, M., Azdimousa, A., Melinte-Dobrinescu, M.C., Drinia, H., Bonno, M., Arnaud, N., Monié, P., Quillévéré, F. and Ben Moussa, A.. (2014). Late Miocene to present-day exhumation and uplift of the Internal Zone of the Rif chain: Insights from low-temperature thermochronometry and basin analysis: Journal of Geodynamics, 77, p. 39–55. doi:10.1016/j.jog.2014.01.006

Ruiz, G.M.H., Sebti, S., Negro, F., Saddiqi, O., Frizon de Lamotte, D., Stockli, D., Foeken, J., Stuart, F., Barbarand, J. and Schaer, J.P.. (2011). From central Atlantic continental rift to Neogene uplift - western Anti-Atlas (Morocco): Terra Nova, 23, p. 35–41. doi:10.1111/j.1365-3121.2010.00980.x

Sabil, N.. (1995). La datation par traces de fission: Aspects méthodologiques et applications thermochronologiques en contexte alpin et de marge continentale: Université de Grenoble, Ph.D. Thesis, 245 p.

Saddiqi, O., Haimer, El, F.Z., Michard, A., Barbarand, J., Ruiz, G.M.H., Mansour, E.M., Leturmy, P. and de Lamotte, D.F.. (2009). Apatite fission-track analyses on basement granites from south-western Meseta, Morocco: Paleogeographic implications and interpretation of AFT age discrepancies: Tectonophysics, 475, p. 29–37. doi:10.1016/j.tecto.2009.01.007

Saint-Martin, J.-P.. (1990). Les formations récifales coralliennes du Miocène supérieur d'Algérie et du Maroc: Mémoires du Muséum National d'Histoires Naturelles de Paris, 56, p. 1–373.

Salles, T., Flament, N. and Müller, D.. (2017). Influence of mantle flow on the drainage of eastern Australia since the Jurassic Period: Geochemistry Geophysics Geosystems, 18, p. 280–305. doi:10.1002/2016GC006617

Samaka, F. and Bouhaddioui, D.. (2003). Evaluation du Potentiel Petrolier du Bassin de Souss et de l'Offshore d'Agadir: ONHYM, Rapport inédit, 34 p.

Sanders, M.T., Bardin, J., Benzaggagh, M. and Cecca, F.. (2015). Early Toarcian (Jurassic) belemnites from northeastern Gondwana (South Riffian ridges, Morocco): Paläontologische Zeitschrift, 89, p. 51–62. doi:10.1007/s12542-013-0214-0

Schneider, D.A., Issler, D.R.. (2019). Application of Low-Temperature Thermochronology to Hydrocarbon Exploration. In: Malusà M., Fitzgerald P. (eds) Fission-Track Thermochronology and its Application to Geology. Springer Textbooks in Earth Sciences, Geography and Environment. Springer, Cham, p. 315-333.

Sebti, S.. (2011). Mouvements verticaux de l'Anti-Atlas occidental marocain (Kerdous & Ifni): Thermochronologie par traces de fission: Université Hassan II, Ph.D. Thesis, 172 p.

Sehrt, M.. (2014). Variscan to Neogene long-term landscape evolution at the Moroccan passive continental margin (Tarfaya Basin and western Anti-Atlas): University of Heidelberg, Ph.D. Thesis, 174 p.

Sehrt, M., Glasmacher, U.A., Stockli, D.F., Jabour, H. and Kluth, O.. (2017b). Meso-/Cenozoic long-term landscape evolution at the southern Moroccan passive continental margin, Tarfaya Basin, recorded by low-temperature thermochronology: Tectonophysics, 717, p. 499–518. doi:10.1016/j.tecto.2017.08.028

Sehrt, M., Glasmacher, U.A., Stockli, D.F., Jabour, H. and Kluth, O.. (2017a). The southern Moroccan passive continental margin: An example of differentiated long-term landscape evolution in Gondwana: Gondwana Research, 53, p. 129–144. doi:10.1016/j.gr.2017.03.013

Segev, A.. (2002). Flood basalts, continental breakup and the dispersal of Gondwana: evidence for periodic migration of upwelling mantle flows (plumes): EGU Stephan Mueller Special Publication Series, 2, p. 171-191.

Scotese, C. R.. (2012). The Paleomap Project: www.scotese.com.

Sibuet, J.-C., Rouzo, S., Srivastava, S., Dehler, S., Deptuck, M. and Karim, A.. (2012). Plate tectonic reconstructions and paleogeographic maps of the central and North Atlantic oceans: Canadian Journal of Earth Sciences, 49, p. 1395–1415. doi:10.1139/e2012-071

Sloss, L.L. and Scherer, W.. (1975) Geometry of Sedimentary Basins: Applications to Devonian of North America and Europe, in: Whitten, E.H.T.. Quantitative Studies in the Geological Sciences, Geological Society of America Memoir, 142, p. 71-88. doi:10.1130/MEM142-p71

Stampfli, G.M. and Borel, G.D.. (2002). A plate tectonic model for the Paleozoic and Mesozoic constrained by dynamic plate boundaries and restored synthetic oceanic isochrons: Earth and Planetary Science Letters, 196, p. 17–33. doi:10.1016/S0012-821X(01)00588-X

Steiner, C., Hobson, A., Favre, P., Stampfli, G.M. and Hernandez, J.. (1998). Mesozoic sequence of Fuerteventura (Canary Islands): Witness of Early Jurassic sea-floor spreading in the central Atlantic: Geological Society of America Bulletin, 110, p. 1304–1317. doi:10.1130/0016-7606(1998)110<1304:MSOFCI>2.3.CO;2

Stets, J.. (1992). Mid-Jurassic events in the western High Atlas (Morocco): Geologische Rundschau, 81, p. 69–84. doi:10.1007/BF01764540

Sømme, T.O., Helland-Hansen, W., Martinsen, O.J. and Thurmond, J.B.. (2009). Relationships between morphological and sedimentological parameters in source-to-sink systems: A basis for predicting semi-quantitative characteristics in subsurface systems: Basin Research, 21, p. 361–387. doi:10.1111/j.1365-2117.2009.00397.x

Tabuce, R., Adnet, S., Cappetta, H., Noubhani, A. and Quillevere, F.. (2005). Aznag (Ouarzazate basin, Morocco), a new African middle Eocene (Lutetian) vertebrate-bearing locality with selachians and mammals: Bulletin de la Société Géologique de France, 176, p. 381–400. doi:10.2113/176.4.381

Tari, G. and Jabour, H.. (2013). Salt tectonics along the Atlantic margin of Morocco: Geological Society, London, Special Publications, 369, p. 337–353. doi:10.1144/SP369.23

Teixell, A., Arboleya, M.-L., Julivert, M. and Charroud, M.. (2003). Tectonic shortening and topography in the central High Atlas (Morocco): Tectonics, 22, TC1051. doi:10.1029/2002TC001460

Teixell, A., Ayarza, P., Zeyen, H., Fernandez, M. and Arboleya, M.-L.. (2005). Effects of mantle upwelling in a compressional setting: The Atlas Mountains of Morocco: Terra Nova, 17, p. 456–461. doi:10.1111/j.1365-3121.2005.00633.x

Teixell, A., Bertotti, G., de Lamotte, D.F. and Charroud, M.. (2009). The geology of vertical movements of the lithosphere: An overview: Tectonophysics, 475, p. 1–8. doi:10.1016/j.tecto.2009.08.018

Hssaida, T., Chahidi, S., Benzaggagh, M., Riding, J.B. and Oumalch, F.. (2014). Associations de kystes de dinoflagellés des séries du Jurassique supérieur (Oxfordien–Tithonien) du Rif externe (Prérif interne et Mésorif, Maroc) et comparaisons régionales: Annales de paleontologie, 100, p. 327–342. Doi : 10.1016/j.annpal.2014.03.001

Trappe, J.. (1991). Stratigraphy, facies distribution and paleogeography of the marine Paleogene from the Western High Atlas, Morocco: Neues Jahrbuch für Geologie und Paläontologie, 180, p. 279–321.

van den Bogaard, P.. (2013). The origin of the Canary Island Seamount Province - New ages of old seamounts: Scientific Reports, 3, 21077. doi:10.1038/srep02107

van der Beek, P., Mbede, E., Andriessen, P. and Delvaux, D.. (1998). Denudation history of the Malawi and Rukwa Rift flanks (East African Rift System) from apatite fission track thermochronology: Journal of African Earth Sciences, 26, p. 363–385. doi:10.1016/S0899-5362(98)00021-9

Verati C., Rapaille R., Feraud G., Marzoli A., Bertrand H., Youbi N.. (2007). $^{40}Ar/^{39}Ar$ ages and duration of the Central Atlantic Magmatic Province volcanism in Morocco and Portugal and its relation to the Triassic-Jurassic boundary : Palaeogeography, Palaeoclimatology, Paleoecology, 244, p. 308-325. doi:10.1016/j.palaeo.2006.06.033

Vermeesch, P. and Tian, Y.. (2014). Thermal history modelling: HeFTy vs. QTQt: Earth Science Reviews, 139, p. 279–290. doi:10.1016/j.earscirev.2014.09.010

Wang, J.. (2018). Controls on the organic-rich mudstones development across the Cenomanian-Turonian Oceanic Anoxic Event (OAE2) in Moroccan Basins: PhD Thesis, University of Manchester, 248p.

Wildman, M., Brown, R., Watkins, R., Carter, A., Gleadow, A. and Summerfield, M.. (2015). Post break-up tectonic inversion across the southwestern cape of South Africa: New insights from apatite and zircon fission track thermochronometry: Tectonophysics, 654, p. 30–55. doi:10.1016/j.tecto.2015.04.012

Wildman, M., Cogné, N., Beucher, R.. (2019). Fission-Track Thermochronology Applied to the Evolution of Passive Continental Margins. In: Malusà M., Fitzgerald P. (eds) Fission-Track Thermochronology and its Application to Geology. Springer Textbooks in Earth Sciences, Geography and Environment. Springer, Cham, p. 351-371.

Wipf, M., Glasmacher, U.A., Stockli, D.F., Emmerich, A., Bechstädt, T. and Baur, H.. (2009). Reconstruction of the differentiated long-term exhumation history of Fuerteventura, Canary Islands, Spain, through fission-track and (U-Th–Sm)/He data: International Journal of Earth Sciences, 99, p. 675–686. doi:10.1007/s00531-008-0415-z

Withjack, M.O. and Schlische, R.W.. (2005). A Review of Tectonic Events on the Passive Margin of Eastern North America: Bob S. Perkins Research Conference, 25, Houston, p. 203–235.

Wold, C.N. and Hay, W.W.. (1990). Estimating Ancient Sediment Fluxes: American Journal of Science, 290, p. 1069–1089. doi:10.2475/ajs.290.9.1069

Wrtiti, M.E., Broutin, J., Freytet, P., Larhrib, M. and Toutin-Morin, N.. (1990). Continental deposits in Permian basins of the Mesetian Morocco, geodynamic history: Journal of African Earth Sciences, 10, p. 361–368. doi:10.1016/0899-5362(90)90067-O

Yamato, P., Husson, L., Becker, T.W. and Pedoja, K.. (2013). Passive margins getting squeezed in the mantle convection vice: Tectonics, 32, p. 1559–1570. doi:10.1002/2013TC003375

Ye, J.. (2016). Evolution topographique, tectonique et sédimentaire syn- à post-rift de la marge transformante ouest africaine : GET Toulouse, PhD Thesis, 273 p.

Ye, J., Chardon, D., Rouby, D., Guillocheau, F., Dall'asta, M., Ferry, J.-N. and Broucke, O.. (2017). Paleogeographic and structural evolution of northwestern Africa and its Atlantic margins since the early Mesozoic: Geosphere, 13, p. 1254-1284. doi:10.1130/GES01426.1

Zarhloule, Y.. (2004). Le gradient géothermique profond du Maroc: Détermination et cartographie: Bulletin de l'Institut Scientifique de Rabat, 26, p. 11–25.

Zeyen, H., Ayarza, P., Fernàndez, M., and Rimi, A.. (2005). Lithospheric structure under the western African-European plate boundary: A transect across the Atlas Mountains and the Gulf of Cadiz. Tectonics, 24, TC2001. doi:10.1029/2004TC001639

Zouhri, S., Gingerich, P.D., Elboudali, N., Sebti, S., Noubhani, A., Rahali, M. and Meslouh, S.. (2014). New marine mammal faunas (Cetacea and Sirenia) and sea level change in the Samlat Formation, Upper Eocene, near Ad-Dakhla in southwestern Morocco: Comptes Rendus Palevol, 13, p. 599–610. doi:10.1016/j.crpv.2014.04.002

Zouhri, S., Kchikach, A., Saddiqi, O., Haimer, El, F.Z., Baidder, L. and Michard, A.. (2008). The Cretaceous-tertiary plateaus. In: Continental Evolution: The Geology of Morocco, Springer, p. 331–3

Tables

t-T modelling studies	Locations	Stratigraphic age (sample)	t-T modelling software	t-T models (n=117)	Failed to meet conditions					t-depth models (n=56)	Comments
					i	ii	iii	iv	v		
Sabil, 1995	Meseta	Palaeozoic	Gallagher et al. (1993)	4	.	4	.	.	.	0	*Program:* Gallagher et al, 1993
Barbero *et al.,* 2007	High Atlas	Pal-Meso-Ceno	AFT-Solve	3							*t-T:* no best-fit or weighted average
Malusa *et al.,* 2007	Anti-Atlas	PC-Pal	HeFTy	3	.	.	.	.	3	0	*Anti-Atlas:* no Mesozoic vertical movements
Ghorbal *et al.,* 2008	Meseta	Palaeozoic	HeFTy	4	.	.	.	.	.	4	*All conditions are met*
Balestrieri *et al.,* 2009	Anti-Atlas	Precambrian	HeFTy	2	.	.	.	.	2	0	*Anti-Atlas:* E.Cretaceous exhumation
Ghorbal , 2009	High Atlas	Pc-Pal-Meso	HeFTy	23	1	.	.	.	4	18	*t-T:* younger than 20Ma; *Anti-Atlas:* E.Cretaceous exhumation
Saddiqi *et al.,* 2009	Meseta	Palaeozoic	AFT-Solve	4	.	.	.	.	.	4	*All conditions are met*
Barbero *et al.,* 2011	Meseta	Palaeozoic	HeFTy	5	.	.	.	.	.	5	*All conditions are met*
Ruiz *et al.,* 2011	Anti-Atlas	Precambrian	HeFTy	5	.	.	.	.	5	0	*Anti-Atlas:* E.Cretaceous exhumation
Sebti, 2011	Anti-Atlas	Precambrian	HeFTy	4	.	.	.	.	4	0	*Anti-Atlas:* E.Cretaceous exhumation
Azdimousa *et al.,* 2013	Rif	Palaeozoic	HeFTy	2	1	.	.	.	.	1	*t-T:* younger than 20Ma
Lepretre *et al.,* 2013	Reguibat Shield	Precambrian	HeFTy	4	.	.	4	.	.	0	*t-T:* corrected models in Lepretre, 2015
Oukassou *et al.,* 2013	Anti-Atlas	Precambrian	HeFTy	2	.	.	.	.	2	0	*Anti-Atlas:* E.Cretaceous exhumation
ElHaimer, 2014	Massif Ancien	Palaeozoic	HeFTy	1							*t-T:* no best-fit or weighted average
Romagny *et al.,* 2014	Rif	Palaeozoic	QTQt	2	1	.	.	.	.	1	*t-T:* younger than 20Ma
Sehrt, 2014	Tarfaya and Anti-Atlas	Meso-Ceno and Precambrian	HeFTy	24	.	.	.	.	14	2	*t-T:* results from wells; *Anti-Atlas:* E.Cretaceous exhumation
Domenech, 2015	Massif Ancien	PC-Pal	QTQt	3	.	.	.	3	.	0	*t-T:* modelled for vertical profiles
Lepretre, 2015	Reguibat Shield	Precambrian	QTQt	14	.	.	.	.	1	13	*Anti-Atlas:* E.Cretaceous exhumation
Gouiza *et al.,* 2017	Anti-Atlas	Precambrian	HeFTy	6	.	.	.	.	.	6	*All conditions are met*
Charton *et al.,* 2018	Anti-Atlas	PC-Meso	HeFTy	2	.	.	.	.	.	2	*All conditions are met*

Table 1. Selection of t-T models for temperature-to-depth conversion and for exhumation and subsidence rate calculations. Conditions: The t-T modelling results had to i) start before 20Ma, ii) be based on HeFTy, AFT solve or QTQt results, iii) for different models based on the same LTT data, be from the most recent and published realizations, iv) should be based on one sample (as opposed to vertical profiles), and v) be compatible with the geological evidences discussed in the text.

			Periods [-]						
			a	***b***	***c***	***d***	***e***	***f***	***g***
Eroded material fluxes [10^3 km^3/Myr]	Interpolation Grid	| preferred scenario	21.6	1.8	22.8	15.7	5.5	11.6	28.7
		| constant geotherm (20ºC/km)	23.6	3.8	29.3	19.3	6.9	14.0	33.5
		| constant geotherm (40ºC/km)	20.7	1.9	14.6	9.6	3.4	6.9	17.0
	Meseta & High Atlas		2.3	0.1	0.6	0.7	0.2	0.1	1.3
	Anti-Atlas		3.6	0.6	8.1	1.0	0.9	1.3	3.0
	Reguibat Shield		1.8	0.6	11.5	8.2	1.6	7.6	10.9
Surface area [10^6 km^2]	Exhuming domain		1.6	0.9	1.2	1.2	0.6	1.0	1.3
	Subsiding domain		0.7	1.4	1.1	1.1	1.7	1.3	1.0

Table 2. Eroded material fluxes and surface areas from Permian (**a**) to Neogene (**g**). Preferred scenario for the geotherms is presented in the text. We estimate the error of these fluxes between 20 and 10% (see discussion).

SandS Map	Outcrop Data	Fossil data
Permian (fig. 12)	Wrtiti et al., 1990 | Central Massif Chalouan et al., 2008 | Rif basin	Doubinger, 1956 | Central Massif Broutin et al., 1989 | Argana valley
Triassic (fig. 13)	Brown, 1980 | Argana valley Chalouan et al., 2008 | Rif basin Ouidi and Elmi, 2000 | Hauts Plateaux	Chalouan et al., 2008 | Rif basin Kammerer et al., 2011 | Argana valley Lagnaoui et al., 2016 | Argana valley
Early Jurassic (fig. 14)	Steiner et al., 1998 | Canary Islands Sanders et al., 2015 | Rif basin Merino-Tome et al., 2017 | Eastern High Atlas	Jenny and Jossen, 1982 | Central High Atlas Lee, 1983 |Central High Atlas Beauvais, 1986 | Eastern High Atlas Bourillot et al., 2008 | Central High Atlas
Middle Jurassic (fig. 15)	Ouajhain et al., 2011 | Essaouira-Agadir basin Charriere and Haddoumi, 2016 | Central High Atlas Merino-Tome et al., 2017 | Central High Atlas Benvenuti et al., 2017 | Ouarzazate basin	Monbaron and Taquet, 1981 | Central High Atlas Mahammed et al., 2005 | Eastern High Atlas Haddoumi et al., 2015 | Central High Atlas Oukassou et al., 2016 |Middle Atlas
Late Jurassic (fig. 16)	Fabre et al., 1996 | Taoudeni Steiner et al., 1998 | Canary Islands Mekahli and Benhamou, 2004 | Eastern High Atlas Ouajhain et al., 2011 | Essaouira-Agadir basin Charrière and Haddoumi, 2016 | Central High Atlas Benvenuti et al., 2017 | Ouarzazate basin	Ourribane et al., 2000 | Essaouira-Agadir basin Nouri et al., 2011 | Central High Atlas Touria Hssaida et al., 2014 | Rif basin
(early) Early Cretaceous (fig. 17)	Fabre et al., 1996 | Taoudeni basin Steiner et al., 1998 | Canary Islands Ali et al., 2014 | Tarfaya basin Charrière and Haddoumi, 2016 | Central High Atlas Benzaggagh, 2016 | Rif basin	Monbaron, 1978 | Middle Atlas Middlemiss, 1980 | Essaouira-Agadir basin Benest, 1985 | Rif basin Ettachfini et al., 1998 | Doukkala basin
middle Cretaceous (fig. 18)	Choubert et al., 1966 | Tindouf basin Fabre et al., 1996 | Taoudeni basin Steiner et al., 1998 | Canary Islands Aquit et al., 2013 | Tarfaya basin Benyoucef et al., 2015 | Guir Hamada	Dhondt et al., 1999 | Tarfaya basin Ait Boughrous et al., 2007 | Guir Hamada Cavin et al., 2010 | Kem Kem beds Ibrahim et al., 2014 | Kem Kem beds Benzaggagh et al., 2017 | Rif basin
(mid-late) Late Cretaceous (fig. 19)	Choubert et al., 1966 | Tindouf basin Fabre et al., 1996 | Taoudeni basin Chalouan et al., 2008 | Rif basin Aquit et al., 2013 | Tarfaya basin Arab et al., 2015 | Rif basin	Andreu and Tronchetti, 1994 | Middle Atlas Dhondt et al., 1999 | Tarfaya basin Ambroggi and Lapparent, 1954 | Essaouira-Agadir basin Mulder et al., 2000 | Essaouira-Agadir basin Rage and Wouters, 1979 | Settat basin Hill et al., 2008 | Taoudeni basin
Palaeogene (fig. 20)	Trappe, 1991 | Ouarzazate basin Chalouan et al., 2008 | Rif basin	Tabuce et al., 2005 | Ouarzazate basin Jouve et al., 2005 | Settat basin Gaffney et al., 2006 | Rif basin Adaci et al., 2007 | Kem Kem beds Hill et al., 2008 | Taoudeni basin Zouhri et al., 2014 | Dakhla basin Gingerich and Zouhri, 2015 | Tarfaya basin Marivaux et al., 2017 | Dakhla basin
Neogene (fig. 21)	-	Dartevelle, 1937 | Canary Islands Ennouchi, 1954 | Rif Chevalier and Choubert, 1962 | Safi basin Koeniguer, 1967 | Dakhla Rage, 1976 | Middle Atlas Best and Boekschoten, 1981 | Porto Santo Saint Martin, 1990 | Rif Blain et al., 2013 | Hauts Plateaux

Table 3. References used in this review to construct the SandS maps.

SandS Map	Paleo-reconstruction*	Provenance study
Permian (fig. 12)	Broutin et al., 1998 | Meseta Ellouz et al., 2003 | Atlas Systems Chopin et al., 2014 | Atlas Systems Najih et al., 2019 | N Morocco	-
Triassic (fig. 13)	Ranke et al., 1982 | Tarfaya basin Le Roy, 1997 | Atlantic Shelf Brahim et al., 2002 | Atlas Systems Leleu et al., 2016 | Morocco Benvenuti et al., 2017 | Massif Ancien	Baudon et al., 2009 | Massif Ancien Domenech et al., 2018 | Massif Ancien
Early Jurassic (fig. 14)	Laville and Pique, 1992 | Atlantic Ellouz et al., 2003 | Atlas Systems Elmi et al., 2009 | Rif basin Sibuet et al., 2012 | Atlantic	Domenech et al., 2018 | Western High Atlas
Middle Jurassic (fig. 15)	Ellouz et al., 2003 | Atlas Systems Guiraud et al., 2005 | Morocco Nemčok et al., 2005 | Morocco Frizon de Lamotte et al., 2011 | Tethys	Stets, 1992 | Massif Ancien Pratt et al., 2015 | Middle Atlas
Late Jurassic (fig. 16)	Ranke et al., 1982 | Tarfaya basin Ellouz et al., 2003 | Atlas Systems Nemčok et al., 2005 | Morocco Sibuet et al., 2012 | Atlantic Lepretre et al., 2018 | Rif-Tethys	Stets, 1992 | Rehamna
(early) Early Cretaceous (fig. 17)	Sibuet et al., 2012 | Atlantic Aloui et al., 2012 | Algeria Ye et al., 2017 | Reguibat Shield Luber, 2018 | Essaouira-Agadir basin Gimeno-Vives et al., 2019 | Rif basin	Ali et al., 2014 | Tarfaya basin Leprêtre, 2015 | Reguibat Shield Pratt et al., 2015 | Rif basin Luber, 2018 | Essaouira-Agadir basin
middle Cretaceous (fig. 18)	Guiraud et al., 2005 | Morocco Ye et al., 2017 | Reguibat Shield	Ali et al., 2014 | Tarfaya basin Pratt et al., 2015 | Rif basin Essafraoui et al., 2015 | Massif Ancien Meister et al., 2016 | Kem Kem beds Mourlot et al., 2018 | DSDP wells Azdimousa et al., 2019 | Rif
(mid-late) Late Cretaceous (fig. 19)	Ranke et al., 1982 | Tarfaya basin Fabre et al., 1996 | Taoudeni basin Brahim et al., 2002 | Atlas Systems Sibuet et al., 2012 | Atlantic van den Bogaard, 2013 | Canary Islands Ye et al., 2017 | Reguibat Shield	Ali et al., 2014 | Tarfaya basin Mourlot et al., 2018 | DSDP wells
Palaeogene (fig. 20)	Ranke et al., 1982 | Tarfaya basin Herbig and Trappe, 1994 | Meseta Brahim et al., 2002 | Atlas Systems Guiraud et al., 2005 | Morocco van den Bogaard, 2013 | Canary Islands Lepretre et al., 2018 | Rif system	Azdimousa et al., 2019 | Rif
Neogene (fig. 21)	Ranke et al., 1982 | Tarfaya basin Lepretre et al., 2018 | Rif system	Ali et al., 2014 | Tarfaya basin Azdimousa et al., 2019 | Rif

Table 3 (continued). * Including paleogeography, depositional environment, and stress / structural maps.

Figures

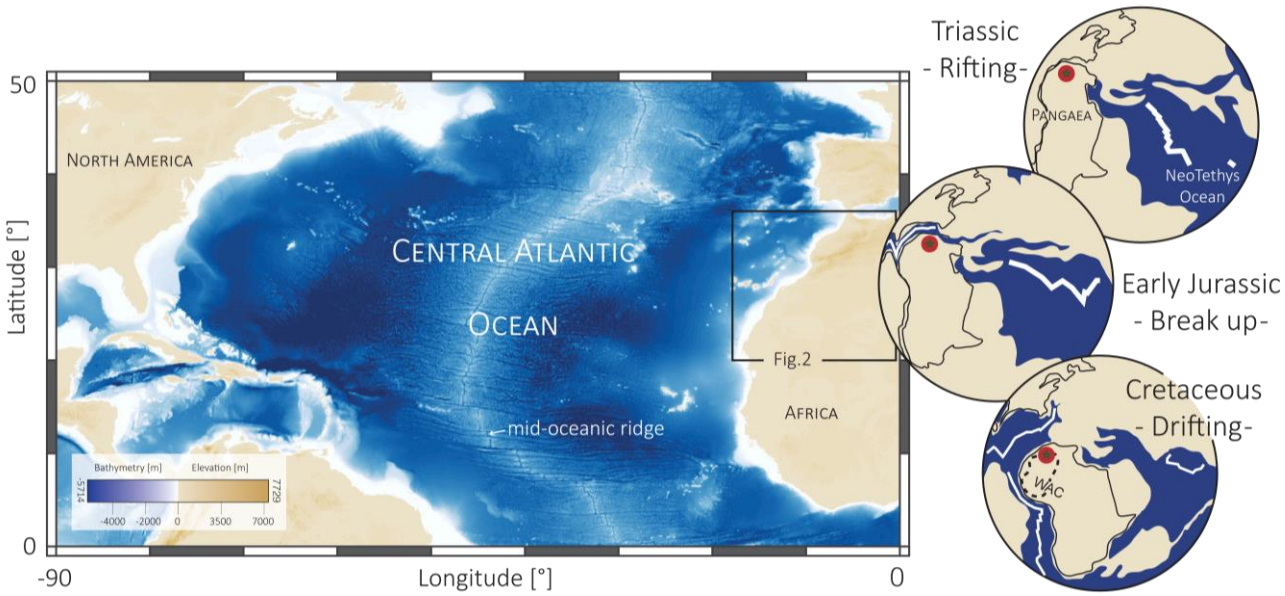

Figure 1. Morphology of the Central Atlantic seafloor and conjugate margins (data: GEBCO_2014_1D). Simplified plate tectonic evolution is after Stampfli and Borel (2002). WAC: Western African Craton.

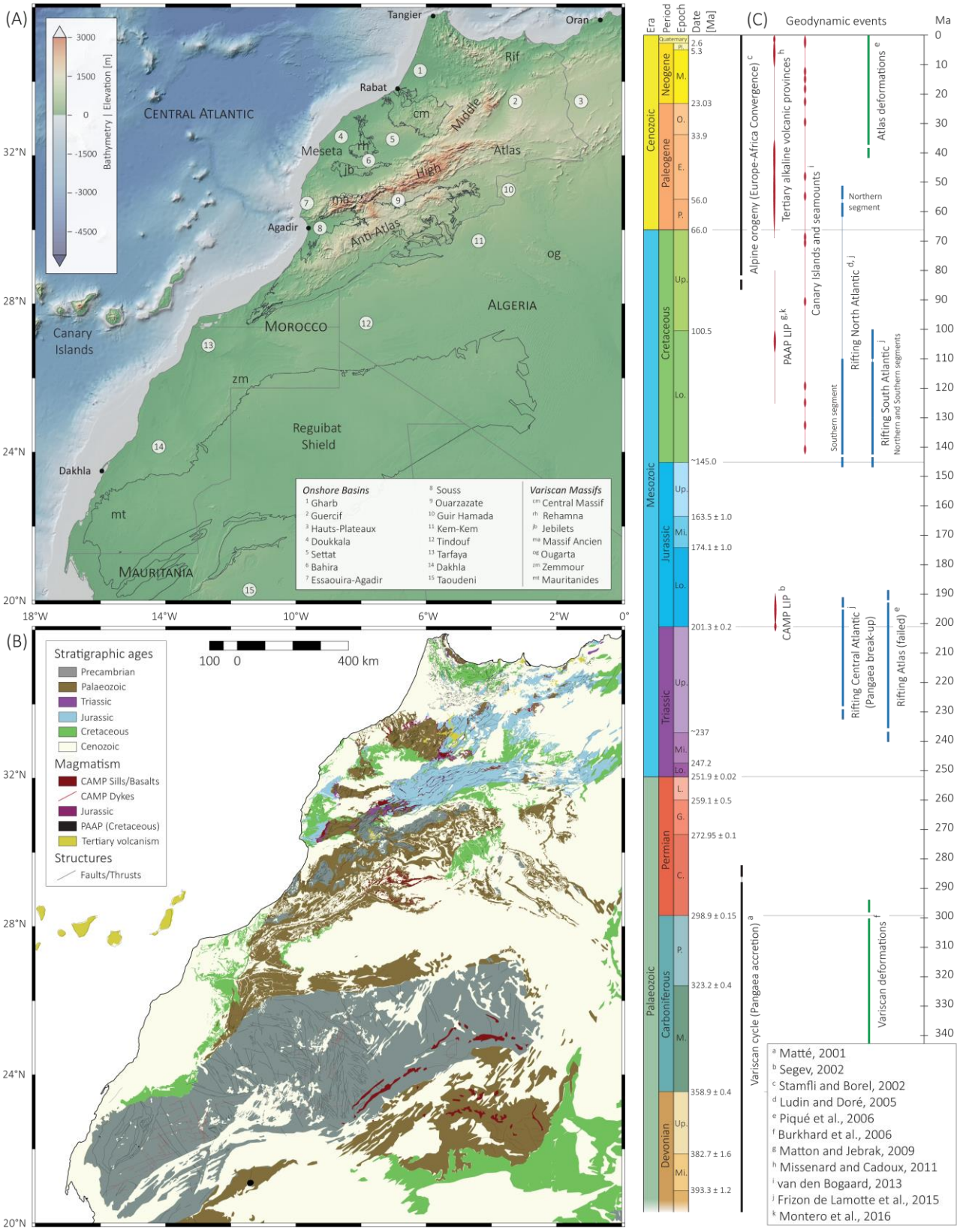
(A)
Tangier
Oran
Rif
Central Atlantic
Rabat
cm
Middle
Atlas
Meseta
rh
jb
High
Atlas
ma
Agadir
Anti-Atlas
og
Algeria
Morocco
Canary
Islands
zm
Reguibat
Shield
Dakhla
mt
Mauritania
Bathymetry | Elevation [m]
3000
1500
0
-1500
-3000
-4500
Onshore Basins
1 Gharb
2 Guercif
3 Hauts-Plateaux
4 Doukkala
5 Settat
6 Bahira
7 Essaouira-Agadir
8 Souss
9 Ouarzazate
10 Guir Hamada
11 Kem-Kem
12 Tindouf
13 Tarfaya
14 Dakhla
15 Taoudeni
Variscan Massifs
cm Central Massif
rh Rehamna
jb Jebilets
ma Massif Ancien
og Ougarta
zm Zemmour
mt Mauritanides
18°W
14°W
10°W
6°W
2°W
0°
32°N
28°N
24°N
20°N
(B)
Stratigraphic ages
Precambrian
Palaeozoic
Triassic
Jurassic
Cretaceous
Cenozoic
Magmatism
CAMP Sills/Basalts
CAMP Dykes
Jurassic
PAAP (Cretaceous)
Tertiary volcanism
Structures
Faults/Thrusts
100 0 400 km
(C) Geodynamic events
Era
Period
Epoch
Date [Ma]
Ma
Cenozoic
Paleogene
Neogene
Quaternary
Pl.
M.
O.
E.
P.
2.6
5.3
23.03
33.9
56.0
66.0
Mesozoic
Cretaceous
Up.
Lo.
100.5
~145.0
Jurassic
Up.
Mi.
Lo.
163.5 ± 1.0
174.1 ± 1.0
201.3 ± 0.2
Triassic
Up.
Mi.
Lo.
~237
247.2
251.9 ± 0.02
Palaeozoic
Permian
L.
G.
C.
259.1 ± 0.5
272.95 ± 0.1
298.9 ± 0.15
Carboniferous
P.
M.
323.2 ± 0.4
358.9 ± 0.4
Devonian
Up.
Mi.
382.7 ± 1.6
393.3 ± 1.2
Alpine orogeny (Europe-Africa Convergence) c
Tertiary alkaline volcanic provinces h
Canary Islands and seamounts i
Atlas deformations e
Northern segment
PAAP LIP g,k
Rifting North Atlantic d, j
Southern segment
Rifting South Atlantic j
Northern and Southern segments
CAMP LIP b
Rifting Central Atlantic j
(Pangaea break-up)
Rifting Atlas (failed) e
Variscan cycle (Pangaea accretion) a
Variscan deformations f
a Matté, 2001
b Segev, 2002
c Stamfli and Borel, 2002
d Ludin and Doré, 2005
e Piqué et al., 2006
f Burkhard et al., 2006
g Matton and Jebrak, 2009
h Missenard and Cadoux, 2011
i van den Bogaard, 2013
j Frizon de Lamotte et al., 2015
k Montero et al., 2016

Figure 2 (previous page). A) Geography of Morocco and its surroundings (data: GEBCO_2014_1D) with main geological domains, sedimentary basins, and Variscan Massifs superimposed. B) Geological map of Morocco and its surroundings (after Hollard et al., 1985). **CAMP**: Central Atlantic Magmatic Province (Triassic); **PAAP**: Peri-Atlantic Alkaline Province (Cretaceous). C) Tectonic chart of the Atlantic realm and Morocco, see references therein (numerical ages after ICS 2016/12). **LIP**: Large Igneous Province; **CAMP**: Central Atlantic Magmatic Province; **PAAP**: Peri-Atlantic Alkaline Pulse.

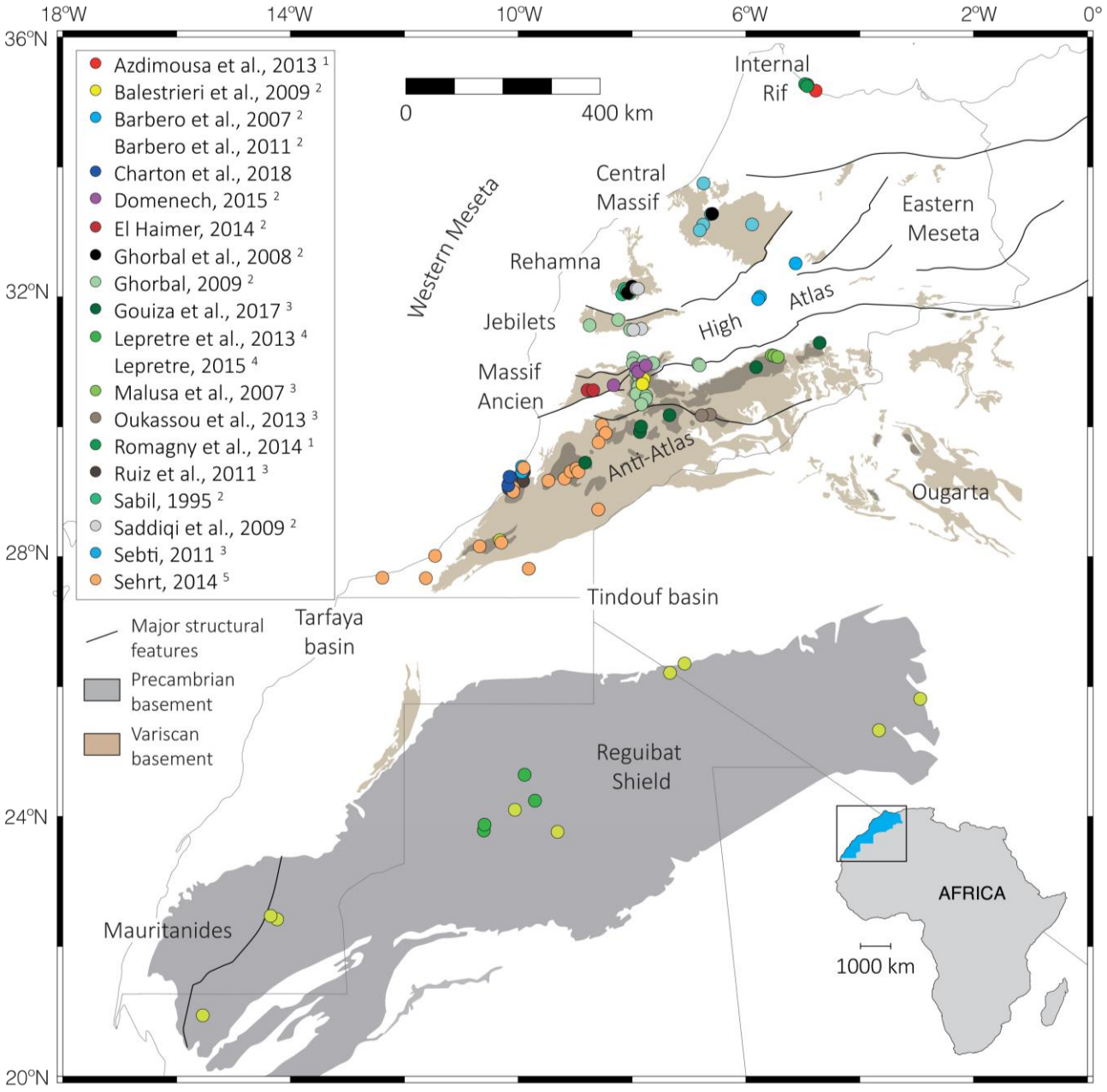

Figure 3. Location of samples used for t-T modelling, located in the Rif[1], the Meseta and High Atlas[2], the Anti-Atlas[3], the Reguibat Shield[4], and the western Anti-Atlas and north Tarfaya Basin[5] (see reference details in table 1).

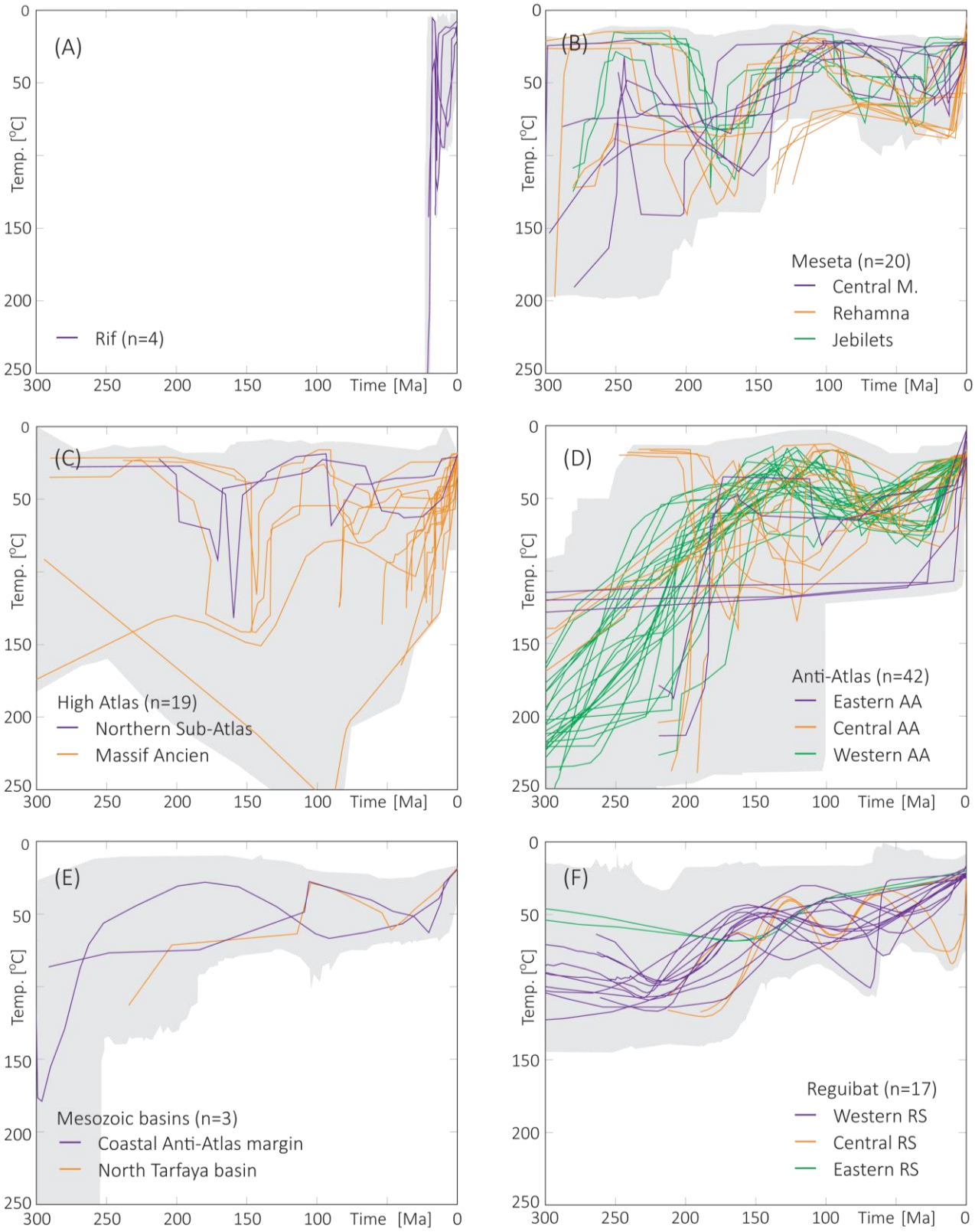
(A)
Rif (n=4)
(B)
Meseta (n=20)
Central M.
Rehamna
Jebilets
(C)
High Atlas (n=19)
Northern Sub-Atlas
Massif Ancien
(D)
Anti-Atlas (n=42)
Eastern AA
Central AA
Western AA
(E)
Mesozoic basins (n=3)
Coastal Anti-Atlas margin
North Tarfaya basin
(F)
Reguibat (n=17)
Western RS
Central RS
Eastern RS
Temp. [°C]
Time [Ma]
0
50
150
200
250
300

Figure 4 (previous page). Digitized t-T modelling weighted averages, best-fit curves, and acceptable envelopes (grey area) for HeFTy results or expected curves, maximum likelihood curves and limits of 2σ confidence level (grey area) for QTQt results (see references in table 1). t-T results for borehole samples from Sehrt (2014), as well as results from El Haimer (2014) and Barbero et al. (2007), for which only envelopes were published, were not included.

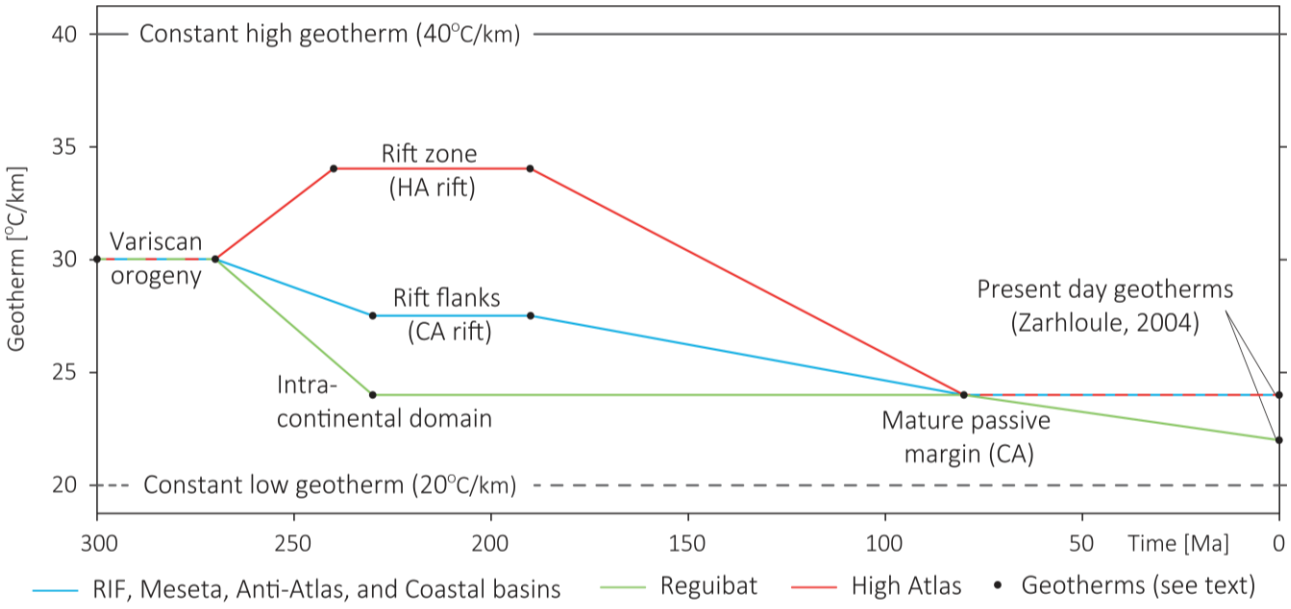

Figure 5. Geothermal gradients used for the depth conversion of the t-T curves. Geotherms: Geothermal gradients documented in literature, from present-day or recent settings similar to ones in Moroccan geological past. See description of the geotherms considered as analogues in the text.

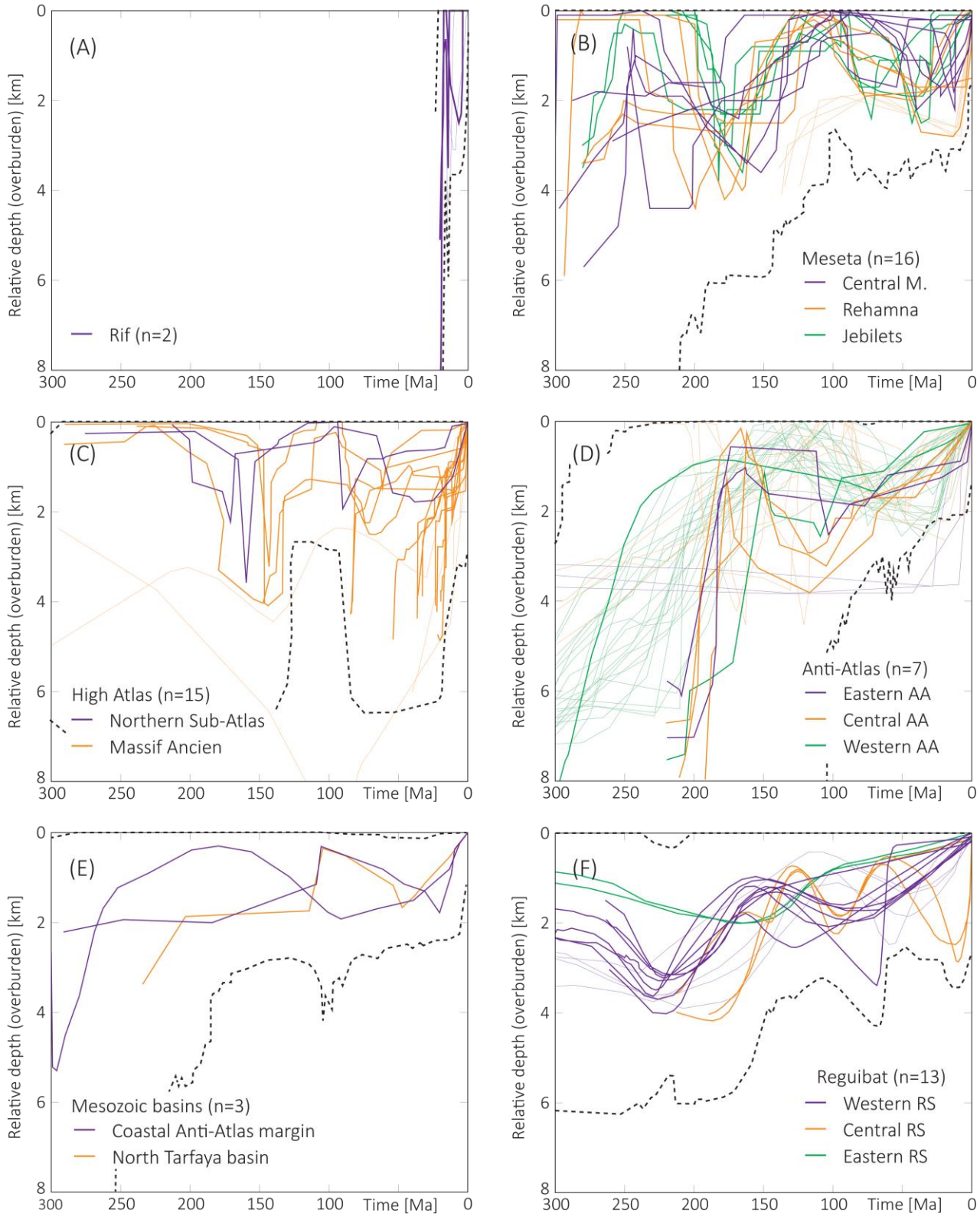
(A)
Rif (n=2)
(B)
Meseta (n=16)
Central M.
Rehamna
Jebilets
(C)
High Atlas (n=15)
Northern Sub-Atlas
Massif Ancien
(D)
Anti-Atlas (n=7)
Eastern AA
Central AA
Western AA
(E)
Mesozoic basins (n=3)
Coastal Anti-Atlas margin
North Tarfaya basin
(F)
Reguibat (n=13)
Western RS
Central RS
Eastern RS
Relative depth (overburden) [km]
Time [Ma]
0
2
4
6
8
300
250
200
150
100

Figure 6 (previous page). Time-depth curves converted from t-T curves shown in figure **4**, assuming geothermal gradients evolving as illustrated in figure **5** and assuming a surface temperature of 20°C. The thicker lines display vertical movement rate calculations; non-selected thinner curves, in the backgrounds, were also converted to depth but were not used in the later study; conditions for result selection are detailed in table **1**. The upper and lower limits (thick dashed lines) are calculated with geothermal gradients of 40 and 20°C/km, respectively.

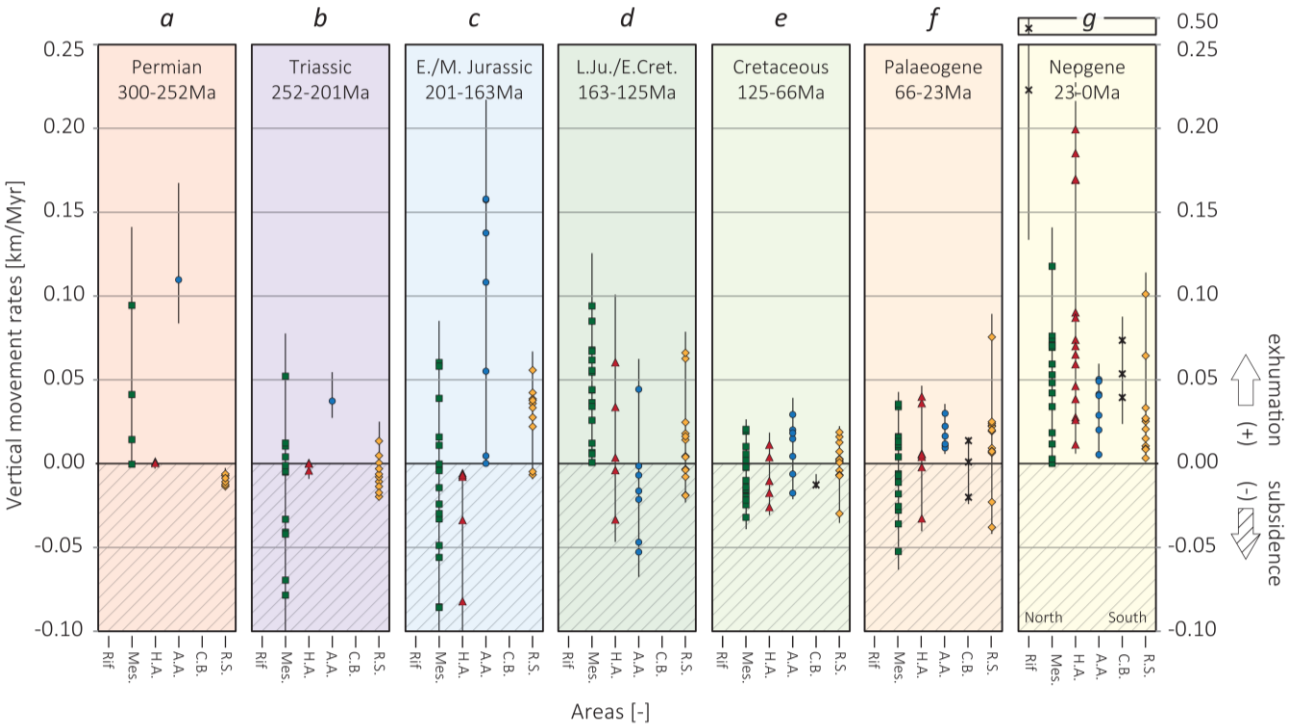

Figure 7. Exhumation and subsidence rates calculated from the 56 selected depth converted curves of figure 5 using the variable geotherms shown in figure A1. The seven defined periods *a* to *g* span between 300 and 0 Ma. The combined uncertainties are extracted from the results of rate calculations using constant geotherms. Mes: Meseta; HA: High Atlas; AA: Anti-Atlas; CB: Coastal Mesozoic basins; RS: Reguibat Shield. Areas, especially if substantially large, may have experienced both exhumation and subsidence, and must not necessarily be an error from the initial t-T models. North and South are only marked for period g because Morocco has been significantly rotated since the Permian (e.g. Scotese, 2012). Note that the x-axis is not time.

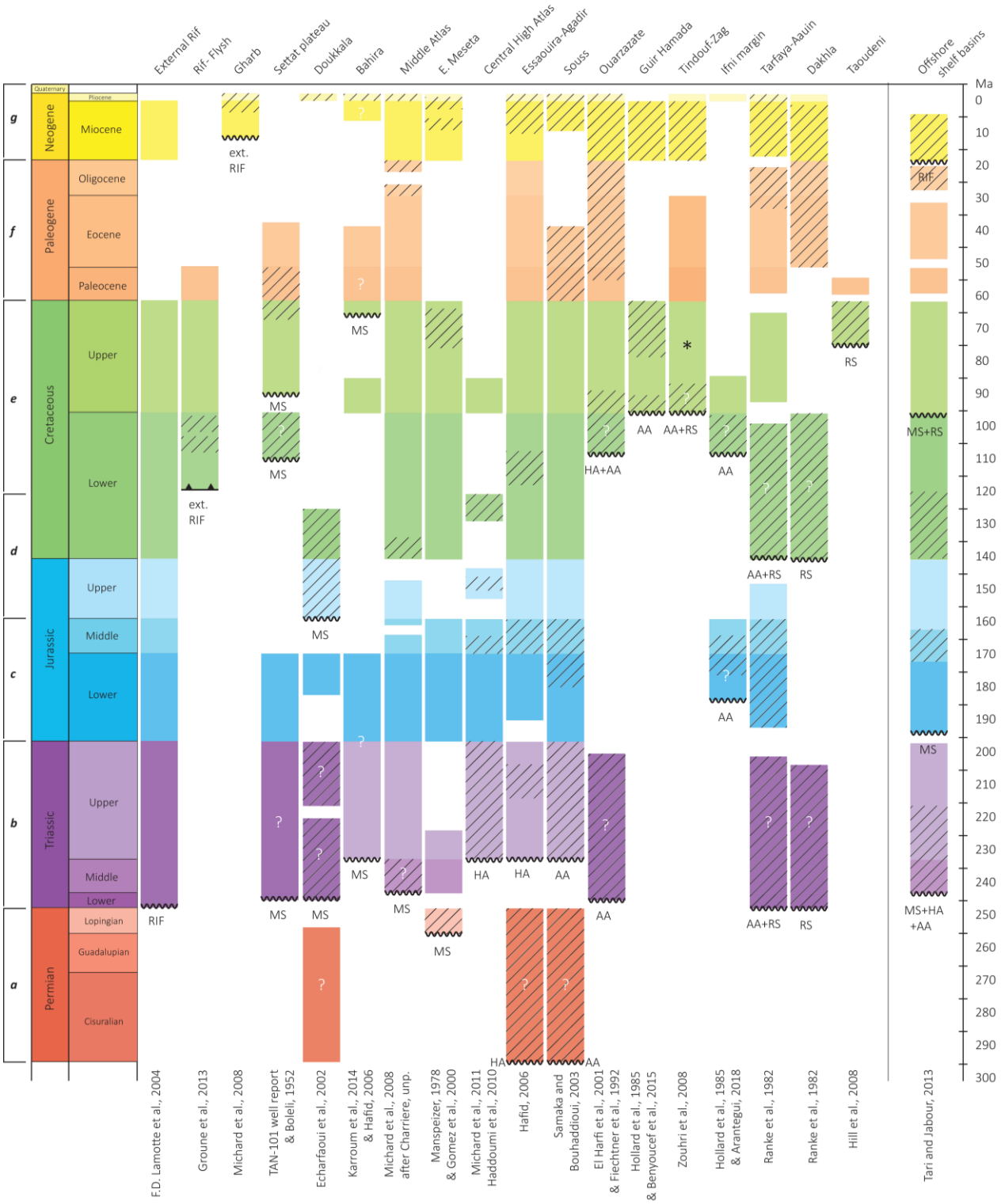
External Rif
Rif- Flysh
Gharb
Settat plateau
Doukkala
Bahira
Middle Atlas
E. Meseta
Central High Atlas
Essaouira-Agadir
Souss
Ouarzazate
Guir Hamada
Tindouf-Zag
Ifni margin
Tarfaya-Aauin
Dakhla
Taoudeni
Offshore shelf basins
Ma
Quaternary
Pliocene
Neogene
Miocene
Paleogene
Oligocene
Eocene
Paleocene
Cretaceous
Upper
Lower
Jurassic
Upper
Middle
Lower
Triassic
Upper
Middle
Lower
Permian
Lopingian
Guadalupian
Cisuralian
g
f
e
d
c
b
a
ext. RIF
RIF
MS
HA
AA
RS
AA+RS
HA+AA
MS+RS
MS+HA +AA
F.D. Lamotte et al., 2004
Groune et al., 2013
Michard et al., 2008
TAN-101 well report & Boleli, 1952
Echarfaoui et al., 2002
Karroum et al., 2014 & Hafid, 2006
Michard et al., 2008 after Charriere, unp.
Manspeïzer, 1978 & Gomez et al., 2000
Michard et al., 2011 Haddoumi et al., 2010
Hafid, 2006
Samaka and Bouhaddioui, 2003
El Harfi et al., 2001 & Fiechtner et al., 1992
Hollard et al., 1985 & Benyoucef et al., 2015
Zouhri et al., 2008
Hollard et al., 1985 & Arantegui, 2018
Ranke et al., 1982
Ranke et al., 1982
Hill et al., 2008
Tari and Jabour, 2013

Figure 8 (previous page). Simplified stratigraphic columns. The hatched parts highlight continental facies and/or coarse to very coarse clastic deposits. The name of the corresponding Variscan/Precambrian basement is shown below the unconformity surfaces (MS: Meseta, HA: High Atlas, AA: Anti-Atlas, and RS: Reguibat shield basements). The seven selected periods (*a* to *g*) are shown on the left. *Late Cretaceous in the Tindouf basin is present in the eastern and western parts, but not in its central part (Hollard et al., 1985).

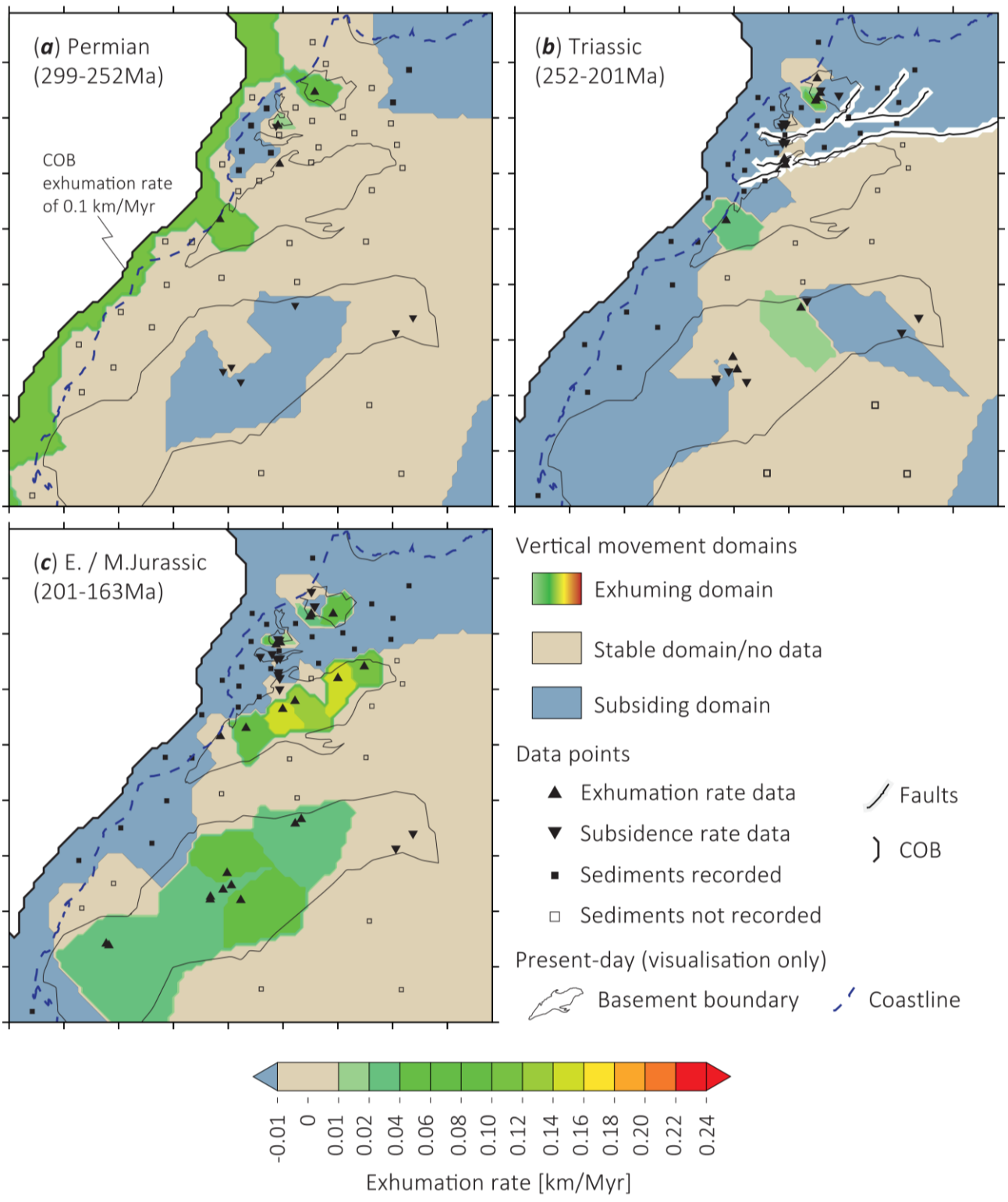
(a) Permian
(299-252Ma)
COB
exhumation rate
of 0.1 km/Myr
(b) Triassic
(252-201Ma)
(c) E. / M.Jurassic
(201-163Ma)
Vertical movement domains
Exhuming domain
Stable domain/no data
Subsiding domain
Data points
Exhumation rate data
Subsidence rate data
Sediments recorded
Sediments not recorded
Faults
COB
Present-day (visualisation only)
Basement boundary
Coastline
-0.01
0
0.01
0.02
0.04
0.06
0.08
0.10
0.12
0.14
0.16
0.18
0.20
0.22
0.24
Exhumation rate [km/Myr]

Figure 9 (previous page). Exhumation maps for the seven selected periods for Morocco and surroundings (***a-c*** on this page and ***d-g*** on the next one) after geological record (fig. 8) and vertical movement rates (fig. 7). Area of interpolation corresponds to area shown in figure 3. Three domains are defined on the exhumation maps: a subsiding domain with rates ≤ -0.011 km/Myr, a stable domain characterised by rates between -0.01 and 0.01, and an exhuming domain with rates ≥ 0.011 km/Myr. Note that the western boundary is the Continent-Ocean Boundary (COB).

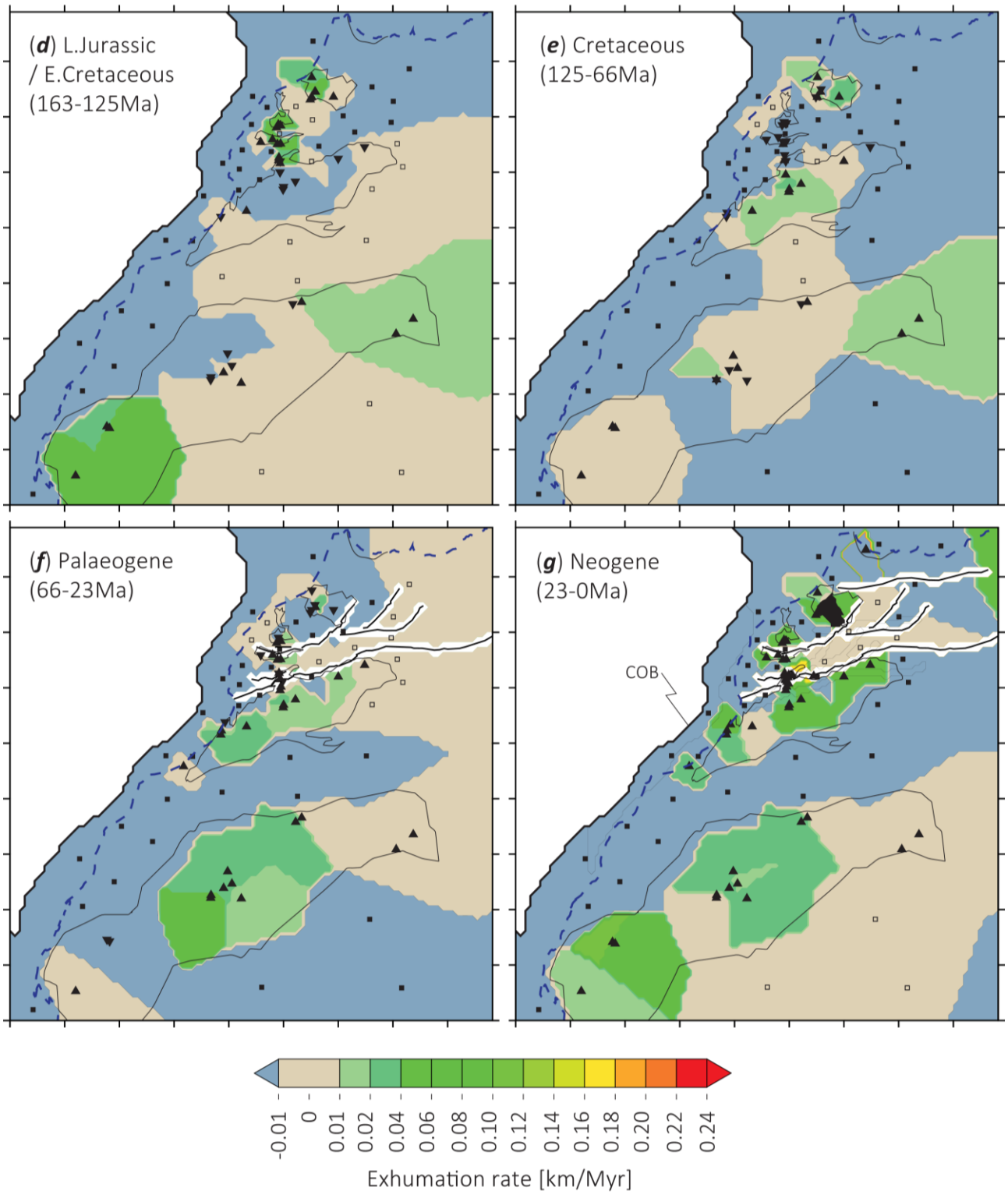

Figure 9. (continued)

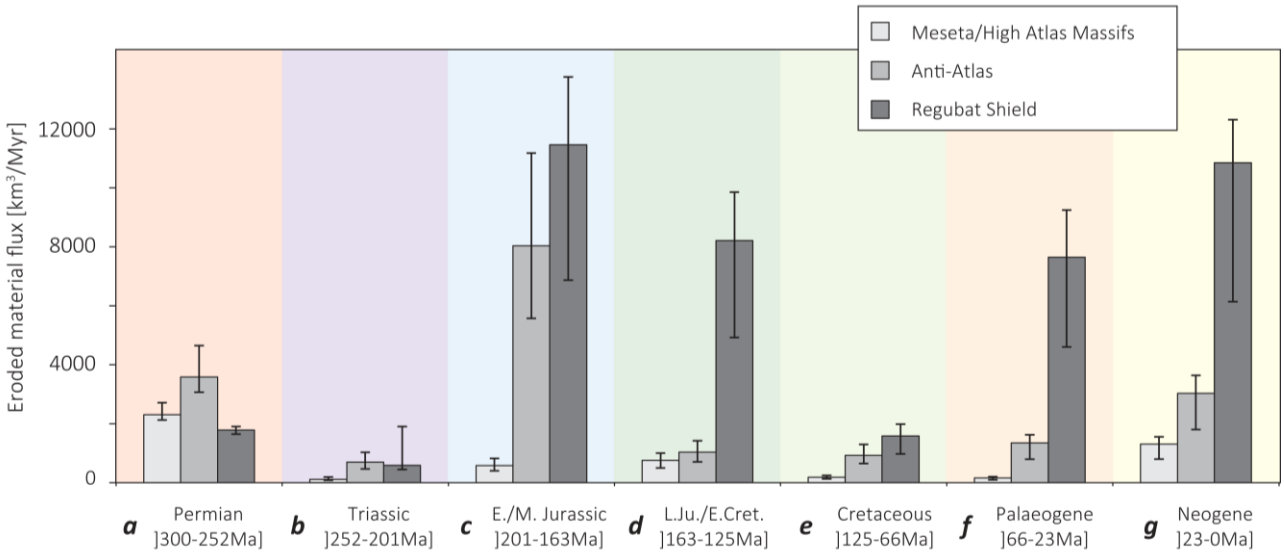

Figure 10. Estimated eroded material flux for the three main sediment sources (Meseta/High Atlas, Anti-Atlas, and Reguibat Shield) for the seven defined periods (**a**-**g**). The eroded material flux is obtained with variable geotherms (fig. **5**), while the ranges are given by calculations done with two constant geotherms of 20 and 40°C/km.

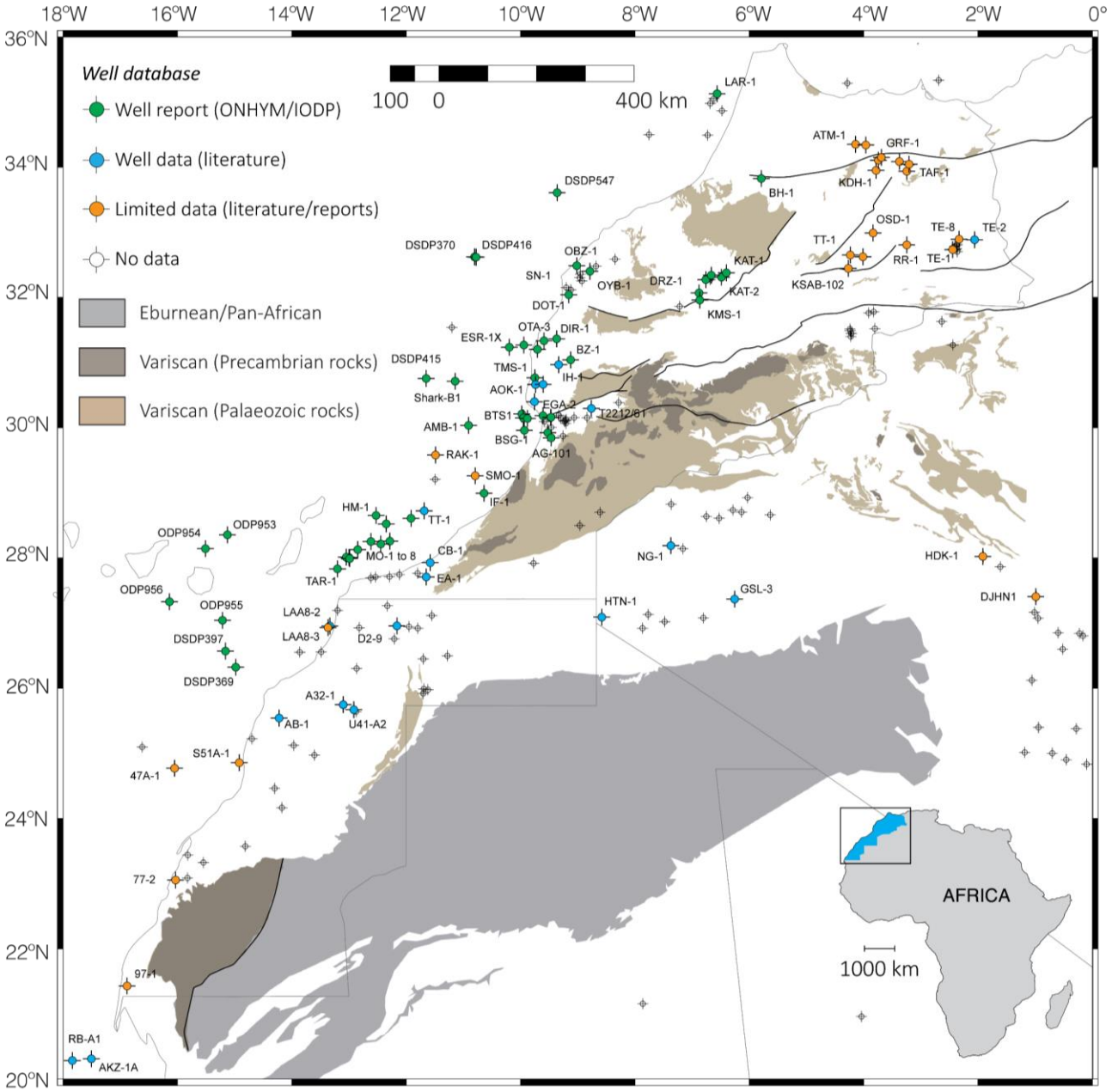

Figure 11. Location of boreholes in Morocco and surrounding NW African countries (non-exhaustive).

Color-coded wells were used in the construction of the SandS maps.

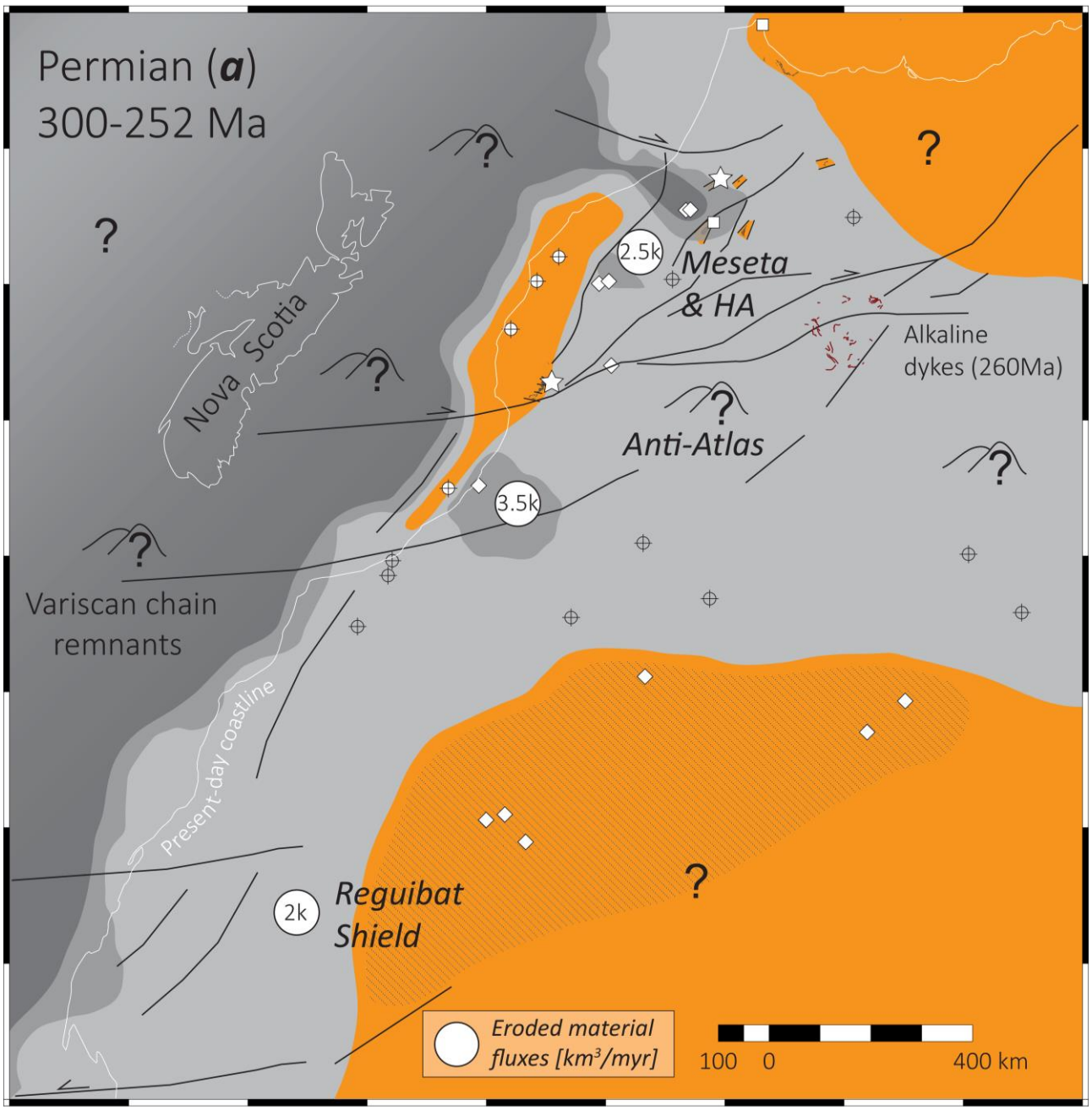

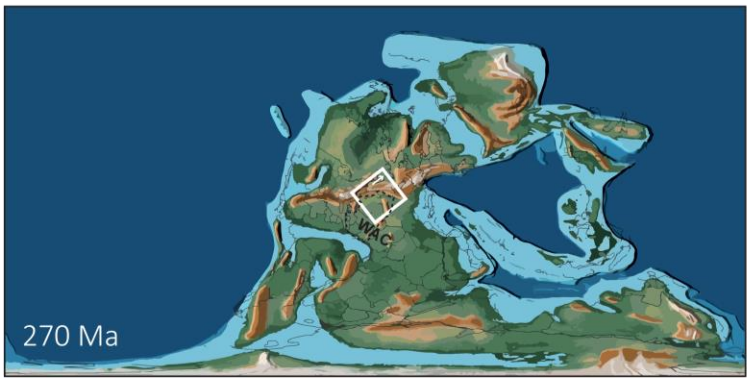

after PALEOMAP project (Scotese, 2012)

Source area

Dominant dep. env.
- Terrestrial
- Transitional
- Shallow marine
- Marine

Control points
- Well data
- Outcrop data
- Fossil data
- t-T modelling

*Source-to-sink**

Geological map
- Outcrops
- Basalts/sills
- Dykes

Exhumation rates
- ≥0.01 km/Myr
- ≥0.05
- ≥0.10

Structural
- Faults
- Local/regional stresses

Figure 12 (previous page). Permian map (period ***a*** as defined in the previous part of this work). See list of references used to build this map, and the following ones, in Table **3**. Dominant dep. env.: Dominant depositional environment. **Source-to-sink***: Simplified source-to-sink systems evidenced with provenance study or paleo-currents. **Well data**: full (white) points mean that sediments of that age were preserved; empty (transparent) points illustrate that sediments were not deposited or not preserved. **WAC**: Western African Craton. Terrestrial domains may also have contain local sedimentary sources, which is highlighted in the SandS maps by with hatched (and dashed) lines.

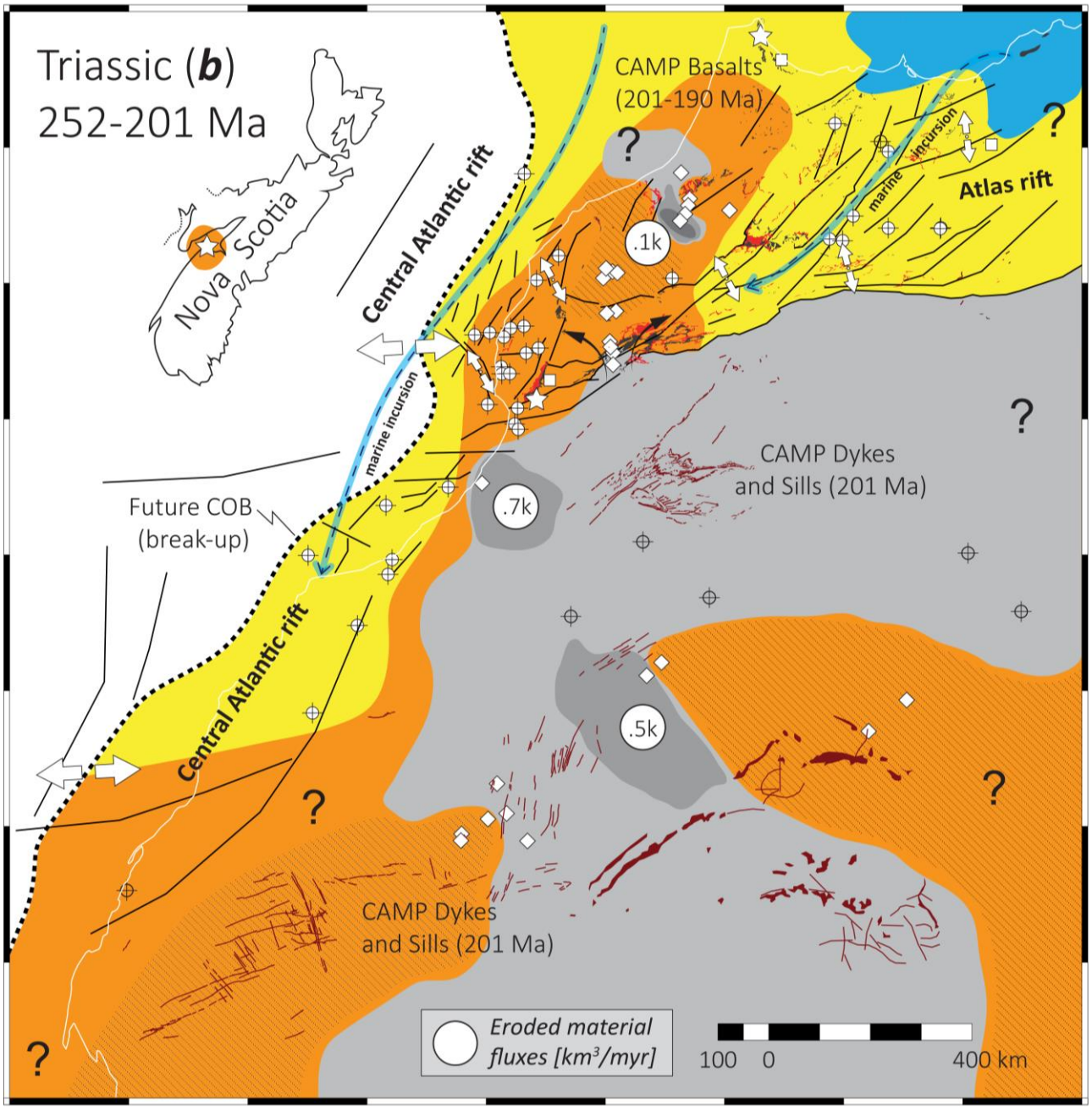

after PALEOMAP project (Scotese, 2012)

Source area

Dominant dep. env.
- Terrestrial
- Transitional
- Shallow marine
- Marine

Control points
- Well data
- Outcrop data
- Fossil data
- t-T modelling

*Source-to-sink**

Geological map
- Outcrops
- Basalts/sills
- Dykes

Exhumation rates
- ≥0.01 km/Myr
- ≥0.05
- ≥0.10

Structural
- Faults
- Local/regional stresses

Figure 13 (previous page). Triassic map (period ***b***). Illustrated dykes and basalts are from the Central Atlantic Magmatic Province (CAMP). See caption of figure 12 for additional information.

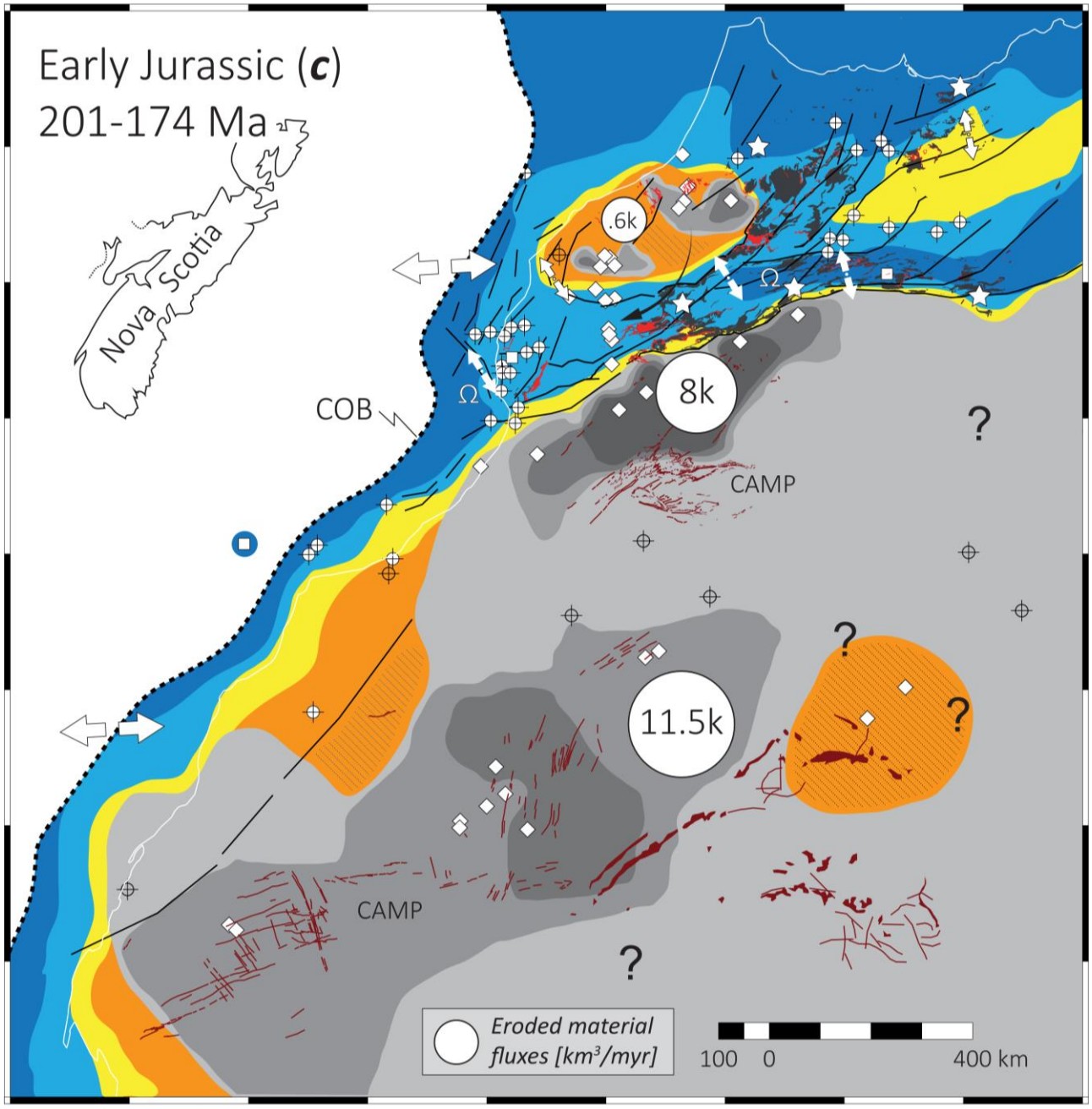

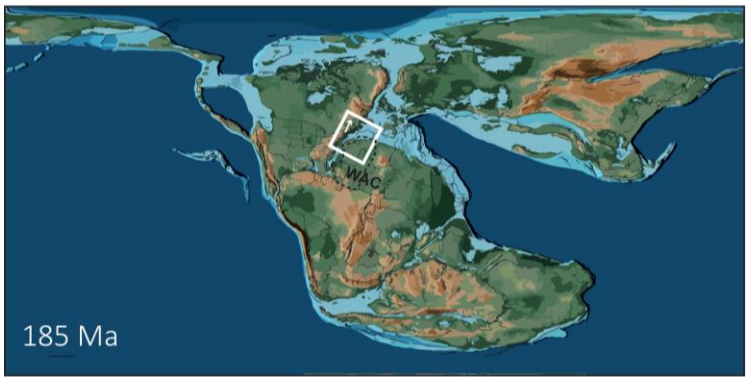

after PALEOMAP project (Scotese, 2012)

Source area
Dominant dep. env.
Terrestrial
Transitional
Shallow marine
Marine
Control points
Well data
Outcrop data
Fossil data
t-T modelling
*Source-to-sink**

Geological map
Outcrops
Basalts/sills
Dykes
Exhumation rates
≥0.01 km/Myr
≥0.05
≥0.10
Structural
Faults
Local/regional stresses

Figure 14 (previous page). Early Jurassic map (period *c*). CAMP: Central Atlantic Magmatic Province. See caption of figure 12 for additional information. Ω: Triassic salt mobilisation (after Moragas et al., 2018).

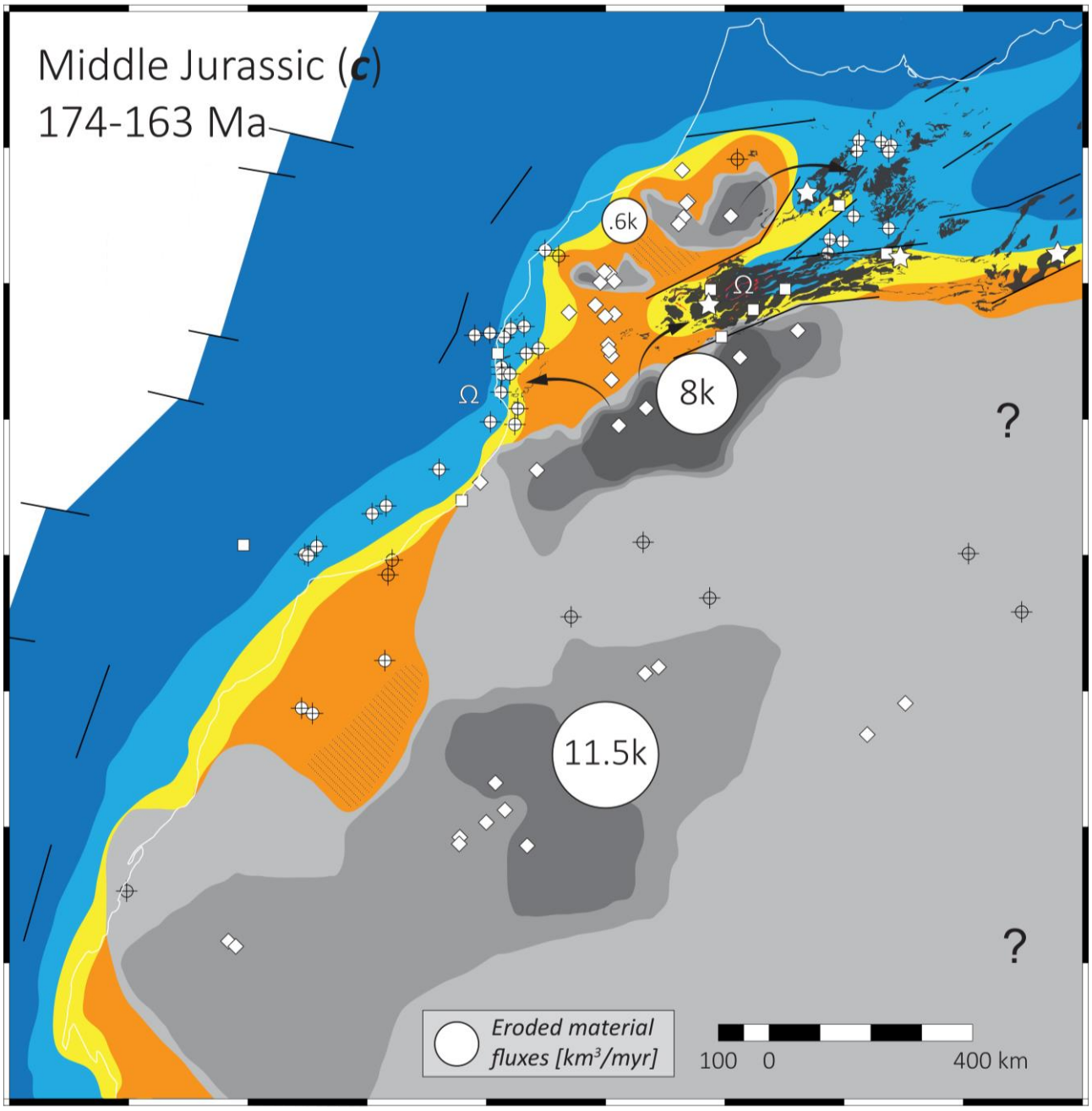

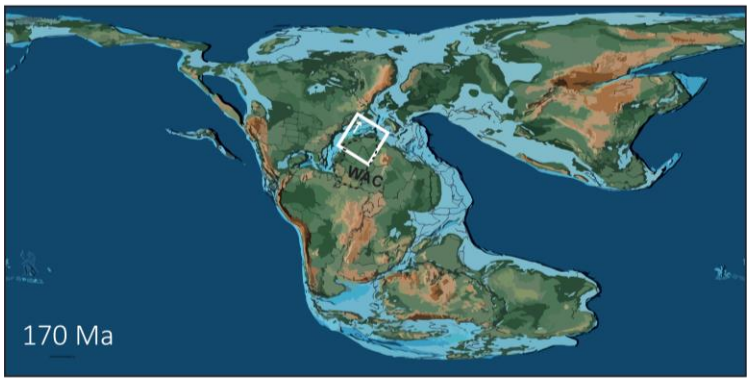

after PALEOMAP project (Scotese, 2012)

Source area

Dominant dep. env.
- Terrestrial
- Transitional
- Shallow marine
- Marine

Control points
- Well data
- Outcrop data
- Fossil data
- t-T modelling

*Source-to-sink**

Geological map
- Outcrops
- Basalts/sills
- Dykes

Exhumation rates
- ≥0.01 km/Myr
- ≥0.05
- ≥0.10

Structural
- Faults
- Local/regional stresses

Figure 15 (previous page). Middle Jurassic map (period ***c***). See caption of figure 12 for additional information. **Ω**: Triassic salt mobilisation (after Moragas et al., 2018).

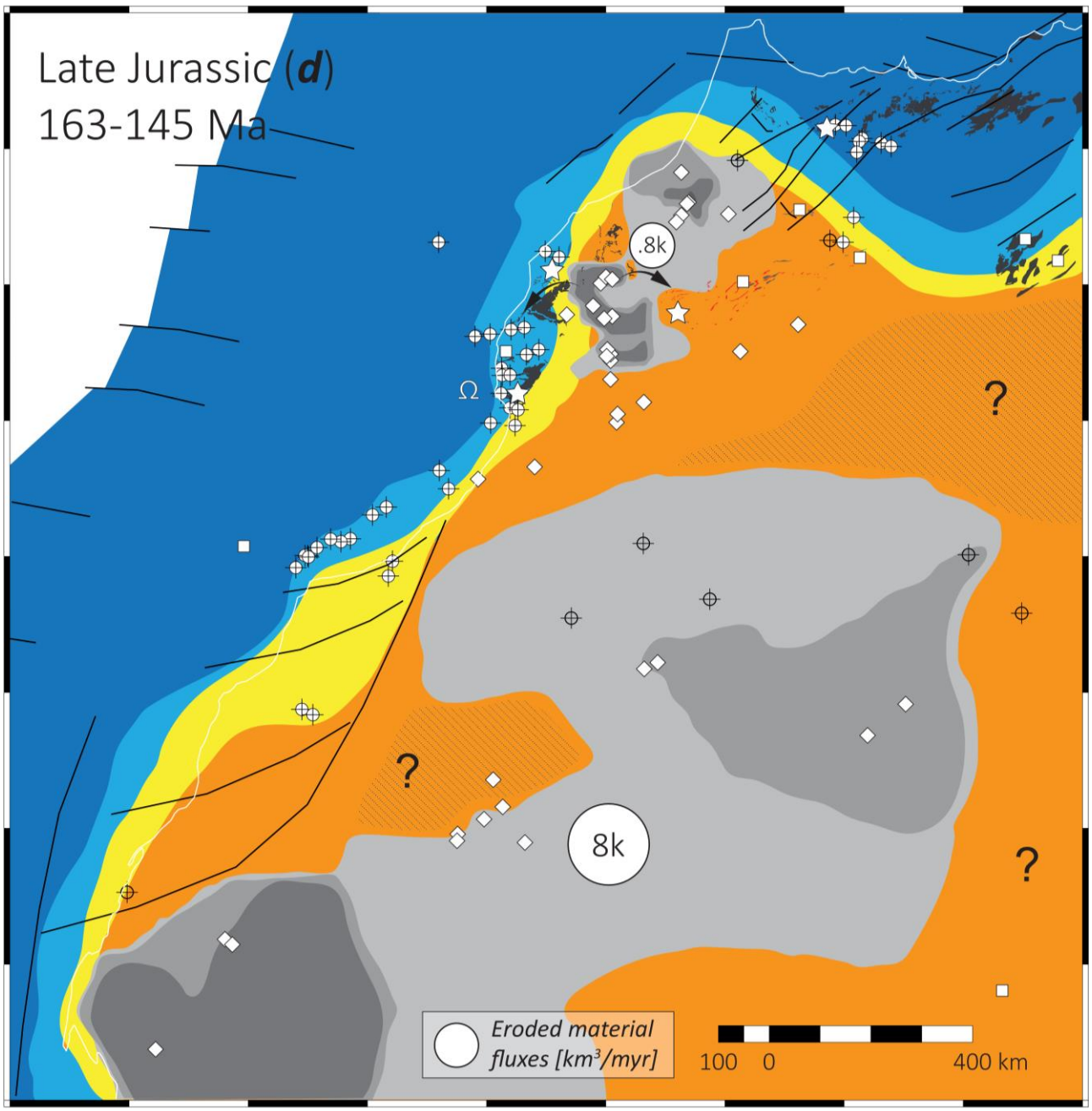

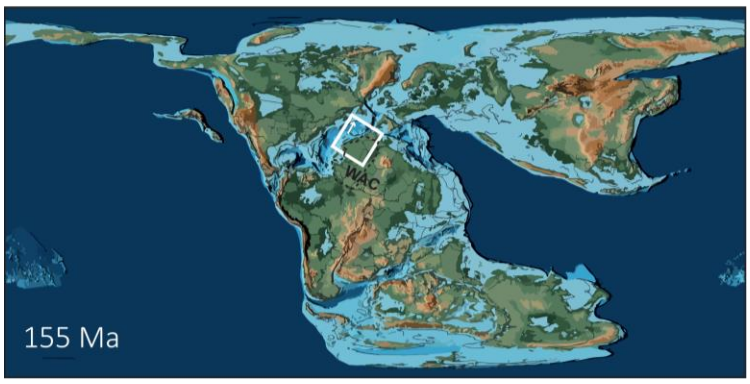

after PALEOMAP project (Scotese, 2012)

Source area

Dominant dep. env.
- Terrestrial
- Transitional
- Shallow marine
- Marine

Control points
- Well data
- Outcrop data
- Fossil data
- t-T modelling

*Source-to-sink**

Geological map
- Outcrops
- Basalts/sills
- Dykes

Exhumation rates
- ≥0.01 km/Myr
- ≥0.05
- ≥0.10

Structural
- Faults
- Local/regional stresses

Figure 16 (previous page). Late Jurassic map (period ***d***). See caption of figure 12 for additional information. **Ω**: Triassic salt mobilisation (after Moragas et al., 2018).

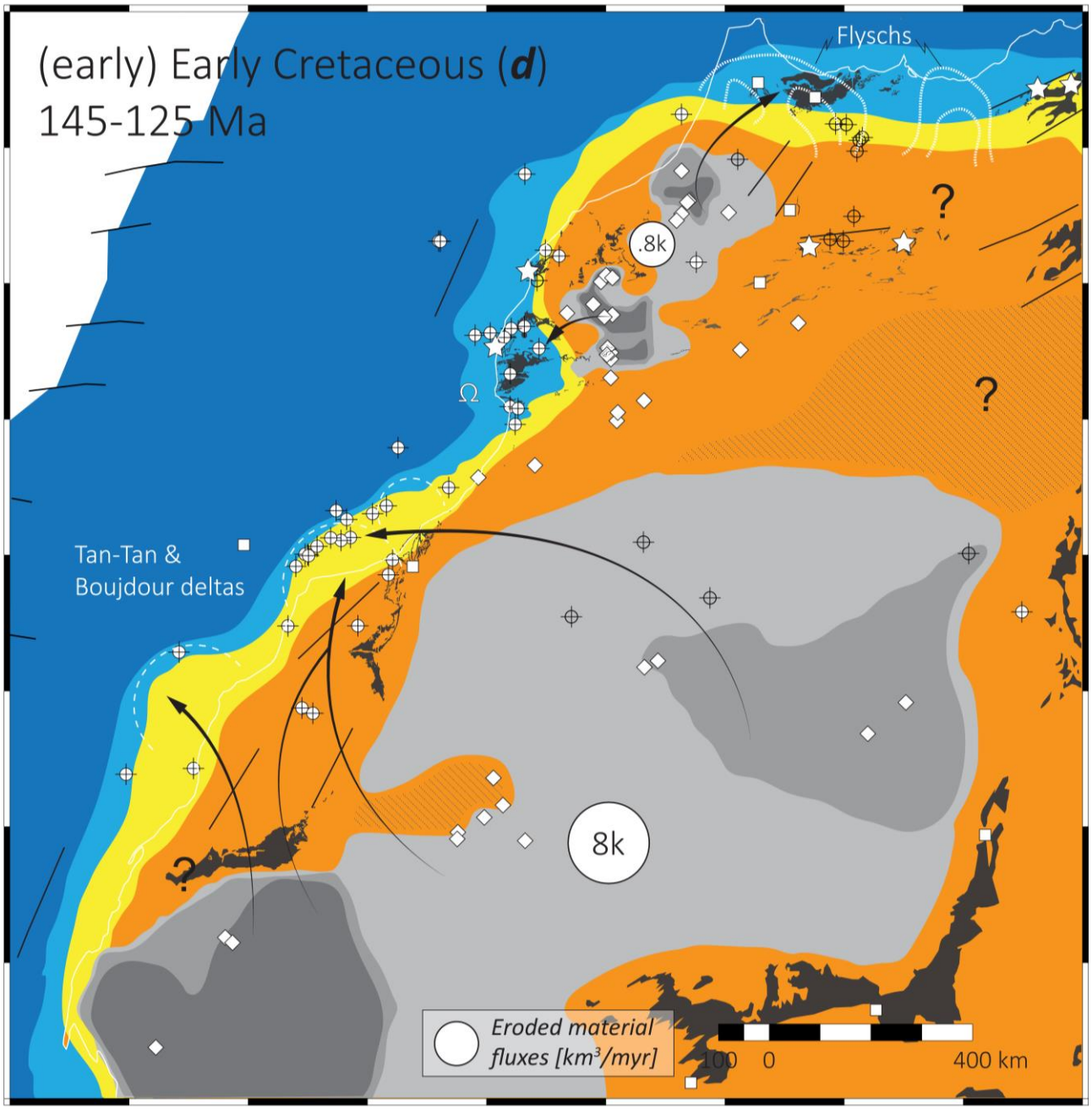

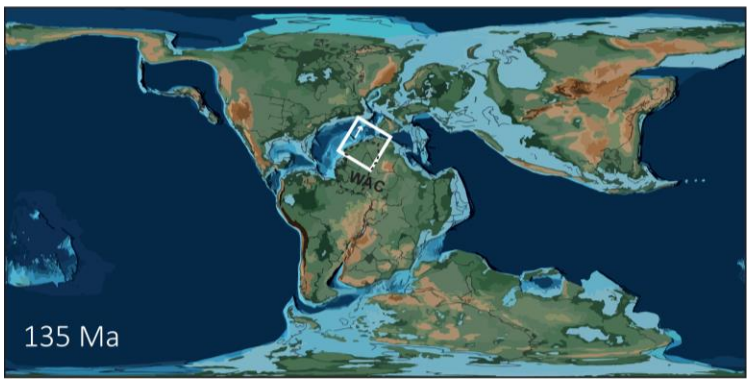

after PALEOMAP project (Scotese, 2012)

Source area

Dominant dep. env.
- Terrestrial
- Transitional
- Shallow marine
- Marine

Control points
- Well data
- Outcrop data
- Fossil data
- t-T modelling

*Source-to-sink**

Geological map
- Outcrops
- Basalts/sills
- Dykes

Exhumation rates
- ≥0.01 km/Myr
- ≥0.05
- ≥0.10

Structural
- Faults
- Local/regional stresses

Figure 17 (previous page). (early) Early Cretaceous map (period ***d***). See caption of figure 12 for additional information. Ω: Triassic salt mobilisation (after Moragas et al., 2018).

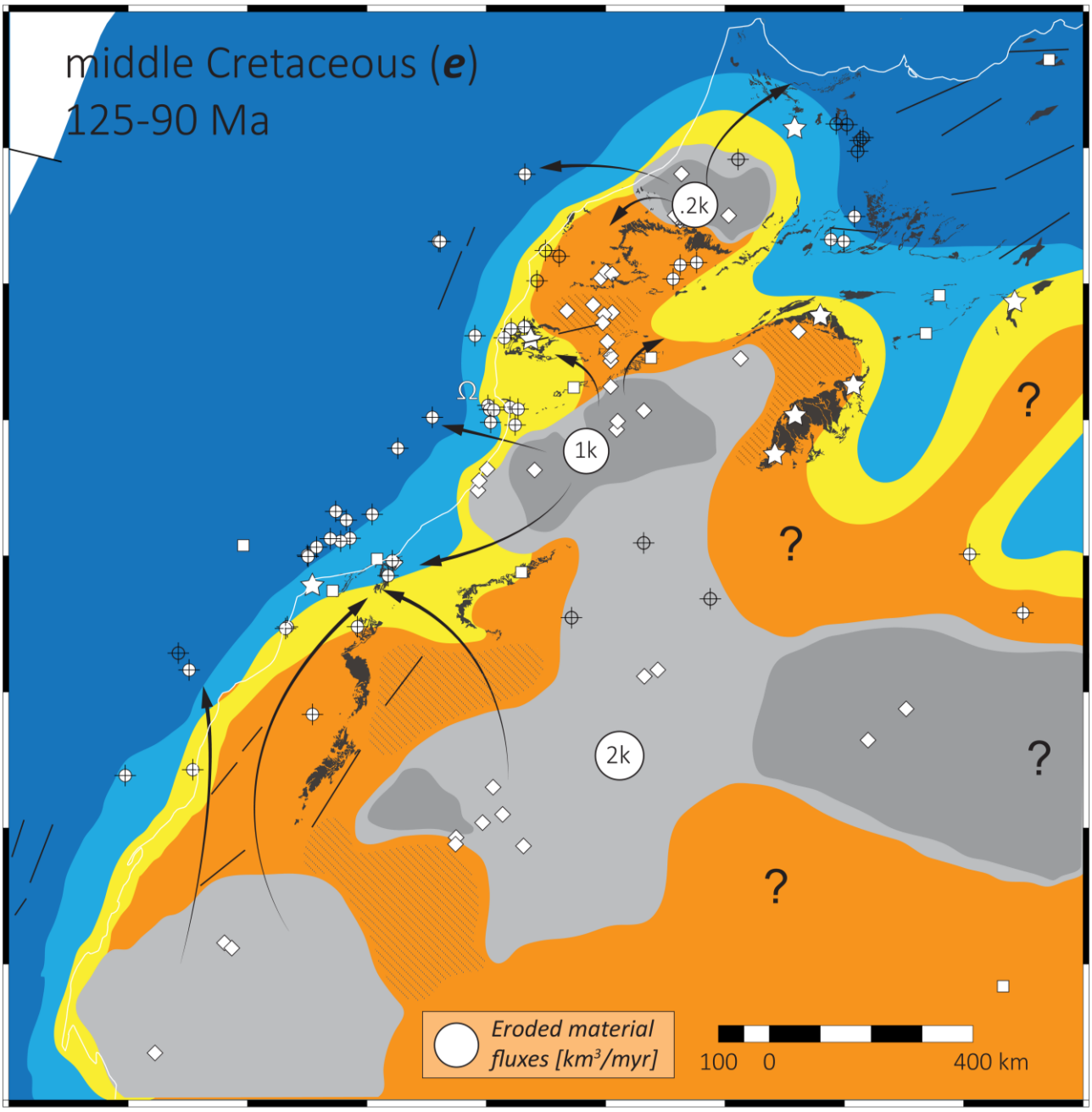

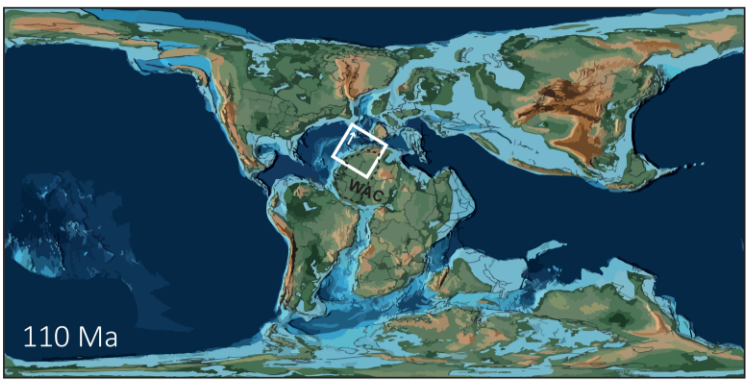

after PALEOMAP project (Scotese, 2012)

Source area

Dominant dep. env.
- Terrestrial
- Transitional
- Shallow marine
- Marine

Control points
- Well data
- Outcrop data
- Fossil data
- t-T modelling

*Source-to-sink**

Geological map
- Outcrops
- Basalts/sills
- Dykes

Exhumation rates
- ≥0.01 km/Myr
- ≥0.05
- ≥0.10

Structural
- Faults
- Local/regional stresses

Figure 18 (previous page). middle Cretaceous map (period ***e***). See caption of figure 12 for additional information. **Ω**: Triassic salt mobilisation (after Moragas et al., 2018).

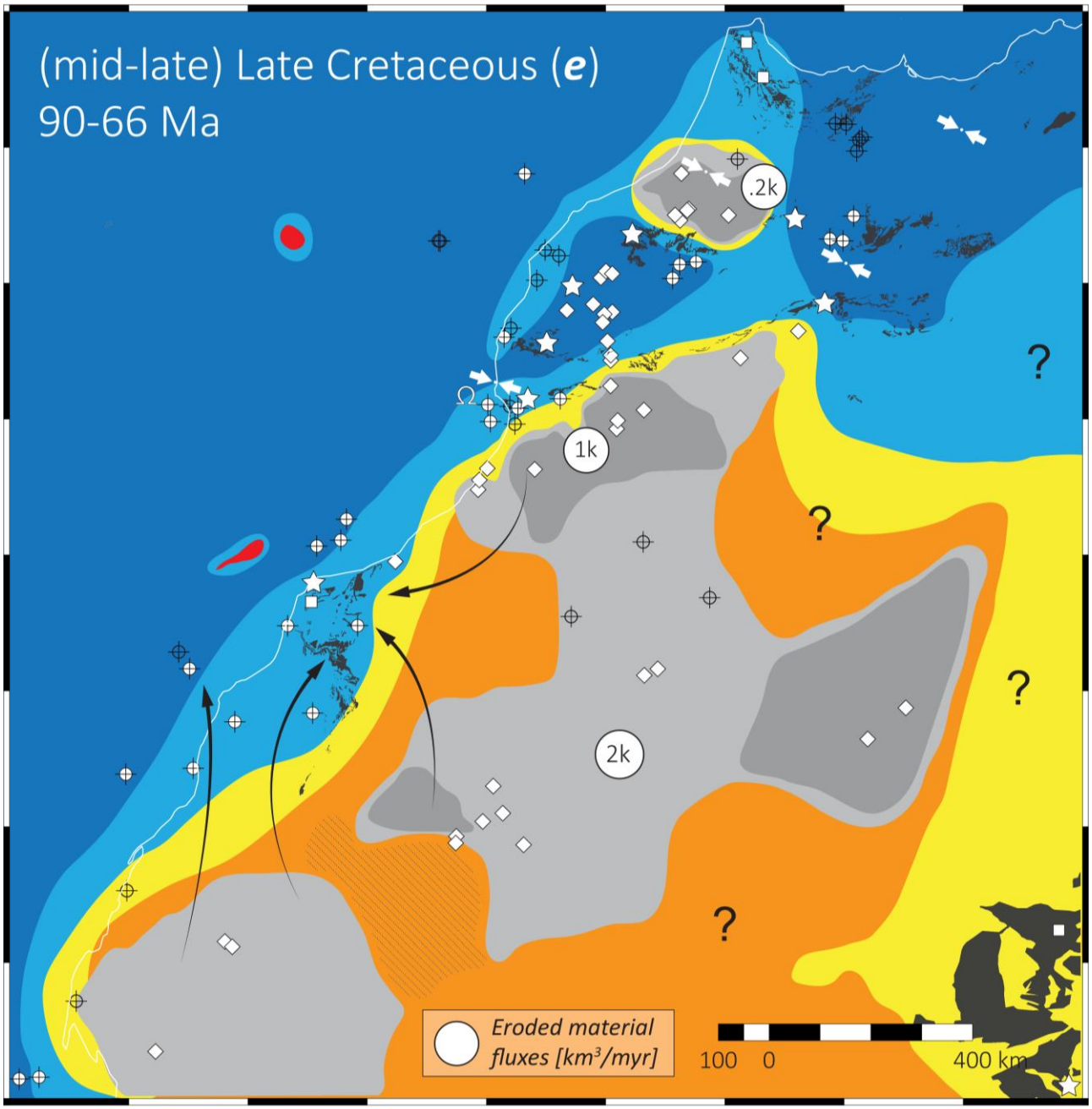

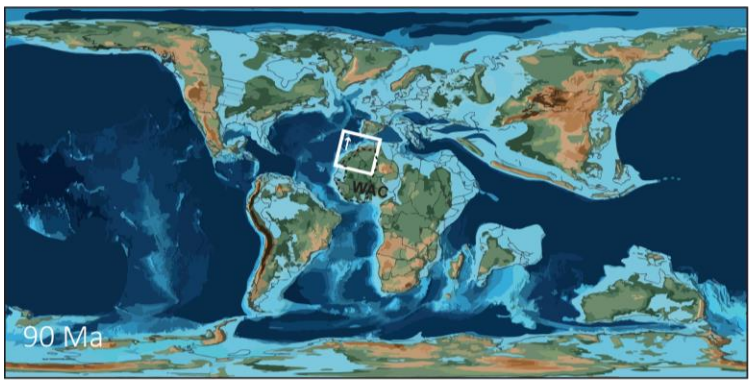

after PALEOMAP project (Scotese, 2012)

Source area

Dominant dep. env.
- Terrestrial
- Transitional
- Shallow marine
- Marine

Control points
- Well data
- Outcrop data
- Fossil data
- t-T modelling

*Source-to-sink**

Geological map
- Outcrops
- Basalts/sills
- Dykes

Exhumation rates
- ≥0.01 km/Myr
- ≥0.05
- ≥0.10

Structural
- Faults
- Local/regional stresses

Figure 19 (previous page). (mid-late) Late Cretaceous map (period ***e***). See caption of figure 12 for additional information. **Ω**: Triassic salt mobilisation (after Moragas et al., 2018).

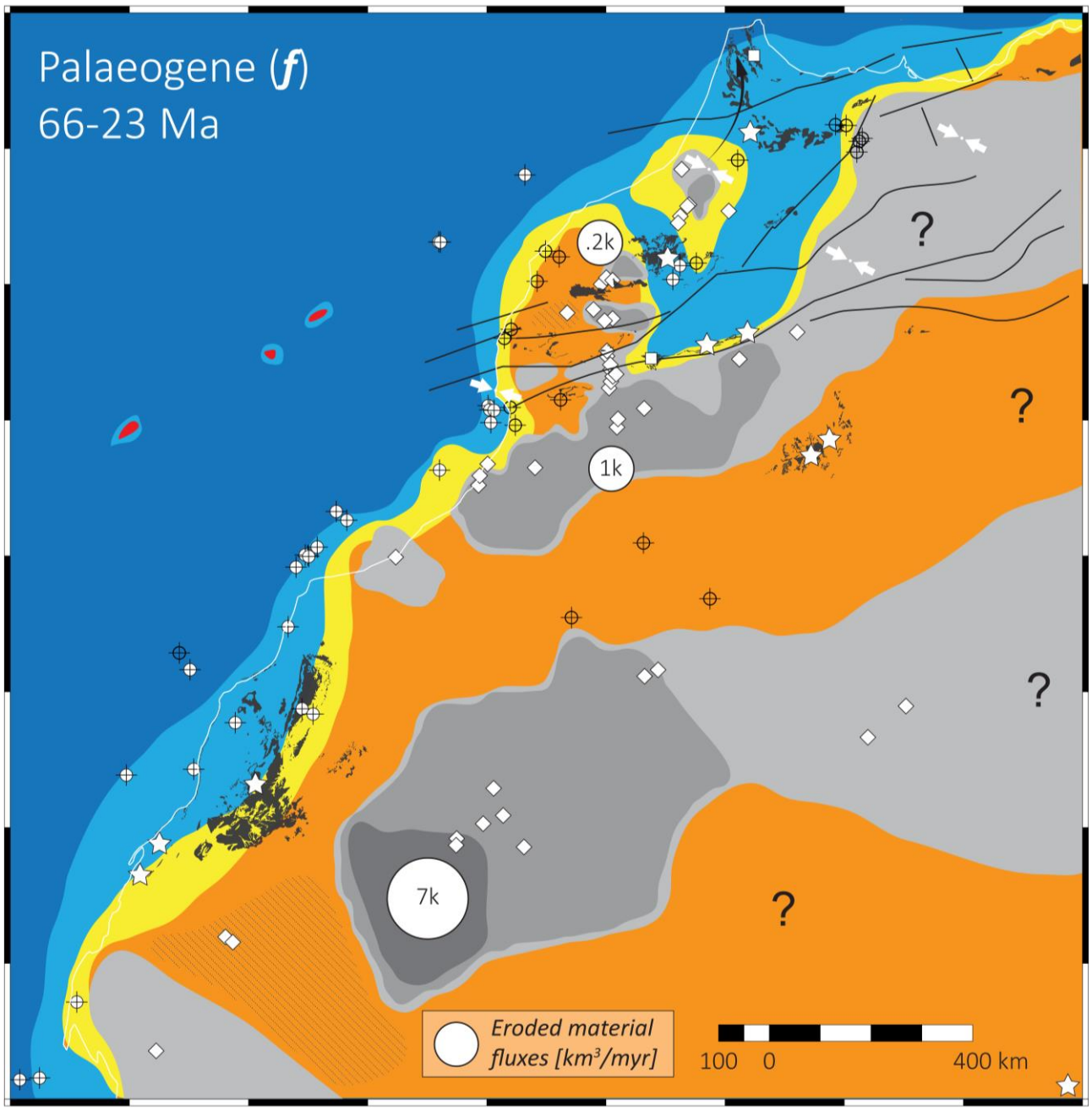

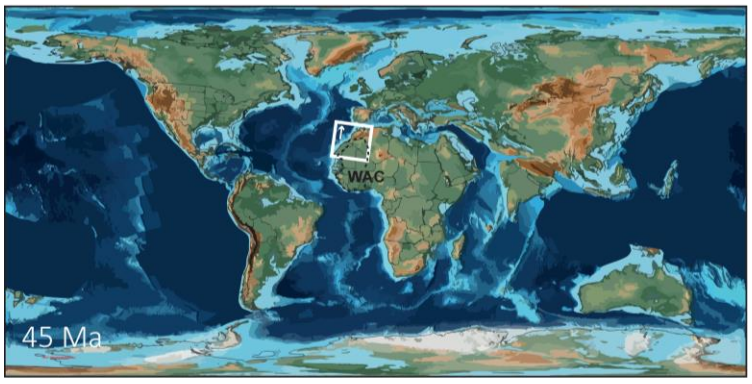

after PALEOMAP project (Scotese, 2012)

Source area
Dominant dep. env.
Terrestrial
Transitional
Shallow marine
Marine
Control points
Well data
Outcrop data
Fossil data
t-T modelling
*Source-to-sink**

Geological map
Outcrops
Basalts/sills
Dykes
Exhumation rates
≥0.01 km/Myr
≥0.05
≥0.10
Structural
Faults
Local/regional stresses

Figure 20 (previous page). Palaeogene map (period ***f***). See caption of figure 12 for additional information.

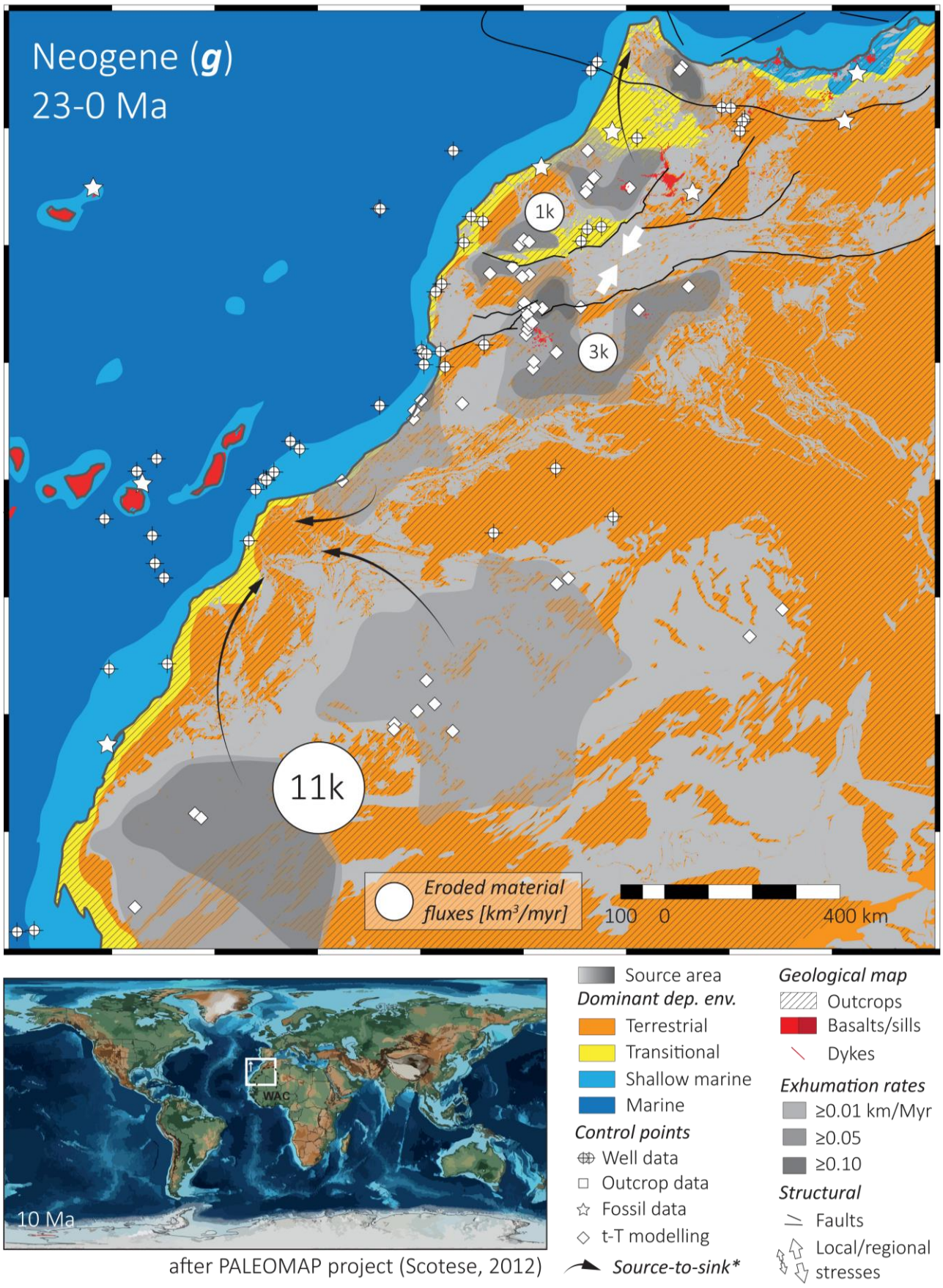

Figure 21. Neogene map (period ***g***). See caption of figure 12 for additional information.

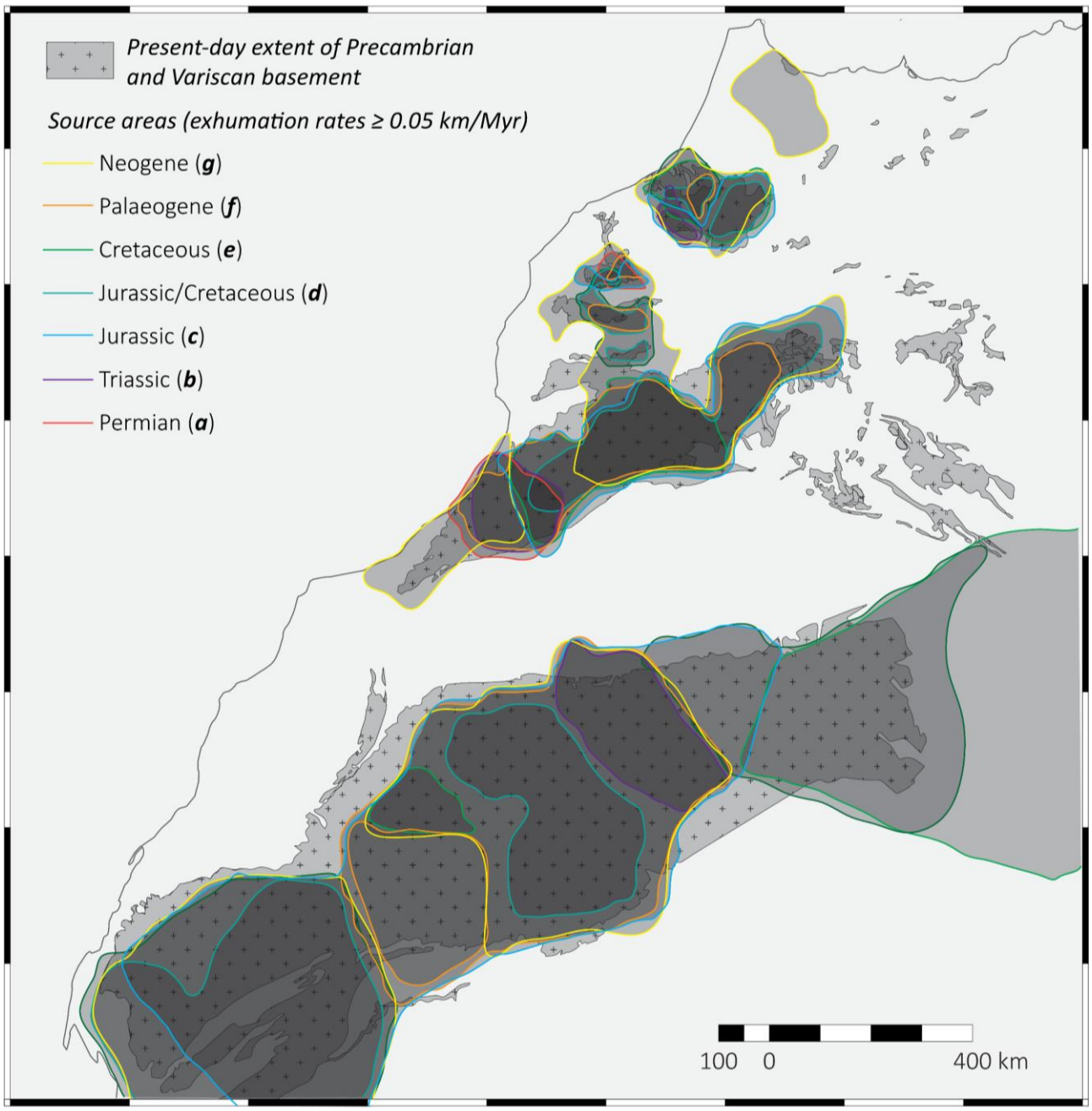

Figure 22. Stacked polygons for exhumation rates ≥ 0.05 km/Myr, for each period of the exhumation maps (fig. 9), superimposed to the extent of Precambrian and Variscan basement outcrops (Hollard et al., 1986).

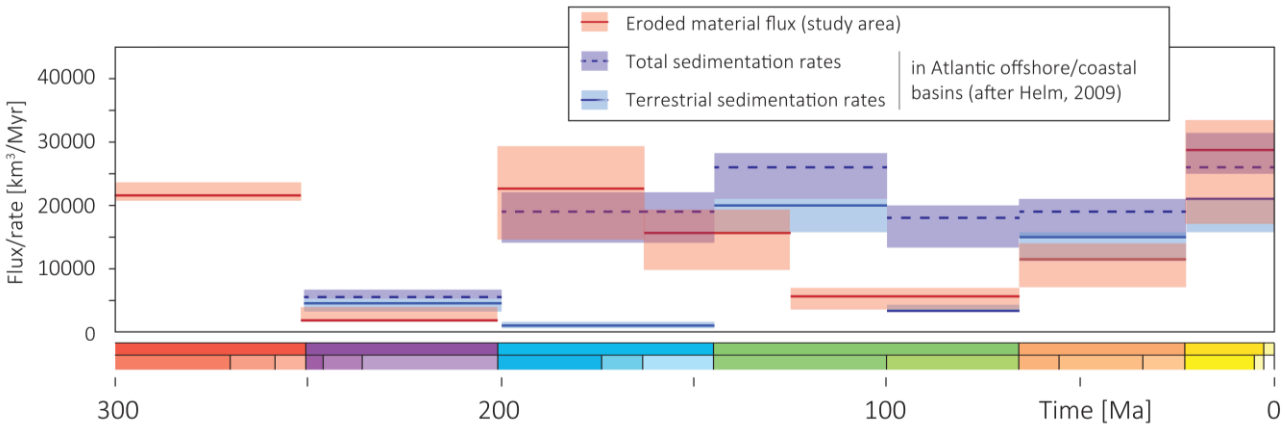

Figure 23. Comparison of the total eroded material flux to sedimentation rates in Moroccan offshore and coastal basins (after Helm, 2009). Note that it may be expected that the results should not match perfectly, as a proportion of the eroded material would be removed as dissolved carbonate or as fines that would have long transport distance into the deep oceanic basins (i.e. eroded material flux – red line v terrestrial sedimentation rates - blue).